Iowa Research Online
The University of Iowa's Institutional Repository

University of Iowa
Iowa Research Online

Theses and Dissertations

Spring 2017

Characterization of wastes pertaining to naturally occurring radioactive materials (NORM) and the nuclear fuel cycle

Eric Steven Eitrheim
University of Iowa

Copyright © 2017 Eric Steven Eitrheim

This dissertation is available at Iowa Research Online: http://ir.uiowa.edu/etd/5464

Recommended Citation
Eitrheim, Eric Steven. "Characterization of wastes pertaining to naturally occurring radioactive materials (NORM) and the nuclear fuel cycle." PhD (Doctor of Philosophy) thesis, University of Iowa, 2017.
http://ir.uiowa.edu/etd/5464.

Follow this and additional works at: http://ir.uiowa.edu/etd


Part of the Chemistry Commons

CHARACTERIZATION OF WASTES PERTAINING TO NATURALLY OCCURRING RADIOACTIVE MATERIALS (NORM) AND THE NUCLEAR FUEL CYCLE

BY

ERIC STEVEN EITRHEIM

A thesis submitted in partial fulfillment
of the requirements for the Doctor of Philosophy
degree in Chemistry
in the Graduate College of
The University of Iowa

May 2017

Thesis Supervisor: Associate Professor Tori Z. Forbes

Copyright by

ERIC STEVEN EITRHEIM

2017

All Rights Reserved

Graduate College
The University of Iowa
Iowa City, Iowa

CERTIFICATE OF APPROVAL

_____

PH.D. THESIS

_____

This is to certify that the Ph.D. thesis of

ERIC STEVEN EITRHEIM

has been approved by the Examining Committee for
the thesis requirement for the Doctor of Philosophy degree
in Chemistry at the May 2017 graduation.

Thesis Committee: _____
TORI Z. FORBES, Thesis Supervisor

_____
MICHAEL K. SCHULTZ

_____
EDWARD G. GILLAN

_____
SCOTT K. SHAW

_____
JOHNA LEDDY

I dedicate this thesis to the inspirational memory of my father.

Without his example, I would not be where I am today.

Nothing in life is to be feared; it is only to be understood.

-Marie Sklodowska Curie
1903 & 1911 Nobel laureate, physicist, chemist

The important thing in science is not so much to obtain new facts as to discover new ways of thinking about them.

– Sir William Lawrence Bragg
1915 Nobel laureate, physicist, X-ray crystallographer

ACKNOWLEDGEMENTS

First of all, I have the utmost thanks for my wife, Sarah, for her support and sacrifices to aid me in pursuing my degree. She has helped provide motivation and clarity of my professional goals. Sarah also put up with the odd hours, unknown end-date, and occasional complaint.

Secondly, a thanks to my advisor, Tori, for her continually guidance and understanding. She helped me navigate the uncertainties associated with entering a career in academia. Tori is more than just an advisor, but really the definition of a mentor who clearly cares about her students and is interested in their personal and professional development. She has been able to direct me and keep me on track. I am not sure that I would have been able to do this without her. She has gone out of her way to provide opportunities for me, including numerous teaching experiences, collaborations, and educational experiences.

Thirdly, I owe more than I can imagine to my co-workers who critiqued me, taught me, and inspired me in various projects. Most notably, my labmates and friends, Andy Nelson, Andrew Knight, Mo Payne, Madeline Basile, Jennifer Bjorkland, Josh de Groot, Ashini Jayasinghe, Dustin May, Ryan Golkowski, and Adam Johns. Undergraduate researchers like Mackenzie Cole and Cyrus Mansouri were also indispensable. This is not an extensive list and I am thankful to others who have helped me in the laboratory. I couldn't have gotten any luckier with co-workers who I have been privileged to work side by side with for so many years.

Additionally, I would also like to thank Michael Schultz for going above and beyond to provide opportunities that added value to my professional development. Without these opportunities in teaching Radiochemistry, gaining industry experience at NorthStar Medical

Radioisotopes, as well as a government lab experience at New Brunswick Lab at Argonne National Lab, I would not feel as confident entering a career in chemistry.

Lastly, I would like to thank the University of Iowa, Department of Chemistry and all of the administrators and staff. They have always treated me with respect and have helped at every chance to aid in my success. Among this list particularly includes my committee who have guided me all of these years providing insight and valuable time. I couldn't be more grateful.

Without all your support, this thesis would not have been possible.

ABSTRACT

Radioactive wastes from a range of sources are of great concern for their potential to negatively affect the environment and human health. There is a substantial need to develop new methods and techniques for management and disposal that are economically feasible and environmentally suitable. Such methods require better characterization and chemical understanding of these wastes, including advancements pertaining to the interaction between radioactive elements and non-radioactive constituents within the complex waste matrix. This thesis focuses on the fundamental chemistry of three types of waste forms: (1) solid drill cuttings from hydraulic fracturing activities; (2) Weapons grade plutonium; and (3) solid aluminum hydroxide phases associated with Hanford Tank wastes.

The first study characterizes naturally occurring radioactive materials (NORM) in solid "drill cuttings" from hydraulic fracturing activities for natural gas extraction. NORM (uranium (U), thorium (Th), radium (Ra), lead (Pb), and polonium (Po) isotopes) associated with three samples from the Marcellus Shale formation were analyzed using radiometric techniques and found to have elevated radioactivity levels and isotopic disequilibria. NORM mobility within a landfill environment was also evaluated and these studies suggested some leaching of NORM from the solid waste form.

Nuclear weapons technologies have also produced significant amounts of wastes, including some forms can be processed into useable, mixed-oxide (MOX) nuclear fuels. MOX solids require a complete separation of the gallium (Ga) originally present in the original weapons materials from Pu and other actinides to ensure the conversion was effective. A radiochemical method for the separation of Ga, Pu, U, Th, and americium (Am) was developed using chromatographic resins

and radiochemical tracers. The innovation within this study included the novel use of ^{68}Ga, an isotope developed for nuclear medicine applications. This research can be translated to nuclear forensics applications because it provides isotope ratios that can be used to determine the method or location of production of the original nuclear weapons material.

The third research area focuses on the fundamental chemistry of the aluminum bearing wastes associated with the Hanford Site in Washington State. These mixed radioactive wastes have large quantities of aluminum (Al) that interferes with effective management and treatment strategies. There is a critical need to improve our fundamental understanding of Al chemistry in these systems to develop methods to improve our ability to work with the current waste streams. For example, Al is known to form oxyhydroxy polyaluminum species, or soluble molecular nanoclusters that exhibit different physical and chemical properties than isolated monomeric or dimeric forms of Al and contribute to much of the problematic chemistry in this system. There are significant challenges for the identification and characterization of these clusters in simple aqueous solutions and in more-complex solutions such as nuclear wastes. This body of work focuses on the isolation and identification of some of these clusters, including three Al_{30} clusters, and their interaction with other contaminants that are likely to be present in nuclear waste streams. Other clusters, including the elusive aluminum octamer, have also been synthesized and isolated, allowing for further characterization and understanding of these model clusters.

PUBLIC ABSTRACT

Wastes produced from industry and government activities need to be characterized and disposed of in a way that is economically and environmentally suitable. To do this, it is crucial to characterize and understand the chemistry of these complex waste streams. Naturally occurring radioactivity is one characteristic of wastes produced in hydraulic fracturing activities. These radioactive materials exhibit distinctive radioactive-decay properties that can be detected in the laboratory, allowing us to determine how a given material will behave and how best to isolate it. This in turn can lead to better management techniques for dealing with these wastes to help preserve human and environmental health.

Other wastes are more directly related to radioactive materials are nuclear wastes. Nuclear wastes, including the complex waste from nuclear weapons production, have large quantities of aluminum that has complicated our ability to treat and manage those wastes effectively. Probing the basic understanding of this element and how it complexes with both itself and other elements can help lead to better methods of handling aluminum-containing wastes. Isolating structures of aluminum with various contaminants can help develop this knowledge. We are able to study these aluminum structures by utilizing a technique called single crystal X-ray diffraction, which can give us a three-dimensional picture of where atoms are located in a structure along with the type of atom (i.e. element) that is located at each position. This technique can assist us in identify new structures and contaminant interactions with aluminum, which may be useful in managing these wastes. This structural understanding helps us determine how aluminum will interact with other chemicals and elements, particularly in a nuclear waste setting.

Another waste stream associated with nuclear weapons production as a by-product of nuclear disarmament. These materials can often be recycled and reprocessed into fuel for nuclear energy production. However, the properties of such fuels are different than the original material required to make a nuclear weapon, and new techniques and methods must be developed to ensure the overall transformation process has occurred correctly. This requires analyzing the elements present in the original material, including radioactive ones because some need to be extracted to create the new fuel material. Appropriately analyzing these waste streams will help us manage these wastes in the future and assure adequate protection for human and environmental health.

TABLE OF CONTENTS

LIST OF FIGURES

LIST OF TABLES

LIST OF ABBREVIATIONS

2,6-NDS	2,6-Naphthalene Disulfonate (Disodium)
2,7-NDS	2,7-Naphthalene Disulfonate (Disodium)
Al_{13}^{k}	Aluminum 13 Keggin
Al_{13}^{f}	Aluminum 13 flat
ACS	American Chemical Society
CERCLA	Comprehensive Environmental Response, Compensation, and Liability Act
DEP	Department of Environmental Protection
DOE	Department of Energy (U.S.) or USDOE
EDTA	Ethylenediaminetetraacetic acid
EPA	Environmental Protection Agency (U.S.) or USEPA
FTIR	Fourier Transform Infrared Spectroscopy
HEDTA	N-(2-hydroxyethyl)-ethylenediaminetriacetic acid
IAEA	International Atomic Energy Agency
MOX	Mixed Oxide Nuclear Fuels
NORM	Naturally Occurring Radioactive Materials
NMR	Nuclear Magnetic Resonance
PXRD	Powder X-Ray Diffraction
ROI	Region of Interest
TOC	Table of Contents
TGA	Thermal Gravimetric Analysis
XRD	X-Ray Diffraction

CHAPTER 1. INTRODUCTION: ADVANCING THE CHEMISTRY OF ELEMENTS PERTAINING TO NORM AND NUCLEAR MATERIALS AND WASTES.

This Chapter is based on a book chapter to be submitted for publication in the American Chemical Society (ACS) Symposium Series: Old Elements, New Discoveries titled, "Advancing the chemistry of elements pertaining to NORM and nuclear materials/wastes." expected in 2017 by Eitrheim, E.S.; Knight, A.W.; Schultz, M.K.; Forbes, T.Z.; Nelson, A.W. The drafted publication has been adapted or augmented and some original material, including wording and figures, has remained intact.

1.1 Introduction

In 2012, the National Academy of Sciences released a report indicating that there were dwindling numbers of radiochemists and nuclear scientists graduating from U.S. graduate programs.[1] The numbers of radiochemists and nuclear scientists graduating from Ph.D. programs is particularly low and expected to be well below the demand by employers in the coming decade. In response to the low rate of Ph.D.-trained radiochemists, the University of Iowa launched an interdisciplinary radiochemistry program that included research and training in medical, environmental, and energy applications of radiochemistry.[2] I was a part of this program with research focusing on radiochemistry topics as they pertain to waste forms. In particular, my research focused on gallium (Ga) and plutonium (Pu) with applications in mixed-oxide (MOX) fuels, naturally occurring uranium-series radionuclides in the environment, and aluminum in nuclear wastes.

1.2 Plutonium Nuclear Materials and Applications in Nuclear Forensics

Plutonium (Pu) nuclear materials originated shortly after discovery of the element by Glenn T. Seaborg and colleagues in December of 1940.[3] This discovery was not initially announced due to the understanding that this new element had application in nuclear weapons technologies.[3] Plutonium was initially produced at the Hanford Site in Washington State using a nuclear reactor; most notably reactor B.[4] While production and isolation of gram quantities of Pu began almost immediately, additional materials engineering and processing was necessary to stabilize Pu for use in nuclear weapons.

One of the most important advancements in this area was the discovery of plutonium-gallium alloys during the Manhattan Project, which effectively stabilized the material for use in nuclear weapons.[5] Pure Pu has six allotropes and the thermodynamically stable phase at standard temperatures and pressures is the high density (19.86 g/cm^3) α-form. The lowest density phase is δ-Pu, which is approximately 25% less dense (16.0 g/cm^3) than the α-phase and can only be stabilized at temperatures between 310 and 425 ^{o}C. Super criticality is only reached through a compression based δ-α transformation, thus maintaining the δ-Pu material under standard conditions is crucial for the design of a functioning nuclear weapon. Creating a Pu alloy stabilizes the δ-phase at room temperature and this is typically achieved by adding ~0.8-1 mol% Ga to the Pu metal. Alloying Ga with Pu also improves the mechanical properties by decreasing corrosion rates, improving the ability to cast, and creating low thermal expansion properties leading to better material processing for nuclear material production.

Thousands of nuclear weapons have been created using Ga-Pu alloys, and consequently these materials pose a nonproliferation risk.[6] According to the International Atomic Energy

Agency (IAEA), eight incidences of theft or loss of plutonium-based nuclear materials has been reported globally, excluding Pu-based smoke detectors, from 1993 through 2015.[7] When the authorities confiscate these now-illicit Pu nuclear materials, identifying isotopic and elemental "signatures" linking them to their last legal owner, production location, facility, or method of production is considered crucial for accountability and legal prosecution.[8] As Pu used in weapons production has been alloyed with Ga, the elemental signature of interest is the Ga/Pu ratio because it unique to the specific to each specific production facility and can be used to pinpoint the initial material processing facility.

This method's usefulness goes beyond nuclear forensics applications and can also be valuable for nuclear energy-producing industries. Decommissioning of the nuclear arsenal has prompted the U.S. to start dismantling numerous nuclear weapons and using the Pu in in MOX (mixed-oxide) nuclear reactors.[9] MOX fuel is the mixture of plutonium and uranium oxides and can be used in place of the traditional isotopically-enriched uranium dioxide fuels. However, the initial alloy has significant amounts of Ga, which is incompatible with practical MOX fuel applications even in small quantities, because it can migrate from the fuel into the zirconium (Zr) cladding, making that cladding more brittle and subject to corrosion.[10-13] In order to down-blend these weapon pits for MOX applications, removal of Ga to approximately a 10^5 decontamination factor is needed to avoid these complications, requiring a final Ga concentration of 0.1 ppm within the solid oxide material.[14] To use MOX fuel from down-blended Pu-bearing nuclear materials in nuclear reactors, there is a need for advancements in separations technologies.

Several methods have been shown to effectively separate Ga and Pu in nuclear weapon pits for application as MOX fuel. For example, a separation of Pu and Ga by ion-exchange

chromatography was proposed by DeMuth at Los Alamos National Laboratory that uses aqueous-based ion-exchange chromatography.[15-16] This method focused on large scale separations instead of isotopic analysis, making it less applicable for nuclear forensics applications.[15-16] A second method utilized high-temperature thermal removal of gallium for industrial MOX fuel production and again focused on large quantities necessary in the nuclear energy industry.[17]

These methods were not designed for, nor are they suitable for, the analytical investigation of gallium, plutonium, or other candidate actinides of interest for nuclear forensics of MOX fuel analysis. In order to address this critical need, methodology was developed at the University of Iowa that provided analysis of various actinide elements and gallium within plutonium nuclear materials, such as nuclear weapon pits and MOX nuclear fuels. Developing a dependable, fast, and accurate analysis method for stable gallium in Pu nuclear materials could be a powerful tool for both nuclear forensics applications and nuclear energy-producing industries. Combining the analysis of Ga with the determination of isotopes of the actinides Pu, U, Th, and Am would increase the efficiency of nuclear forensics investigations.

Using extraction chromatography paired with isotope dilution techniques, a complete radiochemical separation of Ga, Pu, Am, U, and Th was developed for nuclear forensics applications of Pu-bearing nuclear materials.[18] Extraction chromatographic resins (TEVA and TRU Resins from Eichrom Technologies, LLC) were used to prepare elementally pure fractions for isotope analysis (FIGURE 1.1).[18] Preparing and separating samples for analysis requires an accurate and precise method that determines the yield of Ga, even though the complex matrix of Pu-bearing nuclear materials is a hindrance to the analysis of gallium concentrations. A notable contribution to developing these methods was the use of a nuclear medical radioisotope,

^{68}Ga, as an improved alternative to trace stable Ga yields in these separations.[18] Innovative medical radioisotopes, such as ^{68}Ga, are becoming for available and affordable due to recent advancements in their production and isolation.[19] Combining ideas from various areas of radiochemistry, such as nuclear medicine and nuclear forensics, can have substantial impacts on methodology development. Utilizing a medical radioisotope to provide stable gallium signatures in nuclear-forensics applications allows quick and accurate determination of Ga concentrations. The ^{68}Ga nuclear medical radiotracer allows precise, stable gallium determination without interfering with the separation and quantification of other isotopes of radioactive actinides.

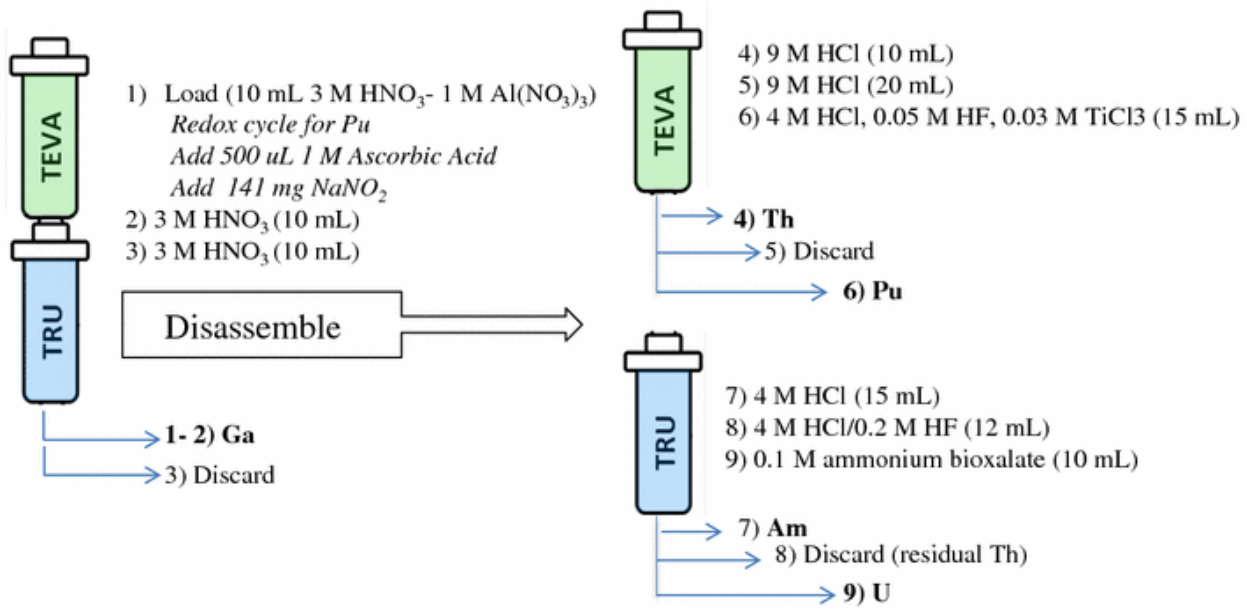

Figure 1.1 Tandem column arrangement of the TEVA/TRU developed for the separation and purification of stable Ga and radioactive isotopes of elements Th, Pu, Am, and U. The load and rinse solutions remove common ions and matrix interferences. The columns are then disassembled. Steps 4-6 (TEVA) may be run concurrently with steps 7-9 (TRU).[18]

1.3 Advancements in Separations and Nuclear Forensics Applications

Methods developed at the University of Iowa provide the separation and analysis of Ga, Pu, U, Th, and Am for the purpose of nuclear forensics and nuclear fuel analysis. Further advancements are needed, however, that include certification of the method for use on various

nuclear materials. This method's applications could potentially be extended into many types of nuclear materials (MOX fuels, Pu-Ga alloys, nuclear wastes), but verification is a crucial step in the process. Accessing nuclear materials is not trivial due to nonproliferation security controls; accessing nuclear materials for peaceful research and development is similarly challenging. Performing this separation on digested nuclear fuels (both pre and post burn-up) as well as Pu-nuclear weapon pits would allow for a more complete understanding of this method's strengths and limitations.

Additional quantification of Ga by ICP-MS would also be a useful improvement as these instruments become more widely used for analysis of trace-level metals. The use of ^{68}Ga as a radiotracer could be performed before the analysis of gallium by ICP-MS, and would likewise provide a precise quantification of the gallium present in a nuclear material. Certifying this method for ICP-MS analysis would widen the scope of sample analysis to include compounds like post-irradiation nuclear materials, which would have a dramatically more complex matrix, including fission products(e.g. ^{137}Cs, ^{90}Sr, ^{131}I, ^{85}Kr, ^{99}Tc, ^{151}Sm, ^{93}Zr, etc.) that complicate analysis of the sample by radiotracers.[20] Additional modifications to the method may be needed with the addition of fission products. For example, additional method verification would be required for various isobaric interferences, which could accompany fission products arising from post-burnup MOX fuels.

Overall, the use of extraction chromatography with the addition of a medical radioisotope tracer helped to advance our methods regarding Pu-bearing nuclear materials. This work highlights the importance of radiochemistry training programs within the university setting, where advancements in one field can be applied to other fields and students involved in

interdisciplinary programs can take advantage of a growing number of interesting isotopes used in a wide range of applications.

1.4 Concerns about Radioactivity in Liquid Waste from Hydraulic Fracturing

When the University of Iowa program launched in 2012, concerns about naturally occurring radium (Ra) isotopes in Marcellus Shale produced fluids had just begun to surface within the scientific community.[21-23] A group at the United States Geologic Survey (USGS) published a detailed study that illustrated the potential for ^{226}Ra and ^{228}Ra to concentrate in produced fluids and brines generated by hydraulic fracturing for natural gas in the Marcellus Shale formation.[21] This report raised numerous questions about radioactivity in hydraulic fracturing flowback water and produced fluids, such as the presence of naturally occurring radionuclides and environmental impacts of waste disposal. The USGS report was followed by a key study by Warner *et al*. (2013) that indicate the presence of high levels of Ra isotopes downstream of wastewater treatment plants handling Marcellus Shale produced fluids, suggesting that certain treatment plants were undertreating the radioactivity associated with these fluids[23]. After the Warner, *et al.* (2013) and USGS studies, it was clear that there were elevated levels of radioactivity in these fluids and that there was the potential for certain isotopes (^{226}Ra and ^{228}Ra) to contaminate the environment. Despite these two observations, there were no validated methods to detect and characterize radionuclides in hydraulic fracturing-produced fluids and brines. The problem presented by this lack of methodology was twofold: (1) without comprehensive methodology for alpha, beta, and gamma emitters, it was unclear whether other radioactive elements were present in the fluids, and (2) the radioactivity concentrations of reported Ra isotopes remained questionable.

1.5 Method Development

By the summer of 2013, the US Environmental Protection Agency (USEPA) had funded a project at the University of Iowa to develop and validate a method to detect gross alpha and beta particles in these fluids.[24] Development of the gross alpha and beta method required a technique that could isolate key radionuclides, including U, Th, Pa, Ra, Pb, Bi, and Po isotopes. Numerous methods to isolate these radionuclides in drinking water exist (e.g. EPA 900.0[25] & ASTM method #D7283[26]); however, these methods are intended for waters with low concentrations of dissolved solids. Water samples with higher levels of dissolved solids are generally unsuitable for a "gross alpha and beta" method due to 1) the need to remove interfering stable elements that would absorb or attenuate the ionizing radiation, and 2) the challenges of separating the numerous radionuclides from stable elements. The sample of Marcellus Shale produced fluids provided to the University of Iowa had exceptionally high concentrations of dissolved solids (~278,000 mg/L).[27] Furthermore, the fluids contained high levels of barium (Ba) salts (>9,000 mg/kg).[28]The problem with Ba for radiochemical separations is that Ba and Ra have very similar chemistry and often co-elute or co-precipitate during chemical separations.[28-31] The high levels of dissolved solids (in particular the high concentrations of Ba) suggested that a low-cost, rapid, practical separation of Ra from the Marcellus Shale fluids would not be possible. Given that Ra had been previously established as a key radionuclide in Marcellus Shale produced fluids and flowback,[21, 32] this suggested that a single gross alpha/beta method was impractical. Thus, we had to split the sample up to measure key alpha emitters (^{238}U, ^{234}U, ^{232}Th, ^{230}Th, ^{228}Th, ^{210}Po) by alpha spectrometry and key beta emitters by gamma spectrometry (^{228}Ac, ^{212}Bi, ^{212}Pb, ^{214}Pb, ^{214}Bi). Note that most key beta emitters of concern in this case also emitted gamma rays (ex: ^{210}Pb; 46

keV)[33]or had short-lived daughters that could be measured by gamma spectrometry, which would allow for modeling their activity (ex: ^{226}Ra released ^{214}Bi and ^{214}Pb).

1.6 Radiochemical Disequilibrium

During the development of the isotope-specific method, we discovered several interesting radiochemical parameters. First, we observed that U levels in the produced fluids were exceptionally low, suggesting that U was insoluble. This is to be expected given that the Marcellus Shale is a reducing zone, meaning that U would be found in the +4 valence state and immobile.[34] The second discovery was that ^{234}U radioactivity concentrations exceeded ^{238}U radioactivity concentrations. This result was surprising at first, given that a system as old as the Marcellus Shale is expected to be in secular equilibrium (meaning ^{238}U and ^{234}U should have the exact same radioactivity concentration; for further reading on radioactive equilibrium we recommend the following references:[35-37]). The discrepancy in radioactivity levels is believed to be attributed to a phenomenon known as alpha recoil enrichment, which results in higher-than-expected concentrations of decay products.[38-39] The third discovery was that Ra activities, as measured by chemical separations, were greatly underestimated. We attributed this discovery to Ba interference during chemical separations, which is further discussed in ESTL and EPSI.[27, 29] Lastly, and perhaps of greatest interest to us, was the apparent absence of ^{226}Ra decay products from the fluids.[40] Given the solubility of Pb in these fluids,[27] we expected ^{210}Pb to be detectable; however, models suggested that ^{210}Pb was absent at the time of extraction and thereby insoluble in the fluids. More studies are needed to fully understand for the chemical reasoning for the ^{210}Pb insolubility in these fluids, but we currently hypothesize that this is caused by the partitioning of ^{222}Rn gas.[41] The absence of ^{210}Po was expected due to the lack of its parent ^{210}Pb.

1.7 Radium Decay Products

As we were investigating the absence of ^{226}Ra decay products in these fluids, Warner *et al.* (2013) documented high levels of Ra isotopes downstream of a wastewater treatment facility processing Marcellus Shale produced fluids but the study did not address Ra decay products. To further explore the environmental transport and mobility of Ra decay products, particularly ^{210}Po and ^{210}Pb, we embarked on a year-long field study near Mannington, West Virginia.[42] Local citizens expressed concerns that the Northern West Virginia Water Treatment Facility was discharging undertreated Marcellus Shale waste into the Hibbs Reservoir. We later discovered through a Freedom of Information Act (FOIA) request that this facility only received coal wastes and that all documented discharges appeared in the range of issued permits.[43] Regardless, we saw this as a unique opportunity to investigate the fate and transport of ^{226}Ra decay products in the environment. After three sampling trips, we discovered that ^{210}Po radioactivity concentrations were approximately 2.3 ± 0.4 (n=12) fold greater than the parent ^{226}Ra.[42]In one sample, the ^{210}Po radioactivity concentration exceeded that of cleanup goals for surface sediments at USEPA CERCLA (Comprehensive Environmental Response, Compensation, and Liability Act of 1980) sites. We were hesitant to publish this result without an appropriate local control site, but many of the lakes in the surrounding area were impacted by oil and natural gas or coal extraction. Therefore, we sampled a lake at F.W. Kent State Park near Oxford, Iowa that was of similar size, but had no documented oil and natural gas or coal extraction in its watershed to serve as a control site.[44] We were shocked to discover that ^{210}Po exceeded ^{226}Ra concentrations by 2.8 ± 0.5 (n=5) at the Iowa site and that the activity concentration was very similar to what we observed at impacted Hibbs Reservoir in West Virginia. The only apparent

source of ^{210}Po for F.W. Kent Lake is background ^{222}Rn, suggesting that ^{210}Po accumulates in lakes in areas with high background ^{222}Rn.

1.8 Drill Cuttings

Although the bulk of discussion on radioactivity related to drilling activities in the Marcellus Shale has focused on liquid waste, we understood that all the radioactivity in liquid waste ultimately came from solids in the subsurface—i.e., the source rock necessarily containing the parents ^{238}U and ^{232}Th.[40] As we were finishing our research on liquid wastes, reports were emerging in popular press outlets that radioactivity levels in solid wastes were potentially at elevated and actionable levels. Specifically, several news sources noted that radioactivity alarms at landfills were activated by trucks carrying drill cuttings (solid waste).[45] These radioactivity alarms were characterized by dose rates, but did not define the radiochemical profile of the drill cuttings. In early 2014, we began efforts to obtain drill cuttings so that we could characterize the disequilibrium status of these cuttings, but were not able to obtain materials until a drilling company directly supplied us with them in late 2015. During this time, Pennsylvania and West Virginia released studies that characterized certain aspects of these drill cuttings (gamma spectrometry-based results); however, the cuttings' radiochemical profiles were not released due to a lack of methodology for alpha spectrometry.

Thus, we saw a critical need to develop methodologies for examining these materials and distribute these methods to other researchers through the peer-reviewed process. Due to the chemical characteristics and high organic content of the cuttings, we tailored these methods from techniques previously developed for asphalt. The method development process is described further in Eitrheim *et al.* (2016).[41] The most interesting aspect of the study is that ^{226}Ra decay

products were in disequilibrium with the supporting parent radionuclides. This continual trend of $^{238}U/^{210}Po$ disequilibrium in environmental radioactivity measurement raises several questions: Where is ^{210}Po going?; How is it getting there?; What are the health implications of ^{210}Po exposure? The following section of this chapter will explore these questions regarding the fate, transport, and health implications of ^{210}Po exposure.

1.9 Aluminum in Nuclear Wastes

Upon the development of the radiochemistry program at the University of Iowa, other projects emerged as being relevant to radiochemistry-related fields. Improvements in the analysis and fundamental understanding of metal hydroxide and oxide chemistry is an important area of study because of its importance as a waste matrix for nuclear materials. Metal oxides and hydroxides, in particularly Al and Fe, are present in numerous waste streams, including that of nuclear weapons production. Notably, the Hanford Site in Washington State, U.S., is the home of the first full-scale plutonium (Pu) production facility for nuclear-weapons purposes.[4, 46] To create the Pu metal needed for nuclear weapons, significant separation and purification processes were utilized that produced a large amount of nuclear waste. Al was an integral part of this purification process, which produced a mixed nuclear waste that included large amounts of Al.

Waste streams from the production of Pu metal were consolidated and stored in large underground tanks at the Hanford Site. Initial estimates of the waste at the site suggests that 53 million US gallons of highly radioactive liquid are stored in these tanks in a slurry form. Al and Na are found in molar quantities. Polycarboxylates, such as EDTA and HEDTA were utilized in the separation process and are also observed in the waste form. Radiolysis of these organic

molecules results in the breakdown of these large ligands into more simple forms. Some of the most important by-products of these larger chelating ligands, which are smaller carboxylate and phosphate containing organic compounds.

The large volume of wastes produced at the Hanford site required the development of large liquid-storage tanks. These tanks were initially built in the 1940's – 1980's and continue to house material. These tanks have recently come under scrutiny due to corrosion and subsequent leaks of highly radioactive materials. This has made additional reprocessing and removal of the waste a high priority, but the protocols have been significantly hampered by the high levels of Al in the waste stream. Aluminum precipitates upon transfer and/or treatment of this liquid waste, causing clogging in filters, pipes, and ion-exchange resins.[47] Current strategies designed to clean up some of this nuclear waste involve very large amounts of sodium or lithium hydroxide to ensure complete dissolution of Al before involving a separation process that currently requires 5M sodium cations (Na+), which is impractical and costly.[47] Given the complexity of the waste forms, predicting the formation of the Al precipitate and then developing protocols to deal with the solid phase is challenging. Probing into the basic Al chemistry in the presence of various anions and organic ligands can help elucidate the fundamental properties of Al in complex waste systems and provide more effective and inexpensive methods for treating these wastes without requiring large quantities of chemicals.

1.10 Aluminum in Environmental Wastes

Aluminum is not only a concern in nuclear wastes, but can also enter aqueous environments through the dissolution of natural Al minerals in soils. Once in an aqueous environment, the chemistry and speciation of Al is vague although a slow increase in our

understanding is currently taking place. Aluminum can complex with organic compounds as well as metals, and these complexes can be influenced by a variety of factors, including pH, ionic strength, temperature, presence of anions and cations, and more. This makes it relatively difficult to gain well-defined insight into their function and speciation in the environment.

To further interfere with our understanding, Al readily forms oxy-hydroxy polyaluminum species through hydrolysis, referred to as "clusters". These complexes exhibit different chemical characteristics, notably in their ability to complex with environmentally persistent organic and inorganic ligands. Understanding Al chemistry is, therefore, critical for our complete understanding of the fate and transport of not only aluminum, but its complexants. A molecular understanding of these systems is needed, including their mechanisms of formation, aggregation, complexation, phase formation, and nucleation. An understanding of the various factors that may influence their speciation is also needed. While aluminum hydrolysis and polymerization in aqueous systems has been studied extensively, the relevant mechanisms and intermediates are still not well clarified.

One of these ways that Al enters the environment is by acid mine drainage, which dissolves some aluminum minerals under acidic conditions. Acid mine drainage allows some solubility and mobility of Al, and in turn of other heavy metals, including radiometals, that have the potential for transportation via adsorption on Al clusters created under these conditions.[48] Understanding aluminum and its speciation, mechanisms of formation, and complexation with contaminants, can better aid our understanding and ability to clean up wastes in situations such as acid mine drainage.

Aluminum-containing wastes are also produced in the Bayer process, which is used to separate Aluminum from ores such as bauxite to produce alumina.[49] This process uses basic conditions and separates Al from mainly iron (Fe) minerals. This process, as in many other industrial chemical processes, is subject to error and environmental contamination. One such example is the Ajka alumina plant accident in Hungary (2010), in which a reservoir break released about one million cubic meters of liquid waste, flooding local villages and affecting 40 square kilometers.[50] This waste eventually made it to the Danube River, three days after killing all life in the Marcal River, the Danube tributary that accommodated the alumina plant. Fe and Al were both present in pronounced quantities, though these elements tend to remain benign to both environmental and human health. The heavy metals that were released, including arsenic (As) and chromium (Cr), were not considered dangerous to the environment, mostly due to their low solubility and high adsorption.[51] These metals will now be present in environments where Fe and Al species are ubiquitous, and the chemistry associated with these heavy metals, including their ultimate fate and transport, could give long-term insight into this and other spills' effects. Identifying the potential aluminum species present, along with their propensity to bind to other naturally occurring complexants, could also provide a model for how some of these interactions might occur. One useful model system could be an isolated aluminum cluster found under similar conditions. Overall, numerous waste and environmental systems would benefit from a better understanding of Al chemistry to potentially allow better treatment of these wastes, and projects in the radiochemistry program at the University of Iowa have started to address these issues.

1.11 Conclusions

As discussed above, the forecasted shortage of radiochemists and radiochemistry graduate programs led to the development of curriculum and expertise at University of Iowa. The first cohort of radiochemistry students focused on Ga and Pu with applications in MOX fuels and naturally occurring uranium-series radionuclides in the environment. Advancing the complete separation of gallium and actinides in nuclear materials for nuclear forensics applications was accomplished yet developments regarding ICP-MS and certification of these methods is still needed. Research in uranium-series radionuclides highlighted the importance of sound methodology and comprehensive analysis of decay products, including ^{210}Po. From our observations of ^{210}Po in aqueous environments, we have begun to probe deeper into the geochemical cycling of ^{210}Po in the Upper Midwest. The newest developments regarding this program involve critical Aluminum chemistry research for applications in advancing our understanding in waste systems. Overall, the University of Iowa Radiochemistry program has contributed to the understanding of these various elements. There is high hope that radiochemistry advancements will continue to contribute to future discoveries regarding elements and their chemistry. This thesis will address many of the issues outlined in this chapter, including those associated with wastes pertaining to NORM and the nuclear fuel cycle, as well as some current research advancements.

1.12 Outline of Thesis

The overall goal of this research is to provide a better understanding of the basic chemistry of a range of radioactive materials and waste forms. The overall research questions are outlined below and a short description of the related work is provided.

Chapter 1 (this chapter) details the projects have tended to focus on nuclear forensics and radiochemical characterization of wastes.

Chapter 2 explores a new method developed for the separation of gallium and plutonium for nuclear forensics applications. This method could also have applications in certifying Pu-containing nuclear fuels that have been recycled from nuclear weapon cores that are now considered wastes.

Chapter 3 presents a detailed radiochemical characterization of solid drill cutting associated with hydraulic fracturing conducted by the oil and gas industries. This includes a brief analysis for potential leachability of these radionuclides in a landfill setting.

Chapter 4 outlines a new method for the synthesis and isolation of an elusive aluminum octamer that may be an important species in aqueous conditions, potentially even in wastes such as those occurring in acid mine drainage and nuclear wastes.

Chapter 5 details three new Al30 clusters with various contaminants adsorbed to their surfaces. This chapter shows that speciation changes in complex mixtures, such as nuclear wastes. A better understanding of these processes of adsorption and speciation could improve knowledge of Al chemistry, allowing better methods for managing Al-rich nuclear wastes such as those at the Hanford Site.

Chapter 6 provides concluding remarks regarding each chapter and future research directions for these projects.

CHAPTER 2. SEPARATION OF GALLIUM AND ACTINIDES IN PLUTONIUM NUCLEAR MATERIALS BY EXTRACTION CHROMATOGRAPHY

This Chapter is based on a publication in the Journal of Radioanalytical and Nuclear Chemistry (J. Radioanal. Nucl. Chem.) titled, "Separation of Gallium and Actinides in Plutonium Nuclear Materials by Extraction Chromatography" in 2015 by Eitrheim, E.S.; Knight, A.W; Nelson, A.W.; Schultz, M.K. The publication has been adapted or augmented and some original material, including wording and figures, has remained intact. The TOC image at the beginning of the chapter depicts a replica of Fat Man, the plutonium-containing nuclear weapon that was exploded on Nagasaki, Japan on August 9, 1945. TOC photo courtesy of the National Archives and An illustrated guide to the Atomic Bombs by Ryan Crierie. The citation for the original journal article is shown here:

J. Radioanal. Nucl. Chem., 2015, *303* (1), pp 123–130

DOI: 10.1007/s10967-014-3310-z

Publication Date (Web): July 27, 2014

Copyright © 2015 Springer

Keywords: gallium; plutonium; radiochemistry; gallium-68; nuclear forensics; nuclear fuel

2.1 Abstract

Analysis of stable gallium in nuclear materials has applications in nuclear fuel characterization and nuclear forensics. The use of positron-emitting gallium isotope ^{68}Ga as a tracer for Ga recoveries for analyses in materials containing actinides was explored. A radiochemical method for the separation of Ga, Pu, U, Th, and Am using commercially-available extraction chromatography resins was developed and evaluated. The method effectively allows precise determination of Ga yield (97±3%) in the analysis of stable Ga (spike recovery 101±1%) and radioactive Pu (radiochemical yield, 82±10%; spike recovery, 96±3%), while also providing

pure elemental fractions of other actinides relevant to materials encountered in the analysis Pu-containing materials.

2.2 Introduction

Determination of the concentration of gallium (Ga) metal in Pu-bearing nuclear materials is recognized as an important analytical parameter of interest to the nuclear power industry and for nuclear forensic analysis of materials.[5, 52-57] For nuclear forensic analysis of suspect plutonium-containing materials, the value of this parameter arises from the use of Ga as an alloy constituent to impart properties to Pu metal that render the material suitable for fabrication of precisely-engineered weapons related devices.[5] For example, so-called Pu "pits" originating from the Manhattan project in the United States, were alloyed with Ga metal primarily to stabilize the δ-phase crystal-structure of Pu metal.[53] The δ-phase of Pu metal is favored for this application because it is the least dense; is the most easily machined; and Pu alloyed with Ga is also highly stable to corrosion.[5] While at standard pressure the δ-phase of pure Pu must be maintained above 310^{o}C to remain stable, suitably fabricated Ga-bearing Pu alloys (3.0-3.5 mol% Ga) preserve the appropriate crystal structure at room temperature.[5, 53] Because the precise Ga/Pu ratio is likely to vary depending on the location and specific fabrication technology applied, the Ga/Pu ratio represents a potential signature that could be used in nuclear forensic analysis of materials.

For nuclear fuel analysis applications, stable Ga is recognized as an important constituent of mixed oxide nuclear fuels (MOX). In this case however, Ga represents a contaminant that is known to migrate from within the MOX fuel matrix and infiltrate surrounding zirconium-based cladding materials. Diffusion of Ga into the Zr cladding causes degradation of its metallic

properties by corrosion and embrittlement.[57] Thus, an upper limit of Ga concentration in MOX fuel must be set to ensure that the integrity of the Zr-based fuel cladding is not compromised. In the United States, the MOX Fuel Fabrication Facility has set a final MOX fuel quality control limit of 0.1 ppm (0.1µg Ga/g Pu), a 10^5 decontamination factor from weapons-grade plutonium.[14]

The above observations establish a need for the development of highly accurate and precise approaches to the analysis of Ga metal for applications in nuclear forensics and in the nuclear fuel cycle. A significant challenge to accurate assessment of the gallium content (and Ga/Pu ratio) in complex matrices for material characterization is a precise method for determination of Ga yield through sample preparation and chemical separations procedures. Previous method development for the analysis of actinides and metal impurities in Pu materials by ion-exchange combined with mass spectrometric techniques in the absence of a yield monitors proved problematic for some metals and for the analysis of U and Th.[55] Previous methods specifically designed for the analysis of stable Ga in these materials have employed radiometric determination of Ga chemical yield using gamma-emitting radionuclide ^{68}Ga.[52] However, no readily-available commercial source of this radionuclide is available and manufacturing requires reactor facilities with high neutron flux capabilities.[52] In addition, previous methods involved the use of cumbersome liquid-liquid extraction techniques, which can potentially involve large volumes of radioactive organic solvent waste.[52] On the other hand, the use of positron emitter ^{68}Ga is on the rise for medical applications and the availability of commercial ^{68}Ga generators is expanding commercially from several sources.[19] Thus, ^{68}Ga is a promising alternative for yield monitoring of the analysis of complex Pu-bearing materials where the chemical yield is required for an accurate determination of stable Ga concentration. Further,

extraction chromatography methods have the potential to provide excellent radiochemical separation performance, while reducing the generation of radioactive organic waste. Within this context, we are exploring the use of positron-emitting Ga isotope ^{68}Ga as a tracer for Ga recoveries for analysis of Ga/Pu ratios in materials containing actinides and other metals. Here, we present a complete radiochemical method for the separation and analysis of Ga, Pu, U, Th, and Am using extraction chromatography resins TEVA and TRU. The method effectively allows precise determination of Ga yield in the analysis of stable Ga and radioactive Pu, while also providing pure elemental fractions of other actinides relevant to materials encountered in the analysis Pu containing materials.

2.3 Experimental

All reagents employed were ACS grade or higher. Radiotracers were prepared in Aristar Ultra (Sigma-Aldrich) nitric acid (HNO_3, metals grade, certified to parts per trillion metal, PPT, purity), which had been diluted to working concentrations using ultra-pure distilled-deionized water of similar certified metal content (Baseline®, Seastar Chemicals, British Columbia, Canada). Tracers were prepared from Standard Reference Materials (SRM's) obtained from the United States (USA) National Institute of Standards and Technology (NIST, Gaithersburg, MD USA) or from NIST-traceable certified reference materials (CRM's, Eckert Ziegler Radioisotopes, Atlanta, GA USA). Tracers were stored in Teflon bottles purchased from Seastar Chemicals, which are certified to ultra-low metal content (PPT). Tracers were prepared within six months of studies presented here and tracer solutions (in Teflon bottles) were further double-sealed in plastic bottles and stored at 5°C continuously to minimize potential evaporation effects. Acids and salts used for radiochemical separations included: nitric acid (HNO_3); hydrochloric acid (HCl);

hydrofluoric acid (HF); sulfuric acid (H_2SO_4); titanium trichloride ($TiCl_3$); ascorbic acid; sodium nitrite ($NaNO_2$); aluminum nitrate ($Al(NO_3)_3$); and ammonium bioxalate [$(NH_4)_2C_2O_4$]); and were ACS reagent grade purity (Fischer Scientific) or higher. Chemicals used for electrodeposition (sodium sulfate, Na_2SO_4; sodium bisulfate, $NaHSO_4$; potassium hydroxide, KOH; ammonium hydroxide, NH_4OH) were reagent grade (Fisher Scientific). Rare-earth fluoride alpha particle counting sources were prepared using stable cerium (Ce) obtained in the chloride form from High Purity Standards (Charleston, SC USA), precipitated with hydrofluoric acid (HF). Half-lives and alpha-particle emission energies stated are values originating from the Evaluated Nuclear Structure Data File (ENSDF) and were obtained through United States National Nuclear Data Center (NNDC, Brookhaven National Laboratory, US Department of Energy, www.nndc.bnl.gov).[33] Unless otherwise stated explicitly, all uncertainties cited are "standard uncertainties," corresponding to a one-uncertainty interval.

2.3.1 Radiotracers

The isotopic tracers for this study were ^{242}Pu ($t_{1/2}$= 3.73x10^4 y), ^{243}Am ($t_{1/2}$=7370 y), ^{232}U ($t_{1/2}$= 69 y), ^{228}Th ($t_{1/2}$= 1.9 y), and ^{68}Ga ($t_{1/2}$= 68 m). The ^{242}Pu tracer (NIST SRM 4334I) and the ^{243}Am tracer (NIST SRM 4332E) were used for quantification of ^{239}Pu and ^{241}Am radionuclide quality control standards by isotope dilution techniques. The ^{232}U tracer (Eckert and Ziegler CRM 92403) and daughter ^{228}Th (certified to be in radioactive equilibrium) were used to quantify the natural U and Th quality control standards in the same manner.[54] ^{68}Ga tracer was eluted from a $^{68}Ga/^{68}Ge$ generator (Eckert and Ziegler Model # IGG100-30M, Reference Date 6 July 2010, ^{68}Ge activity: 1.11 GBq) composed of a borosilicate glass column containing a titanium dioxide bed on

which ^{68}Ge ($t_{1/2}$= 270.8 d) is absorbed. Gallium-68 was eluted and preconcentrated according to routine methods presented by us previously.[19]

Radioactive standard solutions were prepared from the 5 mL flame sealed glass ampoule by serial dilutions, performed volumetrically with gravimetric and radiometric confirmations. Dilution factors for the Pu, Am, U, and Th isotopes were 5 and 500 in 1.0 M Aristar Ultra HNO_3 (Am, U/Th) and 3.0 M Aristar Ultra HNO_3 (Pu). Dilution factors were verified by liquid scintillation counting (LSC) and α-spectrometry to within 2% of the calculated gravimetrically-derived dilution factors for each actinide radiotracer analyzed (Data not shown).

Other radionuclides were selected to simulate the analyte for evaluating the effectiveness of this separation method. For this purpose, natural Uranium (U-NAT), ^{230}Th, ^{239}Pu, and ^{241}Am were obtained, diluted, verified, and stored in the same way as the radiotracers above. The U-NAT standard solutions (Eckert Ziegler CRM 92564) contains Uranium isotopes ^{238}U ($t_{1/2}$= $4.5x10^9$ y), ^{235}U ($t_{1/2}$= $7.0x10^8$ y), and ^{234}U ($t_{1/2}$= $2.5x10^5$ y) in natural abundance.[58] The ^{230}Th ($t_{1/2}$= $7.5x10^4$ y), ^{241}Am ($t_{1/2}$=432.6 y), and ^{239}Pu ($t_{1/2}$=24,100 y) standards were obtained from NIST (SRM 4342A, SRM 4322C, and SRM 4330C, respectively). A certified liquid standard (Lot # 1114303; 1 mg/mL) of stable Ga (High Purity Standards, Charleston, SC) was used to evaluate the use of isotope dilution techniques to quantify stable Ga.

2.3.2 Chemical Separations

The analytical method described here was developed using extraction chromatography resins TEVA and TRU (Eichrom Technologies, Lyle, IL USA), which were obtained in pre-filled (1 mL bed volume) vacuum-ready cartridges from the manufacturer. Each resin is made up of an organic compound adsorbed to a solid-phase support resin bead consisting of Amberchrom CG-

71. The TEVA resin, which has been previously investigated, comprises adsorbed quaternary functionalized ammonium salts as the organic phase with aliphatic chains of two different lengths (n=8, N-methyl-N,N-diocyloctan-1-ammonium chloride; n=10, N-methyl-N,N-didecyldecan-1-ammonium chloride), and is commonly referred to as Aliquot-336.[59] The TRU resin is based on an extraction technology consisting of octylphenyl-N,N-di-isobutyl carbamoylphosphine oxide (abbreviated CMPO; N,N-bis(2-methylpropyl)-1-oxo-2-phenyl-2-phosphanyldecan-1-amine oxide) dissolved in tributyl phosphate (TBP) and was originally developed to extract all actinides from complex matrices.[60-61] These chromatography columns containing the resins were attached in tandem with a 25 mL reservoir (AC-120, Eichrom) integrated with the top cartridge.

Tracer and control standard aliquots for separation experiments presented here were delivered by volume (30-700 µL) to provide nominally equivalent radioactivity levels for tracer and analyte (control standard) using pipets that are tested routinely by gravimetric determination for accuracy and precision. Activities delivered for each separation experiment presented were: $^{232}U/^{228}Th$, 1.0 Bq; U-NAT, 2.3 Bq; ^{230}Th, 1.0 Bq; ^{241}Am, 1.1 Bq; ^{243}Am, 1.1 Bq; ^{242}Pu, 1.0 Bq; ^{239}Pu, 1.0 Bq. Additionally, 37 MBq of ^{68}Ga was used to trace for 200 µg (10 ppm) stable Ga. For experiments presented here, tracer solutions were combined and the starting solutions were adjusted to 3 M Nitric Acid - 1 M Aluminum Nitrate ($Al(NO_3)_3$).[62-63] The tandem TEVA-TRU cartridge setup was preconditioned with a 3 M Nitric Acid, 1 M $Al(NO_3)_3$ solution (10 mL) prior to the commencement of each separation experiment.

2.3.3 Source Preparation

Instrumental methods employed for these studies were carried out via α-spectrometry, γ-spectrometry, and inductively coupled plasma-atomic emission spectroscopy (ICP-AES).

Sources analyzed by α-spectrometry were prepared by routine cerium flouride (CeF_3) microprecipitation (Am, Pu, Th) or electrodeposition (U) techniques described previously.[63-65] Briefly, for microprecipitation, elemental fractions were collected in 50 mL centrifuge tubes. To each tube was added 50 µL 1.00 M cerium solution (50 µg Ce), followed by 2 mL concentrated HF. After 10 minutes, the solution was passed through a 25 mm diameter, 0.1 µm filter (Omnipore) using a polysulfone funnel (Pall). The centrifuge tube, funnel, and filter were rinsed with water (3 x 5 mL), followed by an ethanol rinse to promote drying, and the filters were removed, dried in an oven at 50°C for 1 hour, then fixed to a 25 mm diameter stainless-steel self-adhesive planchette (AF Murphy, Quincy, MA USA).

The U fraction was taken to dryness on a hotplate and redissolved in a buffer containing 5 mL 15% Na_2SO_4, 2.5 mL 5% $NaHSO_4$, and 2 mL of H_2O. The contents were transferred to plastic electrodeposition cells, which have been fitted with a stainless steel planchette (19 mm outer diameter, AF Murphy, Quincy, MA USA), with 3 rinses of 1 mL of H_2O. Once the module was assembled, a platinum electrode was inserted and the current was adjusted to 0.5 amps for 5 minutes, and then kept at constant current (0.75 amps) for 90 minutes using a commercially-available electrodeposition module (EP-4, Phoenix Scientific Sales, Roswell, GA USA). To terminate the deposition, 2 mL of 25% KOH was added (dropwise) with constant current for 1 minute, followed by removal of the current and discarding of the solution. A final rinse of the inside wall of the cell was performed with 5% NH_4OH. The planchets were then removed from the cell and rinsed with minimal volumes of NH_4OH, ethanol, and acetone to clean and dry the counting source. Once dry, the sources could be analyzed by alpha- spectrometry.

2.3.4 Source Counting by Alpha Spectrometry

Elemental sources for alpha spectral analysis of Am, Pu, Th, and U were counted in vacuum-controlled alpha spectrometry chambers (Alpha Analyst, Canberra, Meridan, CT USA) equipped with 450 mm^2 passivated ion-implanted silicon (PIPS, Canberra) detectors, with a source-to-detector distance of about 10 mm, representing a counting efficiency of approximately 18%. Detector efficiencies used to determine tracer yields were obtained using NIST traceable multiline alpha spec standard sources (Canberra) and an internal ^{230}Th standard source prepared by careful application of the CeF_3 microprecipitation and electrodeposition techniques. Quantitative isotopic microprecipitation and electrodeposition of the ^{230}Th source prepared in our laboratory was confirmed by analysis of the supernatant solutions following CeF_3 source preparation and the electrodepostion buffer. No evidence of residual ^{230}Th was observed in counting these validation sources for several days by alpha spectrometry (data not shown). Daughter recoil contamination of solid state alpha detectors was prevented using thin-films prepared and applied as described by us previously.[66] Sufficient counts in the region of interest (ROI) for tracer and analyte peaks were generally achieved with a 24 hour count time and appropriate matched-count-time ROI background corrections were applied.

2.3.5 Gallium-68 yield Determination by Ionization Chamber Measurement

^{68}Ga activities were determined using a well-type ionization chamber (CRC-15R, Capintec, Inc., NJ USA, often referred to as a radionuclide calibrator) by inserting the eluted ^{68}Ga fractions (contained in standard 20 mL liquid scintillation counting vials) directly into the well of the instrument. The manufacturer's calibration dial setting was used for ^{68}Ga activity measurements according to manufacturer's recommendation.

2.3.6 Quantification of Stable Ga with ICP-OES by Isotope Dilution

The quantification of stable Ga was performed using a Varian Inductively Coupled Plasma Optical Emission Spectrometer (ICP-OES; Palo Alto, CA). For these analyses, the Ga fraction (following radiochemical separations) was allowed to stand approximately 5 hours, after radiometric yield determination of ^{68}Ga using the ionization chamber, to ensure that the level of radioactivity was negligible. The ICP-OES was purged with ultra high purity argon (Praxair; Danbury, CT) and the torch was ignited. The analysis protocol consisted of a calibration curve with 3 standards (5 ppm, 10 ppm, and 20 ppm) with a blank of the same chemical matrix using emission wavelengths 250.019, 287.423, 294.363, 294.418, and 417.204 nm. Once the calibration was accepted, the stable Ga eluted from the columns was quantified. To determine the overall spike recovery, the concentration of stable Ga determined from the ICP-OES measurement was divided by the radiochemical yield of ^{68}Ga.

2.4 Results and Discussion

The primary objective of the proposed investigation was to determine the feasibility of the use of radioisotope ^{68}Ga as a yield tracer for the analysis of stable Ga in complex matrixes containing actinides. A yield tracer enables accurate determination of stable Ga where the matrix under investigation requires multiple wet chemical and radiochemical preconcentration and separation steps. Previous methods for stable Ga analysis have employed radionuclide ^{72}Ga for yield monitoring. While ^{72}Ga is recognized as an acceptable radionuclide for application of the isotope dilution approach, there is no commercial manufacturer and a reactor with high neutron flux irradiation capabilities is required for preparation of ^{72}Ga standards.[52] On the other hand, multiple manufacturers of ^{68}Ga generators are emerging and the availability of ^{68}Ga continues to

increase.[19] Further, the half-life of ^{68}Ga (68 m) is favorable compared to ^{72}Ga (14 h) for this application; allowing for radiometric yield determination and decay to near background within 5 hours prior to transfer of the Ga fraction to a non-radioactive measurement facility. Within this context, we employed a method based on previously published approaches to efficiently isolate elementally-pure fractions of U, Th, Pu, Am, and Ga using a tandem arrangement of commercially-available extraction chromatography resins (TEVA and TRU, **Figure 2.1**).

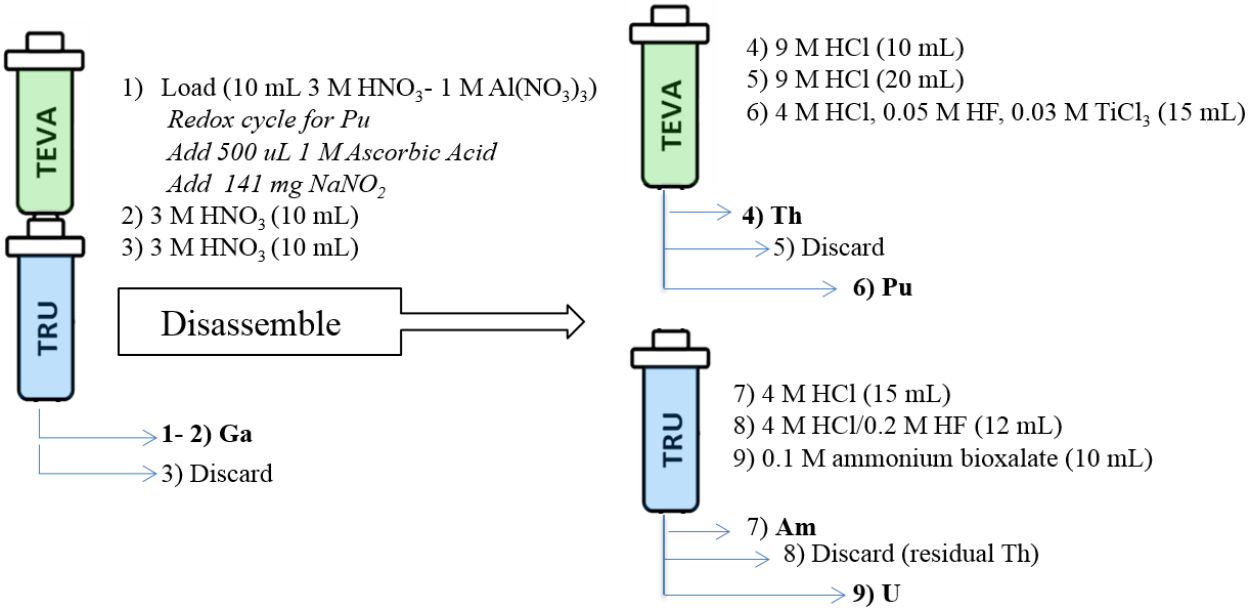

Figure 2.1 Tandem column arrangement of the TEVA/TRU developed for the separation and purification of stable Ga and radioactive isotopes of elements Th, Pu, Am, and U. The load and rinse solution remove common ions and matrix interferences. The columns are then disassembled. Steps 4-6 (TEVA) may be run concurrently with steps 7-9 (TRU).

The use of ^{68}Ga as a radioisotopic tracer for the determination of stable Ga is desirable because the positron emission provides easily measured 511 keV gamma rays for direct measurement by ion chamber. In addition, because the half-life of ^{68}Ga is relatively short (68 min.), the sample can be measured for yield determination and then allowed to decay to baseline levels rapidly prior to determination of non-radioactive constituents by mass spectral or other analytical-instrumental methods. One potential drawback of the use of ^{68}Ga for this application is that stable decay product zinc-68 (^{68}Zn) represents a potential isobaric interference in later mass spectral determination of stable Ga (^{69}Ga and ^{71}Ga). However, our estimates of this contribution are negligible within the range of activity required for a yield determination. For example, for our investigation, approximately 37 MBq of ^{68}Ga (at the time of elution of the generator) was used to study the elution behavior of Ga. While smaller amounts of ^{68}Ga could be used to establish a yield determination, this level of ^{68}Ga radioactivity represents approximately 25 pg of ^{68}Ga, which we expect is sufficiently low to allow for accurate determination of stable Ga without contributing significantly to an interfering signal via Zn hydride formation of ^{68}Ga daughter ^{68}Zn. Further, for our measurements by OES, isobaric interferences do not represent an impurity that will result in measurement interference.

Table 2.1 Elution profile of ^{68}Ga at the load and rinse steps (3 M HNO_3) of the developed procedure. 68Ga passes directly through the TEVA/TRU tandem column arrangement (Fig. 2.1) and is recovered quantitatively in the load and rinse steps. The use of ^{68}Ga as an isotope dilution tracer allows for corrections to be made in the dissolution and concentration steps in the analysis of Pu containing materials.

Step	Trial 1 Recovery (%)	Trial 2 Recovery (%)	Trial 3 Recovery (%)
Load (10 mL)	78	85	79
Rinse 1 (5 mL)	18	14	16
Rinse 2 (5 mL)	0	1	0
Rinse 3 (5 mL)	0	0	0
Total Activity	**96**	**100**	**95**

The separation method is based on previously published approaches to separations of actinides using TEVA and TRU resins.[60-62] The method involves an initial column load [10 mL 3 M HNO_3-1 M $Al(NO_3)_3$] and rinse (10 mL 3 M HNO_3) sequence, which effectively separates Ga from the constituent actinides, followed by separation of the columns for an efficient isolation of Th/Pu on TEVA and Am/U on TRU (**Figure 2.1**). Analysis of the elution behavior of Ga (based on ion chamber measurements of ^{68}Ga and verified by ICP-OES analysis of stable Ga) demonstrates that Ga is quantitatively collected by passing the load solution and one to two rinses of 3 M HNO_3 (**Table 2.1**). The average total recovery of ^{68}Ga measured in this way was 97$\pm$3% of the expected known total activity of ^{68}Ga. The spike recovery of stable Ga observed was 101± 1%, while also providing pure elemental fractions of other actinides relevant to materials encountered in the analysis Pu-containing materials (**Figure 2.1**; **Table 2.2**). These results suggest that ^{68}Ga is a promising tracer for stable Ga in the analysis of complex mixtures of actinides, including Pu.

Table 2.2 Radiochemical yield, control spike recovery, and alpha spectral resolution obtained using the tandem TEVA/TRU column arrangement (Figure 2.1) in the analysis of spiked aqueous samples prepared to evaluate the method for analysis of Ga in mixed actinide matrices. Alpha sources were prepared by cerium fluoride microprecipitation. Radiochemical yield of U was lower than expected, but can be attributed to losses at the source preparation step.

Element	Radiochemical Yield (%)	Spike Recovery (%)	Resolution (keV)
U	63 ± 12	101 ± 5	63 ± 12
Th	109 ± 6	101 ± 2	42 ± 5
Pu	82 ± 10	96 ± 3	51 ± 7
Am	94 ± 12	92 ± 4	46 ± 6
Ga	97 ± 3	101 ± 1	N/A

Table 2.3 Analytes, Radiotracers, and Methods of Detection

Element	Analyte	Tracer used	Method of detection
Ga	Stable Ga (Ga-69, Ga-71)	Ga-68	Ionization Chamber
Pu	Pu-239	Pu-242	Isotope dilution alpha spectrometry
Th	Th-230	Th-228	
U	U-Nat: U-238, U-235, U-234	U-232	
Am	Am-241	Am-243	

Experiments were conducted also to evaluate the radiochemical yield, control spike recovery, and achievable alpha spectral peak resolution (measured at full width at half maximum amplitude, FWHM of alpha peaks) with the use of the tandem column arrangement for the analysis of Am, Pu, Th, U and stable Ga (via ^{68}Ga; **Figure 2.1**; **Table 2.2**; **Table 2.3**). Radiochemical yields for the actinides were excellent for Am, Pu, and Th using the method as described in Figure 1. A somewhat lower yield for U may reflect mass-loading effects at the column step due to the level of natural U added with ^{232}U tracer for the evaluation or at the CeF_3 source preparation step and optimizing these parameters is part of ongoing methods development in our laboratories. The isotope dilution approach was employed to measure the activities of control spike activities in these experiments for Am, Pu, Th, and U – achieving excellent radiochemical control spike recoveries for all actinides. Acceptable alpha peak resolution was achieved for all actinides, with baseline peak separation observed for Pu, Th, and U alpha sources (**Figures 2.2-2.4**), while a slight amount of overlap of the ^{241}Am and ^{243}Am full energy peaks was observed for Am sources (**Figure 2.5**). While it is understood that increasing the source to detector distance could be an effective approach to improving the peak separation for Am source activity determinations, the slight peak overlap was considered acceptable for our initial evaluation of the use of ^{68}Ga for stable Ga recovery monitoring in samples containing multiple actinide analytes.

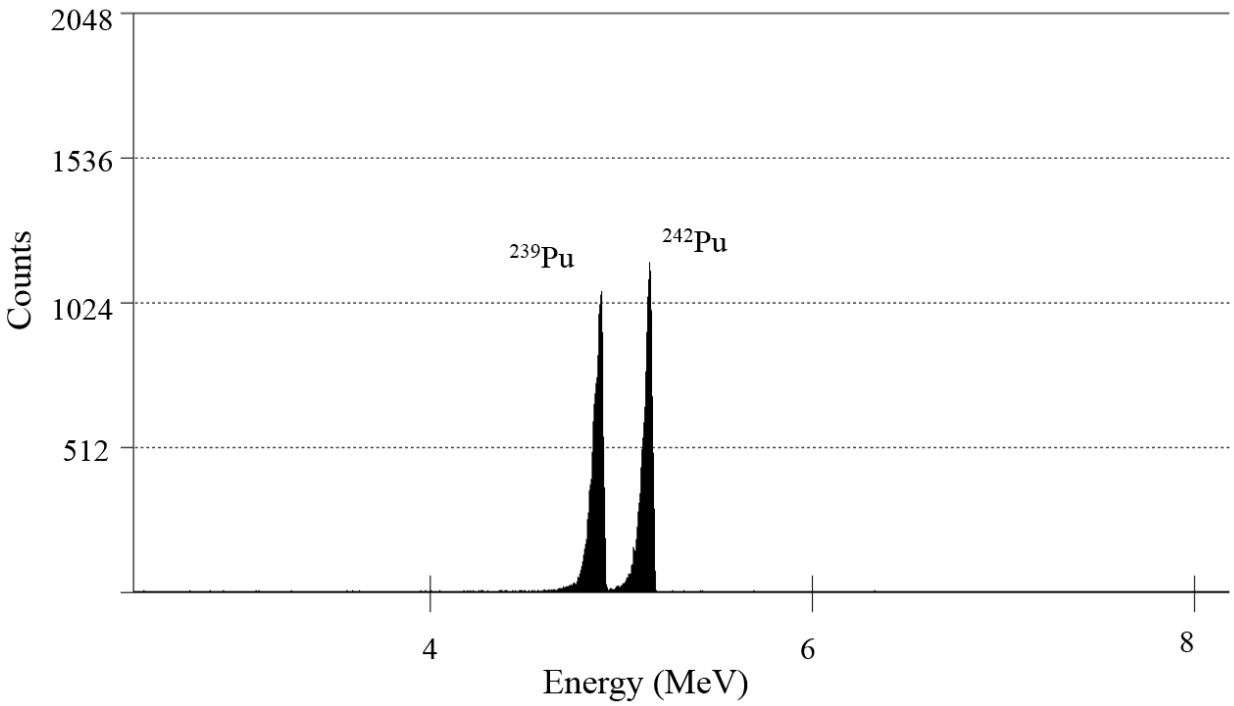

Figure 2.2 Typical alpha spectrum of Pu obtained in the analysis of control-spiked aqueous samples to evaluate the tandem TRU/TEVA method for the analysis of stable Ga in mixed actinide matrices. Near baseline separation of alpha full energy peaks is observed (see Table 2.2).

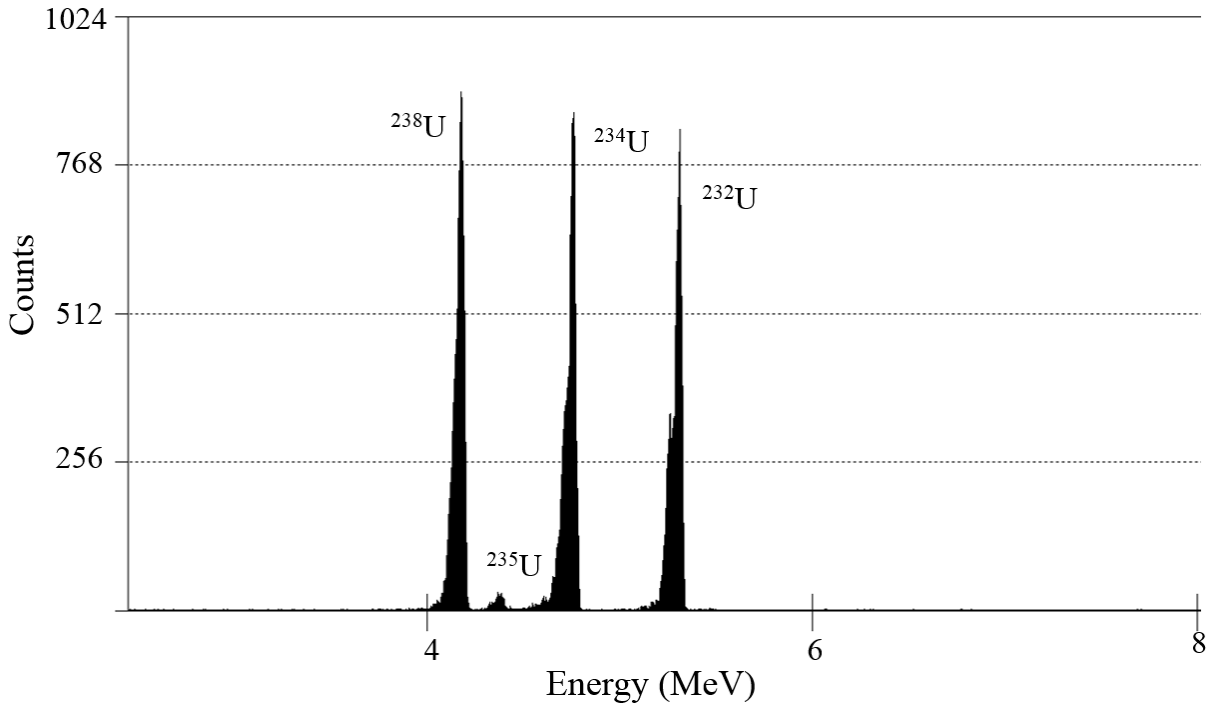

Figure 2.3 Typical alpha spectrum of natural U obtained in the analysis of control-spiked aqueous samples to evaluate the tandem TRU/TEVA method for the analysis of stable Ga in mixed actinide matrices. Near baseline separation of alpha full energy peaks is observed (see Table 2.2).

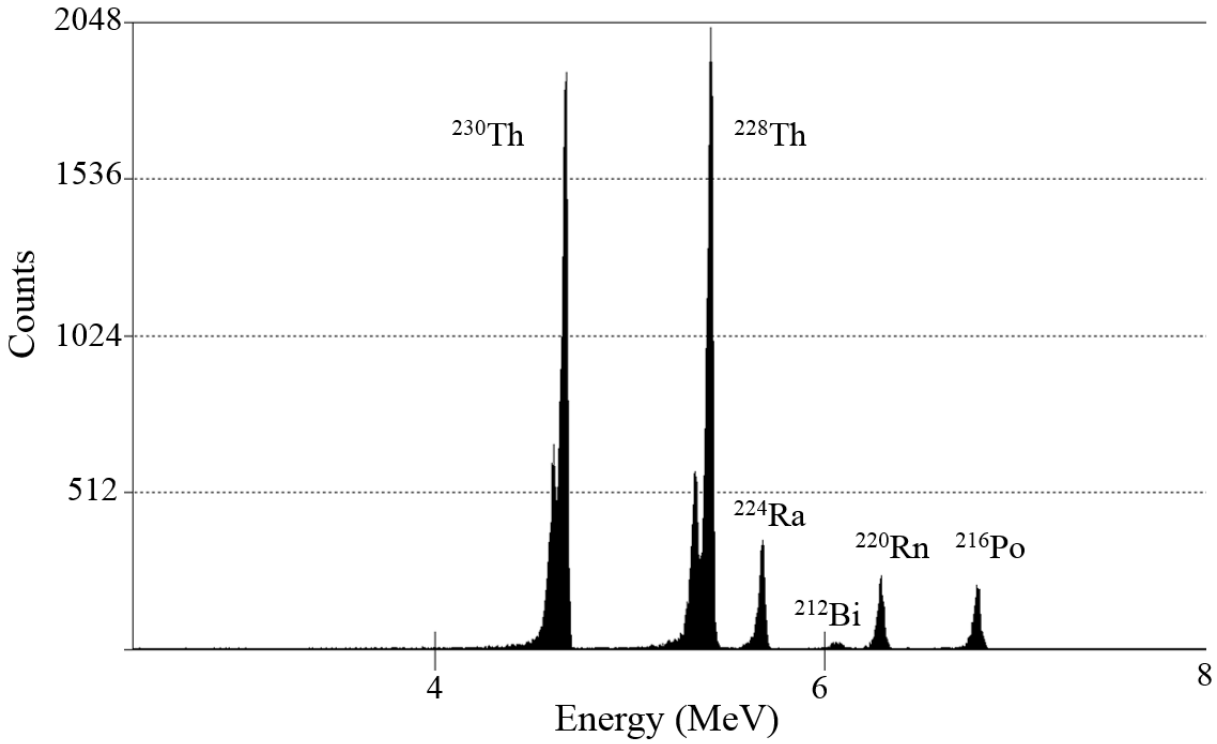

Figure 2.4 Typical alpha spectrum of Th obtained in the analysis of control-spiked aqueous samples to evaluate the tandem TRU/TEVA method for the analysis of stable Ga in mixed actinide matrices. Near baseline separation of alpha full energy peaks is observed (see Table 2.2).

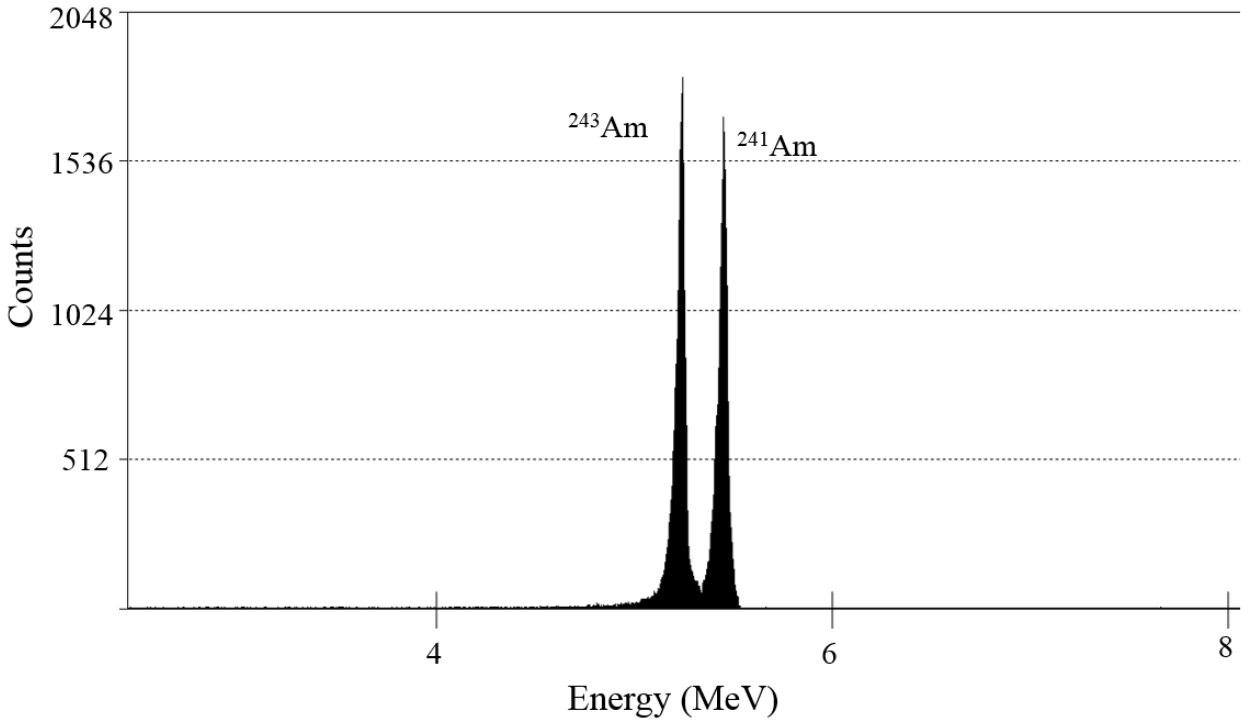

*Figure 2.5 Typical alpha spectrum of Am obtained in the analysis of control-spiked aqueous samples to evaluate the tandem TRU/TEVA method for the analysis of stable Ga in mixed actinide matrices. Near baseline separation of alpha full energy peaks is observed (see **Table 2.2**).*

2.5 Conclusions

Here we describe an effective method for the separation of Ga, Pu, U, Th, and Am, using extraction chromatography resins TEVA and TRU, for use in nuclear material quality control and nuclear forensics. Our results demonstrate that positron-emitting ^{68}Ga can be used as a radioanalytical tracer for stable Ga for complex matrix analysis. The method effectively allows precise determination of Ga yield (97±3%) in the analysis of stable Ga (spike recovery 101±1%) and radioactive Pu (radiochemical yield, 82±10%; spike recovery, 96±3%), while also providing pure elemental fractions of other actinides relevant to materials encountered in the analysis Pu-containing materials. Ongoing studies are aiming to employ the method for the analysis of stable Ga using mass spectral techniques and to expand the method to include further separation of

various isobaric interferences that may be present in nuclear materials that could hinder the quantification of Ga by mass spectrometry.

2.6 Acknowledgements

This material is based upon work supported by the U.S. Department of Homeland Security under Grant Award Number, 2012-DN-130-NF0001-02. The views and conclusions contained in this document are those of the authors and should not be interpreted as necessarily representing the official policies, either expressed or implied, of the U.S. Department of Homeland Security.

A special thanks to Phil Horwitz and Dan McAlister at Eichrom Technologies, LLC for helpful conversations and assistance in obtaining unpublished k' values for TEVA and TRU resins to assist us in optimizing the method.

CHAPTER 3. DISEQUILIBRIUM OF NATURALLY OCCURRING RADIOACTIVE MATERIALS (NORM) IN DRILL CUTTINGS FROM A HORIZONTAL DRILLING OPERATION

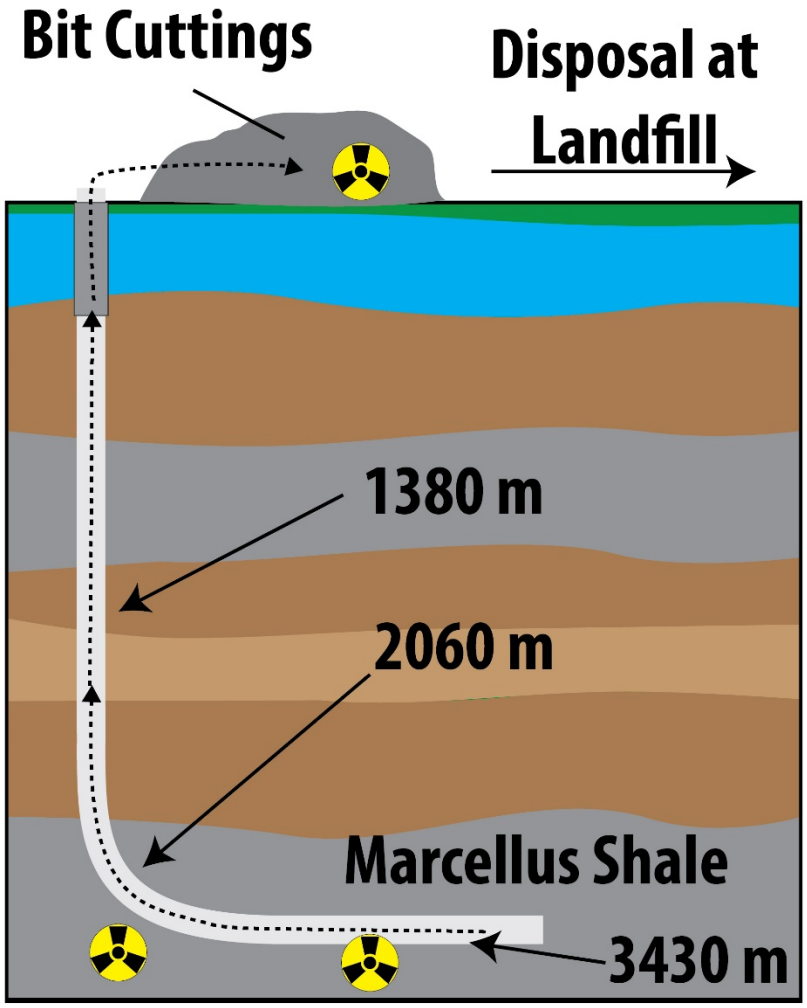

This Chapter is based on a publication in the Environmental Science and Technology Letters (*Environ. Sci. Technol. Lett.*) titled, "Disequilibrium of Naturally Occurring Radioactive Materials (NORM) in Drill Cuttings from a Horizontal Drilling Operation" in 2016 by Eitrheim, E.S.; May, D.; Forbes, T.Z.; Nelson, A.W. The TOC image at the beginning of the chapter depicts the horizontal drilling operation schematic, including the locations of our samples and was originally published in this journal article. The publication has been adapted or augmented and some original material, including wording and figures, has remained intact. The citation for the original journal article is shown here:

Environ. Sci. Technol. Lett., 2016, *3* (12), pp 425–429

DOI: 10.1021/acs.estlett.6b00439

Publication Date (Web): November 23, 2016

Copyright © 2016 American Chemical Society

3.1 Abstract

Naturally occurring radioactive materials (NORM) in solid waste or "drill cuttings" produced from unconventional drilling for natural gas extraction wells potentially pose environmental contamination risks; however, NORM composition and mobility in these solid wastes are poorly understood. In this study, the composition of NORM, including uranium, thorium, radium, lead, and polonium isotopes was evaluated in three samples of drill cuttings extracted from a well drilled into the Marcellus Shale formation. Leachability of NORM in drill cuttings was characterized by leaching the solid waste with dilute acetic acid at four different pH values. The uranium-series radionuclides in cuttings and leachate samples displayed isotopic disequilibrium, suggesting some environmental mobility of radionuclides in these shale formations. Our results

indicate that isotopic analysis of uranium-series radionuclides is needed for a more complete understanding of the potential environmental contamination risks associated with these solids wastes.

3.2 Introduction

Although there are numerous socioeconomic benefits related to increased domestic energy production, unconventional drilling produces large volumes of wastes that may result in long-term undesirable environmental impacts.[1–3] While a range of chemical contaminants have been documented in both solid and liquid wastes, naturally-occurring radioactive materials (NORM) from the uranium-238 (^{238}U) and thorium-232 (^{232}Th) series may also be cause for concern.[4,5] Liquid waste (produced fluids and flowback waters) from unconventional wells have received considerable attention from numerous stakeholders due to the large volumes of radium (Ra)-enriched fluids that are produced and the risks these fluids pose to riparian environments.[6–16] Less attention has been paid to the NORM levels in solid wastes (termed drilling cuttings). Despite the 2.37 million tons of drill cutting extracted in Pennsylvania (PA) in 2011 alone, very little information is available about the radiochemical profile of these materials.[17]

Accurate analysis of NORM in drill cuttings and leachates from drill cuttings requires a multitude of radiochemical techniques that are tailored to the physicochemical and/or radiochemical nature of any given isotope. In 2015, PA and WV (West Virginia) released studies on the NORM content of Marcellus Shale cuttings indicating that radioactivity levels in cuttings from horizontal portions of an unconventional well were higher than vertical portions.[18,19] The studies also concluded that drill cuttings pose minimal risk to the general public. Although this

conclusion may be the case, these reports only focused on several long-lived radionuclides from the ^{238}U series, specifically, ^{238}U and ^{226}Ra. Other key ^{238}U-series radionuclides, such as pure alpha-emitting radionuclides, ^{234}U, thorium-230 (^{230}Th), and polonium-210 (^{210}Po) and the low-energy beta-emitter, lead-210 (^{210}Pb), were not explicitly reported. The PA and WV reports also indicated that leachates from landfills accepting drill cuttings contained NORM, and in some cases the ^{226}Ra concentrations in these samples were above action levels.[18,19] WV and PA did not report levels of ^{238}U in leachates; however, results from sequential leach studies suggest that ^{238}U in Marcellus Shale cuttings is relatively mobile and may contribute to elevated levels of ^{238}U in landfill leachates.[20] While new information on ^{238}U and ^{226}Ra in Marcellus Shale cuttings and leachates is emerging, relative concentrations and mobility of other environmentally-persistent radionuclides in the ^{238}U series, including ^{234}U, ^{230}Th, ^{210}Pb, and ^{210}Po, remain unexplored. These radionuclides may provide important information for environmental contamination risk and source apportionment.

Here, we characterize NORM in cuttings associated with horizontal drilling activities in the Marcellus Shale formation. First, using new and modified radiochemical methods, we quantitate and assess the equilibrium status of environmentally-persistent ^{238}U series radionuclides (^{238}U, ^{234}U, ^{226}Ra, ^{210}Pb, ^{210}Po) in three solid samples from a horizontal well within the Marcellus Shale formation (**Figure 3.1**). Second, the potential for NORM to leach from cuttings extracted from the horizontal portion of the well was assessed using a modified US Environmental Protection Agency (EPA) Toxicity Characteristic Leaching Procedure (TCLP).[21] We hypothesized that ^{238}U-series radionuclides in Marcellus Shale drill cuttings would be in secular

equilibrium (steady-state) and that ^{238}U-series radionuclides would partition into TCLP leachates with decreasing pH.

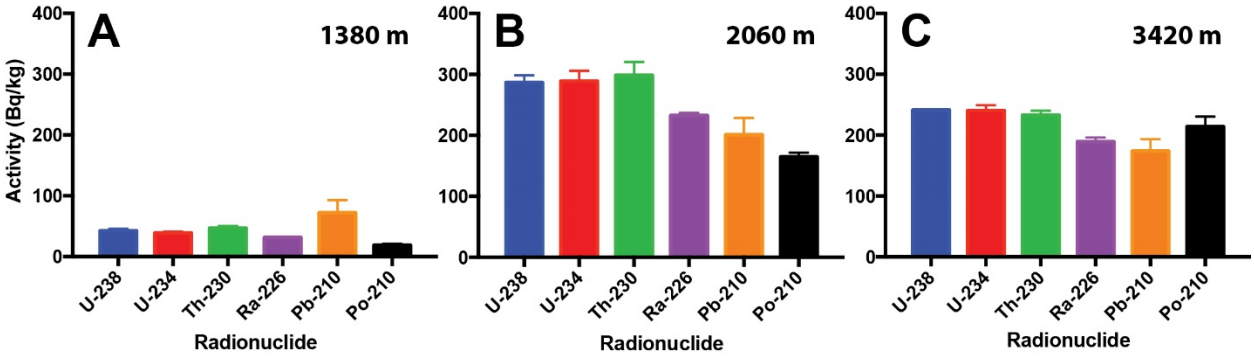

Figure 3.1 Levels of U-238 series radionuclides in three drill cutting samples from an unconventional drilling operation targeting the Marcellus Shale: (A) sample from vertical portion of the well at 1380 m, (B) sample from horizontal drilled portion of well at 2060 m, and (C) sample from horizontal drilled portion of well at 3430 m.

3.3 Materials and Methods

3.3.1 General

All chemicals were ACS reagent grade or higher. The University of Iowa State Hygienic Laboratory (SHL, Coralville, IA, USA) analyzed the solid samples for relevant metals, inorganics, and organics content (**Table 3.1, Figure 3.2**). High purity germanium (HPGe) gamma spectrometry of drill cuttings was performed at the SHL using 500 cm^3 Marinelli beakers on an ORTEC system calibrated to a mixed gamma source (Standard Reference Source 101582, Eckert and Ziegler (E&Z), Atlanta, GA, USA) using previously described methodology.[10,11] Separation and gas flow proportional counting (GFPC) of ^{210}Pb in drill cuttings was performed by PACE Analytical (Greensburg, PA, USA). Alpha spectrometry was performed at the University of Iowa. Radionuclide tracers included: ^{232}U standard 92403 (E&Z), ^{229}Th standard 4328C (National Institute of Standards and Technology (NIST), Gaithersburg, MD, USA),^{209}Po standard 92565 (E&Z), and the cyclotron-produced ^{203}Pb (Lantheus Medical Imaging, Billerica, MA, USA). Emission energies and half-lives were taken from the NUDAT database from the US National Nuclear Data

Center (NNDC Brookhaven National Laboratory, US Department of Energy).[22] The only exception is for ^{209}Po, a half-life of 128.3 yr was used, as evidence suggests that half-life is longer than previously established.[23] All samples were decay corrected to the time of extraction using standard decay correction equations.[24]

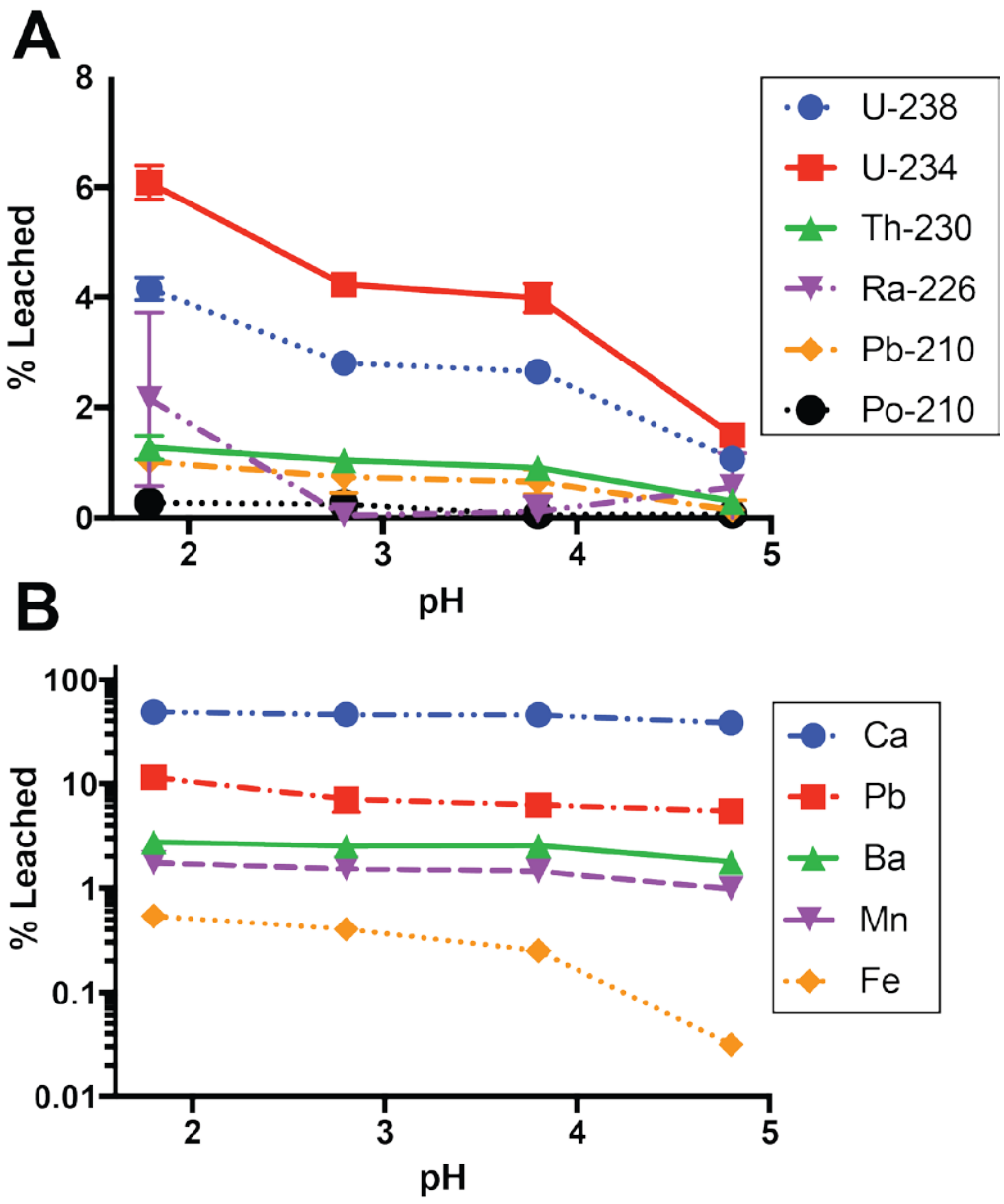

Figure 3.2. Percentage of (A) radionuclides (Figure 3.1) and (B) metals leached by acetate buffer at pH 1.8, 2.8, 3.8, and 4.8 from 2060 m drill cuttings (normalized to dry weight).

3.3.2 Drill Cuttings Sample

Three solid samples were obtained from a single well in northern PA. The first sample was taken from the vertical, air-drilled section (1380 m) extracted in mid-November 2015 and the two other samples were extracted from the horizontal section (2060 m and 3430 m) in mid-December 2015. Samples were received January 8, 2016 and homogenized. Subsamples for U, Th, Ra, and Pb isotopic analysis were dried at 110°C until a stable weight was achieved. Due to the volatility of ^{210}Po, analysis was performed on 'wet' sample.

3.3.3 Methods of Analysis

3.3.3.1 Uranium and Thorium

^{238}U, ^{234}U, and ^{230}Th were prepared by a slightly modified rapid method developed for the analysis of actinides in asphalt.[25] First, 50 mBq of ^{232}U and ^{229}Th tracer were added to the samples (1.0 g) and the dried drill cuttings were ashed in a muffle furnace (600°C, 1 h) in a platinum crucible. The samples were then rapidly fused in NaOH (10 g, 600°C, 15 min), before removal from the salt matrix using H_2O. Initially the samples were precipitated with calcium phosphate ($Ca_3(PO_4)_2$), followed by a second precipitation with cerium fluoride (CeF_3). CeF_3 solids were then dissolved (10 mL, 3M HNO_3/0.175% boric acid; 10 mL 3M HNO_3/1M $Al(NO_3)_3$) and separated by Eichrom method ACW01.[26] Elemental fractions were prepared for alpha spectrometry by cerium fluoride (CeF_3) microprecipitation as previously described.[27]

3.3.3.2 Radium

Samples (1000 cm^3) for ^{226}Ra analysis were dried, sealed (>21 days, for ^{222}Rn ingrowth), and quantitated by HPGe gamma spectrometry (SHL) as previously described.[10,11]

3.3.3.3 Lead

^{210}Pb was separated and quantitated by PACE Analytical (Greensburg, PA, USA) according to Eichrom method PBS01.[28]

3.3.3.4 Polonium

^{209}Po tracer (~50 mBq) was added to 0.5 g subsamples, and then digested with 11 mL aqua regia overnight on hot plate. Samples were then precipitated (H_2O_2, few drops; $Fe(OH)_3$; manganese dioxide (MnO_2); and NH_4OH), centrifuged, and washed (H_2O) as described for methodology developed for Marcellus Shale produced fluids.[11] Pellets were dissolved (HCl, 0.1 M, 20 mL; hydroxylamine ($NH_2OH{\bullet}Cl$), 2 mL, 25% w/v) and autodeposited onto nickel (Ni) disks and counted by high resolution alpha spectrometry.[11]

3.3.3.5 Leaching Studies

Leaching was performed using a modified EPA TCLP.[21] Centrifugation was used instead of filtration to allow for inclusion of colloid-bound radionuclides. For Pb, Po, U, and Th leaches, 100 mL of acetate buffer adjusted to pH 1.8, 2.8, 3.8, and 4.8 (n=4) was added to 10.0 g of sample. Due to higher detection limits for ^{226}Ra, samples were increased to 20.0 g drill cuttings and 200 mL acetate buffer. All samples were then mixed for 24 hours, centrifuged, and the leachates were placed into glass beakers prior to separation and quantitation.

3.3.3.6 Uranium and Thorium

^{232}U and ^{229}Th tracers were added and the sample was subjected to a $Fe(OH)_3$ and $Ca_3(PO_4)_2$ coprecipitation. The resulting solid pellets were dissolved (10 mL, 3M HNO_3/1M $Al(NO_3)_3$) separated, and prepared for alpha spectrometry as described above.

3.3.3.7 Radium

Leachates were prepared by the EPA 903.0 method at the SHL.[29] The only modification to this procedure was that yields were determined by barium-133 (^{133}Ba) using HPGe gamma spectrometry *en lieu* of gravimetric determinations. ^{226}Ra was quantitated by GFPC.

3.3.3.8 Lead

^{203}Pb tracer was added and then the leachates were then subjected to a $Fe(OH)_3$ precipitation. The resultant pellet that was dissolved in 10mL of 1M HCl and separated on Pb resin according to Eichrom method PBW01.[30]. Yield of ^{203}Pb were determined by sodium iodide (NaI) gamma spectrometry.[9] Activities of ^{210}Pb were determined by ingrowth of ^{210}Po via liquid scintillation on an alpha/beta discriminating liquid scintillation counter at the SHL.

3.3.3.9 Polonium

^{209}Po was added as a tracer and the leachate was acidified to pH 1-2 using HCl $NH_2OH{\cdot}Cl$ was added (5 mL, 25% w/v), Po was then autodeposited at 90°C on a Ni planchet, and quantitated by alpha spectrometry. [11]

3.3.3.10 Metals

Using the modified EPA TCLP,[21] each acetate buffer (10 mL, pH 1.8, 2.8, 3.8, 4.8; n=3 for each pH) was added to the drill cuttings (2060 m sample) and homogenized for 24 hours. The samples were then centrifuged, decanted, and acidified (100 µL, HNO_3, 16 M) prior to analysis by at SHL.

Metal, Organic, & Inorganic Composition of Drill Cuttings (**Table 3.1**) and Radioactivity Concentrations in Drill Cuttings (**Table 3.2**) are given at the end of the chapter.

3.4 Results and Discussion

3.4.1 Chemical Characterization

Cuttings from each location were analyzed for common organic and inorganic constituents that could interfere with radiochemical separations. The shallowest sample (1380 m) was extracted by air drilling from the vertical portion of the well, whereas the deeper two samples from the horizontal section (2060 m and 3430 m) were removed by diesel-based drilling techniques. All three samples had high levels of organic fractions, with ethylbenzene (38,000-63,000 μg/kg), xylenes (270,000-450,000 μg/kg), diesel fuel (70,000-120,000 μg/kg), and total extractable hydrocarbons (70,000-120,000 μg/kg) notably elevated (**Table 3.1**). The 1380 m sample is chemically distinct from the deeper Marcellus Shale samples (2060 m and 3430 m), which were characteristic of marine black shales as evidenced by enrichment of trace elements cadmium (Cd), copper (Cu), vanadium (V), zinc (Zn), arsenic (As), and selenium (Se).[31]

3.4.2 NORM Characterization

Environmentally-persistent radionuclides from the natural ^{238}U series (^{238}U, ^{234}U, ^{230}Th, ^{226}Ra, ^{210}Pb, and ^{210}Po) were quantified in each drill cutting location (**Figure 3.2A-B, Table 3.2**). Based upon the chemical analysis and the potential for interference of organic constituents on radiochemical separations, the cutting samples were fired in a muffle furnace. NaOH fusion, based on methods developed for actinide analysis in asphalt, was used to ensure total dissolution of solid material [25] Drill cuttings are exceptionally challenging samples for radiochemical separations. For example, radiochemical yields for uranium in this study were 40 ± 10%. Previous radiochemical analysis of drill cutting material reported radiochemical yields substantially lower (i.e., ~2% recovery).[18] These results suggest that new, more robust methods for analysis of drill

cutting solid waste are needed. ^{226}Ra analyses are simplified for this complex matrix by elevated abundance and the high-energy gamma emissions of ^{226}Ra decay products (^{214}Bi and ^{214}Pb) for HPGe gamma spectrometry with little sample preparation (apart from a 30-day hold to allow for decay product ingrowth). The high density of the drill cuttings can interfere with direct measurement of ^{210}Pb (46 keV, 4%) by gamma spectrometry, [32,33] therefore, ^{210}Pb was quantitated by methods developed for ^{210}Pb in soil.[28] ^{210}Po was extracted by aqua regia and H_2O_2, because ^{210}Po can adhere to organic matter in the soil [34] and volatilize in dry samples through elevated temperatures (>100°C) [35] or by biological processes under ambient conditions.[36]

The deep drill cuttings (2060 m and 3430 m) have significantly higher levels of ^{238}U series radionuclides than the shallower location (1380 m). These results are consistent with the WV and PA studies that indicate horizontal drill cuttings from the Marcellus Shale are elevated in ^{238}U and ^{226}Ra relative to the vertical portions.[18,19] The lower levels of ^{226}Ra relative to ^{238}U is likely attributable to the partitioning of ^{226}Ra into Marcellus Shale brines which are characteristically elevated in ^{226}Ra.[6,8,10,11] As expected, the horizontal portions are also elevated in environmentally-persistent radionuclides, ^{234}U, ^{230}Th, ^{210}Pb, and ^{210}Po. Contrary to our hypothesis, the ^{238}U-series radionuclides were not in secular equilibrium. In all samples, ^{226}Ra levels were lower relative to ^{238}U, ^{234}U, and ^{230}Th, which is consistent with other observations.[18,19] Similarly, levels of ^{210}Pb and ^{210}Po were decreased relative to ^{226}Ra. This disequilibrium is likely attributable to partitioning of the noble gas, radon-222 (^{222}Rn), in the subsurface as is expected of gaseous hydrocarbons. The disequilibrium between ^{226}Ra and ^{210}Pb is likely explained by partitioning of ^{222}Rn and could be explored as a tool for determining gas migration in the subsurface.[37] These results suggest that radiochemical equilibrium of ^{238}U series radionuclides

cannot be assumed in Marcellus Shale drill cuttings; accurate assessment of environmental contamination risk by ^{238}U series radionuclides must include detailed radiochemical analyses.

3.4.3 Leaching

Drill cuttings in the Marcellus Shale region are primarily (98.4%) disposed at landfills;[38] however, the stability of NORM in drill cuttings is uncertain. To assess the potential for ^{238}U-series radionuclides to leach from drill cuttings, we employed a simple, acetate-buffer leaching protocol based on the EPA TCLP method,[21] which the EPA believes simulates the leaching that occurs in landfills.[39] We chose to analyze sample 2060 m as it had the highest levels of all ^{238}U-series radionuclides and would allow for shorter counting times and lower detection limits. In general, we observed negative correlations for percent radionuclide leached with respect to pH for the ^{238}U-series radionuclides tested (^{238}U, R^2 = -0.96; ^{234}U, R^2 = -0.96; ^{230}Th, R^2 = -0.95; ^{226}Ra, R^2 = -0.62; ^{210}Pb, -0.96; ^{210}Po, R^2 = -0.91) (**Figure 3.2A**). Fe and Mn displayed similar trends with greater percentages leaching as pH decreased (Fe, R^2 = -0.99; Mn, R^2 = -0.95) (**Figure 3.2B**). The partitioning of ^{238}U-series radionuclides into the acetate solution may in part be explained by the desorption from hydrous of Fe- and Mn-oxide minerals, which are well known to adsorb heavy metals.[40]

3.4.4 Uranium and Thorium

We observed that ^{238}U and ^{234}U were the most leachable radionuclides (4.2% and 6.1% leached at pH 1.8, respectively), which may be explained by the increased solubility of U when complexed with the acetate anion.[41] Interestingly, ^{234}U had a mean radioactivity concentration 1.5 ± 0.1 times higher than ^{238}U across all leachate samples. This result was unexpected because

^{234}U and ^{238}U were in secular equilibrium in the drill cuttings. However, the isotopic enrichment of ^{234}U is well-known in natural systems due to alpha recoil enrichment,[42] which occurs when ^{238}U decays and releases high energy alpha particles that break chemical bonds. This allows decay products (ex: ^{234}U) to be forcefully extruded from the crystal lattice and deposits larger amounts of ^{234}U on the outside of the mineral grain, leading to higher leaching rates. ^{230}Th was not leached as readily as U, as expected by the relatively low solubility in environmental systems. Th is particle reactive in most environmental systems and tends to remain adsorbed onto mineral surfaces at pH greater than 2.[43]

3.4.5 Radium, Lead, and Polonium

Interestingly, only 2.1 $\pm$ 1.6 % of ^{226}Ra leached at pH 1.8, which is consistent with the analogous Ba data, which indicated that the percent leached was 2.76 $\pm$ 0.03 %. This is surprising, given that high levels of Ba and Ra isotopes were previously reported in Marcellus Shale produced fluids.[6,10] The amount of ^{210}Pb leached was positively correlated with stable Pb extraction (R^2 = 0.84), though at much lower quantities (1.0 $\pm$ 0.1 % versus 11.5 $\pm$ 0.6 %, respectively). The difference in extractability between ^{210}Pb and stable Pb may be a reflection of their geochemical microenvironment, which has been observed for other radionuclides.[44] ^{210}Po was the least soluble radionuclide tested in this system, with only 0.28 $\pm$ 0.01 % leached at pH 1.8. We expected ^{210}Po to partition into the acetate buffers as ^{210}Po is known to be soluble in acetate.[35] Yet, the low solubility of ^{210}Po can be explained by its strong particle reactivity and tendency to adhere strongly to organics.[34] Interestingly, recent reports have indicated that ^{210}Po in reduced sediments can be volatilized by aerobic marine microorganisms.[36] Drill cuttings from the

Marcellus Shale could serve as an interesting medium for future studies on the volatility of Po from ancient marine sediments.

3.5 Conclusion

Although previous studies have suggested that NORM in drill cuttings pose minimal health risk to the general public when disposed in landfills,[18,19,45] our results indicate that Marcellus Shale drill cuttings warrant further radiochemical investigations. More studies are needed to develop robust, rapid methods that are suitable for a variety of complex matrices typified by drill cuttings. Additionally, field studies are needed to determine the stability of radionuclides in landfills and the potential for NORM from drill cuttings to migrate into landfill leachates. Studies assessing the risks for NORM exposure should include analysis of pure-alpha emitters (^{234}U, ^{230}Th, ^{210}Po) and the low-level beta emitter (^{210}Pb). For example, the most leachable isotope in these drill cuttings was ^{234}U, which is typically not detected or reported by standard environmental monitoring methods. Accurate assessment of the human health risks associated with drill cuttings should include isotopic analysis of all environmentally-persistent radionuclides.

Table 3.1 Metal, Organics & Inorganic Composition of Drill Cuttings

Samples (*dry weight)	1380m	2060m	3430m	Method
chloride (mg/kg)*	7300	8700	9500	EPA 300.0
sulfate (mg/kg)*	4200	9800	6400	EPA 300.0
bromide (mg/kg)*	<0.5	<0.5	120	EPA 300.0
aluminum (mg/kg)*	19000	8300	5800	EPA 6020
barium (mg/kg)*	2700	810	1400	EPA 6020
cadmium (mg/kg)*	<2.0	7.1	3.5	EPA 6020
chromium (mg/kg)*	29	13	16	EPA 6020
copper (mg/kg)*	18	92	120	EPA 6020
lead (mg/kg)*	23	14	20	EPA 6020
manganese (mg/kg)*	500	140	150	EPA 6020
nickel (mg/kg)*	44	140	120	EPA 6020
strontium (mg/kg)*	190	180	480	EPA 6020
vanadium (mg/kg)*	38	100	230	EPA 6020
zinc (mg/kg)*	66	640	280	EPA 6020
arsenic (mg/kg)*	6.9	24	24	EPA 6020
iron (mg/kg)*	37000	29000	18000	EPA 6020
selenium (mg/kg)*	<1.0	7.2	5.4	EPA 6020
calcium (mg/kg)*	35000	30000	120000	EPA 6010C
magnesium (mg/kg)*	8500	2600	7000	EPA 6010C
potassium (mg/kg)*	5000	4200	2700	EPA 6010C
sodium (mg/kg)*	1000	810	670	EPA 6010C
benzene (µg/kg)	<25000	<25000	<25000	EPA 8260
toluene (µg/kg)	37000	<25000	28000	EPA 8260
ethylbenzene (µg/kg)	58000	38000	63000	EPA 8260
total xylenes (µg/kg)	390000	270000	450000	EPA 8260
gasoline (µg/kg)	<1500	<2400	<2500	Iowa OA-2
mineral spirits (µg/kg)	<1500	<2400	<2500	Iowa OA-2
kerosene (µg/kg)	<1500	<2400	<2500	Iowa OA-2
diesel fuel (µg/kg)	70000	100000	120000	Iowa OA-2
motor oil (µg/kg)	<1500	<2400	<2500	Iowa OA-2
total extractable hydrocarbons (µg/kg)	70000	100000	120000	Iowa OA-2
dry weight	91.40%	89.30%	86.60%	
Date Collected	18-Nov-16	10-Dec-16	12-Dec-16	

*dry weight

Table 3.2 Radioactivity Concentrations in Drill Cuttings

Sample	1380 m		2060 m		3430 m	
	Activity±SD[d] (Bq/kg)	MDA[e] (Bq/kg)	Activity±SD[d] (Bq/kg)	MDA[e] (Bq/kg)	Activity±SD[d] (Bq/kg)	MDA[e] (Bq/kg)
U-238[a]	43±3	<1	287±12	<1	241±1	<1
U-234[a]	39±3	<1	289±17	<1	241±9	<1
Th-230[a]	47±4	<1	298±22	<1	233±7	<1
Ra-226 (Pb-214)[b]	31±1	1	233±5	2	189±7	1
Pb-210[c]	72±21	22[f]	201±27	12[f]	174±20	14[f]
Po-210[a]	19±2	<1	165±7	<1	214±16	<1

[a] alpha spectrometry

[b] high purity germanium (HPGe) gamma spectrometry

[c] gas flow proportional counting

[d]SD refers to 1 standard deviation

[e] minimum detectable activity determined by the Currie Limit

[f] minimum detectable activity determined by ANSI N42.23 and N13.30

3.6 Acknowledgements

We kindly thank the staff at PACE Analytical Labs for contributing time and resources to this study. Funding for these studies was provided by the Center for Global and Regional Environmental Research (CGRER) at the University of Iowa. The authors declare no competing financial interest.

CHAPTER 4. SYNTHESIS OF THE ALUMINUM HYDROXIDE OCTAMER BY A SIMPLE DISSOLUTION METHOD

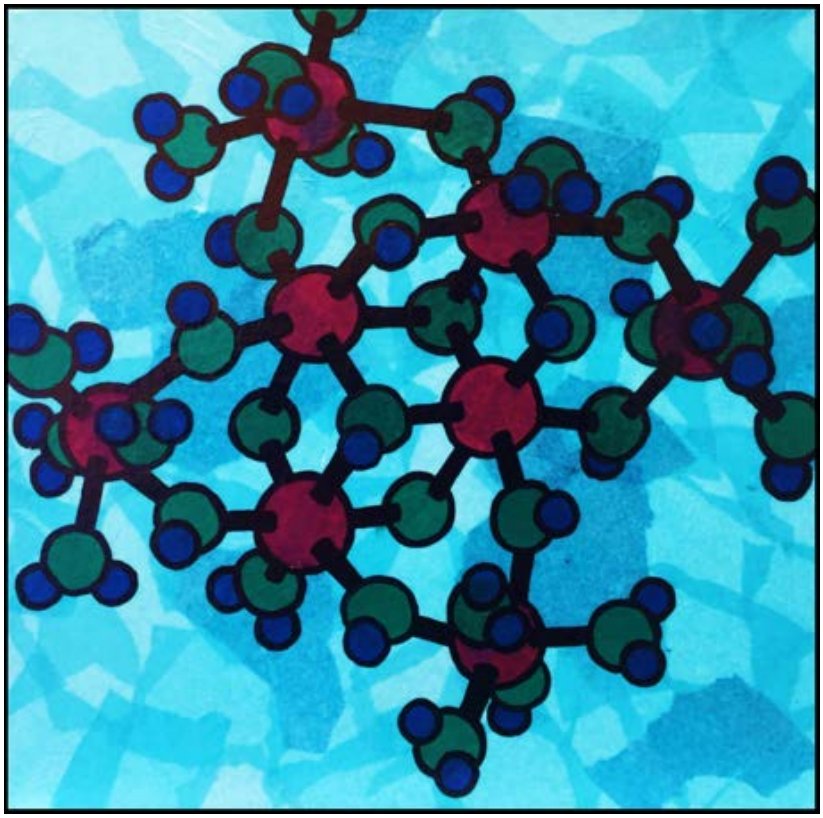

This Chapter is based on the reviewed and accepted communication in Angewandte Chemie International Edition (Angew. Chem. Int. Ed.) titled, "Synthesis of the aluminium hydroxide octamer by a simple dissolution method" accepted to be published in 2017 by Perkins C.K.; Eitrheim, E.S.; Fulton, B.L.; Fullmer, L.B.; Colla, C.A.; Park, D-H.; Oliveri, A.F.; Hutchison, J.E.; Nyman, M.; Casey, W.H.; Forbes, T.Z.; Johnson, D.W.; Keszler, D.A. The TOC image at the beginning of the chapter depicts the cluster with aluminum red spheres, oxygen green, and hydrogen blue (Dr. Anna Oliveri). The publication has been adapted or augmented and some original material, including wording and figures, has remained intact. I am responsible for the synthesis and crystallography components of this work, while other instrumentation and analysis is the input of other authors.

Keywords: aluminum clusters, ^{27}Al NMR, polyoxocations, Small- and wide-angle X-ray scattering, mineral dissolution

4.1 Abstract

Multimeric oxo-hydroxo Al clusters function as models for common mineral structures and reactions. In this role, they help us understand mechanisms of important geochemical reactions and translate natural processes to improve materials properties and function. Cluster research, however, is often slowed by the lack of methods to prepare clusters in pure form and in large amounts. Here, we report a facile synthesis of the recondite cluster $Al_8(OH)_{14}(H_2O)_{18}(SO_4)_5$ (Al_8) by a simple dissolution method. We confirm its structure by single-crystal X-ray diffraction and show by ^{27}Al NMR spectroscopy, electrospray-ionization mass spectrometry, and small- and wide-angle X-ray scattering that it also exists in solution. We speculate Al_8 may form in natural

water systems by dissolution of aluminum-containing minerals in acidic sulfate solutions, such as those that could result from acid rain or mine drainage. Additionally, the dissolution method produces a discrete Al cluster at scale for studies and applications in materials science. This dissolution method, when utilizing sulfuric acid, isolated the Al_8, while using Selenic Acid, isolated a monomer not previously reported. Spectroscopic evidence does indicate that the Al_8 does form under both conditions in solution, despite not isolating the Al_8 with selenate.

4.2 Introduction

Cluster synthesis and isolation remains difficult due to numerous factors. Spectroscopic techniques for identifying clusters in solution is challenging, especially in complex systems like the environment or waste streams. Likewise, the crystallization process is still not completely understood, making cluster isolation, and therefore study, problematic. A number of syntheses, spectroscopic techniques, and methods for crystallization are being developed to address these problems.

4.2.1 Spectroscopic Techniques for Detecting Aluminum Clusters

Utilizing spectroscopic techniques can be challenging for many practical reasons, including sample stability, changing speciation, and interpretation of the spectral bands. The crystals can degrade quickly or dehydrate in the process of preparing the sample. Likewise, speciation and therefore, cluster identification can change upon degradation of the material or dissolution of the solid-state phase in aqueous solutions. These sample issues also exacerbate the issue of band assignment, leading to misinterpretation of the spectroscopic evidence and misidentification of the aluminum hydroxide clusters.[67]

Cluster discovery usually originates with a solid-state single crystal X-ray structure to get a structural characterization of these soluble precursors, which leads to a topological model of the cluster composition, size, and shape. In addition, characterizing these clusters by diffraction techniques provides bond distances and angles and subsequent bond valence calculations leads to information regarding protonation of the cluster. The atomistic understanding of the structure is the most important tool in explaining the function of the cluster and can be utilized by computational chemists as input files for density functional theory calculations.

Nuclear Magnetic Resonance (NMR) techniques can also be used to get a structural understanding of these clusters in both the solid-state and in solution. Single Crystal X-ray diffraction (XRD) is a solid-state technique and require highly crystalline material to provide precise determination of atom locations and bond distances. NMR shifts can add insights where diffraction techniques fail, including coordination geometries about the metal center and information regarding the electronic environment (i.e. electronegativity of nearby atoms). In addition to the ^{1}H and ^{13}C techniques routinely utilized in organic chemistry, quadrupolar ^{27}Al (nuclear spin quantum number, $I > ½$) can also be probed by NMR spectroscopy.[68-69] This nuclei is somewhat hindered by peak-broadening, yet can sometimes be circumvented by the advent of very high magnetic fields as well as ultra-fast magic-angle spinning (MAS) NMR. Characteristic ^{27}Al NMR peaks can be observed for tetrahedrally coordinated ligands found in the Keggin Al_{13} isomers and Al_{30} clusters. For example, the well-known ε-Keggin of aluminum has a characteristic ^{27}Al peak at 63 ppm, and recent ventures have utilized ^{27}Al techniques to even help distinguish the various Keggin isomers due to this tetrahedral peak's chemical shift.[70] NMR techniques have proven a useful addition in the characterization and speciation of cluster chemistry in solution.

Scattering techniques can also be used for the investigation of aqueous cluster chemistry. Small and Wide Angle X-ray Scattering (SWAXS) is one scattering method often used to help elucidate some information regarding the structure of the clusters in solution.[71] Most notably, the dynamic radii can be observed which indicates the shape of the particles in solution. Due to the small shape of these discrete clusters, this is rarely a "stand-alone" technique. A second factor that hinders the use of SWAXS is that the aluminum clusters often have a similar shape and therefore cannot be distinguished in solution, let alone when they are part of a heterogenous mixture.

Other spectroscopic techniques for the identification of aluminum clusters include vibrational spectroscopy (i.e. Raman and Infrared (IR) spectroscopy). IR spectroscopy can often give information regarding the presence of certain functional groups. Raman spectroscopy has the benefit of a very low background signal, yet typically experiences high limits of detection due to low photon scattering. A major advantage is the simple sample prep along with the non-destructive nature of these analytical techniques.

In addition to these techniques, computational methods that both help confirm experimental results or direct experimentation are valuable and can enhance our chemical understanding of the system and interpretation of the data collected by these methods. For example, identifying the species associated with a specific peak in a Raman spectra is not trivial and can more reasonably be completed with confirmation via computational methods that predict the Raman bands for the material. Similar reliance can be seen for NMR, IR, and SAXS data processing and interpretation.

Specifically, with the polyaluminum clusters synthesized in our lab, we utilized primarily single crystal X-ray diffraction, along with NMR and IR techniques. This is in part due to the early stages of Al_{30} chemistry where identifying them in solution is not easy, especially if you are interested in their local environment (i.e. contaminants adsorbed to the surface). After characterizing these new Al_{30} clusters, we attempt to identify if there are characteristic NMR signals that can help identify them in a more complex solution (i.e. nuclear wastes or environmental systems).

4.2.2 Techniques for Synthesizing Aluminum Clusters

4.2.2.1 Classic Base Hydrolysis Approach

The original synthesis of the aluminum tridecameric Keggin was achieved using Al^{3+} aqueous solution with the addition of a hydroxide base to a specific ratio, referred to as the "hydrolysis ratio" with respect to initial Al concentration. Upon changing this hydrolysis ratio, specific aluminum clusters can be synthesized in aqueous solutions. A dimer, trimer, and even the tetramer was reported to exist in solution when the hydrolysis ratios were 1, 1.33, and 1.76, respectively.[69, 72] The synthesis of larger polyaluminum cations, such as the Al_{13} and Al_{30} cluster, are achieved with higher ratios. The well-known ε-keggin, for example, can be synthesized in high yields with hydrolysis ratios of about 2.5 and higher values initiates the precipitation of insoluble polymeric aluminum hydroxide solids.[73-75]

4.2.2.2 Thermolysis: Hydrolysis with Heat

Additional clusters can be formed using hydrolysis method described in the previous with the previous method followed by a moderate heat treatment. [74] For example, the polycation Al_{30}

can be formed by an initial hydrolysis ratio of 2.25-2.4, followed by heating in a gravimetric oven at 80 ^{o}C for 1-3 days.[73-74] Extended heating can lead to Al_{30} molecules becoming the dominant species in solution due to the increased hydrolysis prompted by heating.[68] Aging the solution at temperature likely promotes additional hydrolysis reactions and does not cause the steep pH gradient that would result from the addition of a concentrated droplet of base.

4.2.2.3 Hydrolysis with Zn Metal Redox

Another facile synthesis of the flat tridecameric aluminum cluster (Al_{13}^{f}) that can be performed at room temperature is the treatment of an aluminum (III) nitrate solution with zinc-metal powder.[76] This simple methodology results in yields of 55%, but small amounts of zinc remain in the solid. The residual metal could be considered as a contaminant for some applications and may not be easily removed from the system. Further studies have not been performed to determine if this is a suitable synthesis technique for other aluminum clusters.

4.2.2.4 Nitroso Organic Additives

Another quick and easy synthesis of the flat tridecameric aluminum cluster (Al_{13}^{f}) has been reported using an organic additive (nitrosobenzene).[77] An initial hydrolysis ratio of 1.3 along with the addition of nitrosobenzene in methanolic solutions led to 47% yields, which can be important for utilizing these clusters as precursors for various applications. The use of large amount of organics, however, is not suitable for current sustainability models and the nitrobenzene itself has significant safety concerns. In addition, the aluminum clusters are formed in the presence of a black viscous polymer, which makes product recovery difficult.

4.2.2.5 Hydrolysis with an Electrolytic Cell

Hydrolysis for the synthesis of aluminum clusters can also be achieving utilizing an electrolytic cell that slowly hydrolyzes an Al^{3+} solution by reducing water *in situ*. This can limit the number of additives for a well-defined system, but the yields and reproducibility has been an problematic for this technique. Synthesis of multiple other polyaluminum clusters is likely achievable using electrochemical methodology, yet remains untested in the aluminum hydroxide system.

4.2.2.6 Dissolution Approach

A different approach for attempting to synthesize aluminum clusters involves approaching the solubility of the aluminum hydroxide system from the opposite direction. Instead of starting with acidic Al^{3+} in aqueous solutions and adding a base, we can also start with basic aluminum hydroxide ($Al(OH)_3$) dissolved with an acid of choice. (**Figure 4.1**) Starting with an Al^{3+} solution involves starting with, most commonly, aluminum (III) nitrate or aluminum (III) chloride. There is an increasing understanding that anions can influence the speciation and synthesis of these clusters in solution; thus, the dissolution approach provides better control over

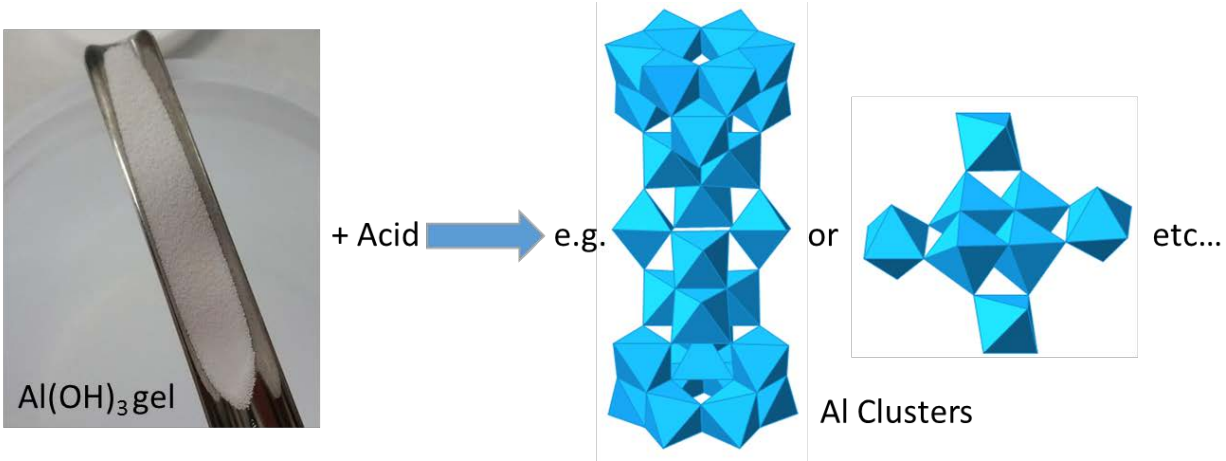

Figure 4.1 Dissolution method approach. $Al(OH)_3$ dried gel dissolved with various acids can form numerous Al clusters, including Al_{13}^f, Al_{13}^k, Al_{30}, and Al_8.

the identity of the cations and anions present in solution. The anion is only introduced in the form of an acid (i.e. formic, phosphoric, hydrochloric, nitric, sulfuric, selenic acid, etc.) The introduction of one anion can allow a more precise study of the anion effects on speciation and potentially an improved and clean synthesis of specific clusters of choice. This chapter (Chapter 4) utilizes this dissolution method with sulfuric and selenic acid to synthesize both the aluminum hydroxide octamer and a monomer, respectively. The next chapter (Chapter 5) will utilize this dissolution method using formic acid to isolate three Al_{30} clusters.

4.3 Synthesis and Characterization of the Aluminum Octamer with Sulfate

Aqueous aluminum chemistry displays a rich array of oxo-hydroxo clusters, exemplified by *flat*-Al_{13} $[Al_{13}(OH)_{24}(H_2O)_{24}{}^{15+}]$,[76, 78] isomers of the Al_{13}-Keggin ion $[Al_{13}O_4(OH)_{24}(H_2O)_{12}]^{7+}$,[79-80] and larger clusters like the Al_{30} cation $[Al_{30}O_8(OH)_{56}(H_2O)_{26}]^{18+}$.[81-82] Although researchers have explored this chemistry for more than a century, novel species continue to emerge. In 2005, Casey and co-workers reported the octameric aluminum hydroxide cluster $Al_8(OH)_{14}(H_2O)_{18}(SO)_5$ (Al_8) as a side product of the aqueous synthesis of the aluminum sulfate dimer $Al_2(OH)_2(H_2O)_8(SO_4)_2$.[83] The octamer was harvested from the reaction solution after nearly 7 years.[83] This long period of time raises questions about whether the cluster may be readily synthesized and whether it even exists in solution. A 2016 report[84] describes the second example of an Al_8 cluster; in this case, the cluster is isolated from an organic solvent and stabilized with trisilanol capping ligands.

To develop a comprehensive understanding of aqueous aluminum chemistry, we must look into scalable synthesis methods and characterize those simple species that exist under consonant reaction conditions. Nature lends insight to potential synthesis methods. Clusters may form along

pathways involving dissolution of aluminum hydroxide solids and clays,[84-87] for example, as products of mineral dissolution in low-pH waters caused by acid-mine drainage or acid rain. Here, we exploit this natural pathway to prepare Al_8 directly and in high yield via dissolution of solid aluminum hydroxide in sulfuric acid. The crystal-producing solutions also aid speciation studies wherein hydroxo and aqua ligands dominate coordination to Al.

Interest in Al_8 extends to geochemistry and beyond, as the precise knowledge of cluster structures enables model studies of mineral-surface interactions and chemistries. Clusters help us describe the bonding of adsorbates to soil minerals, and they aid studies of reaction kinetics at the molecular scale, thereby avoiding extraordinarily complex experiments with minerals suspended in liquids. This understanding may be help in events of environmental contamination events, including the Ajka alumina plant accident in Hungary (2010). Gaining insight into hyroxo-

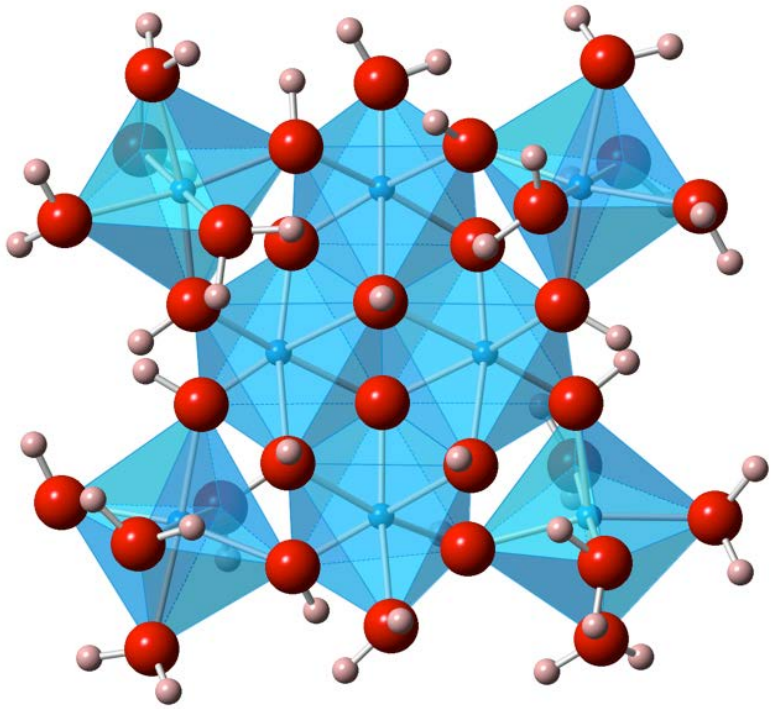

Figure 4.2 Polyhedral structure of the Al_8 cluster (SO_4^{2-} omitted for clarity); blue spheres – Al, red spheres - O, coral spheres – H.

Al cluster chemistry could enable more complete or efficient environmental cleanup as well as an analysis on the potential ramifications of said event. Also, our understanding of hydroxo-Al cluster chemistry guides and advances solution deposition of functional films[88] and improves the performance of high-resolution inorganic nanopatterning.[89]

Here, we prepare Al_8 by a top-down synthesis, i.e., by dissolution of $Al(OH)_3 \bullet 0.7H_2O_{(s)}$ in $H_2SO_{4(aq)}$. Excess $H_2SO_{4(aq)}$ effects full dissolution of aluminum hydroxide at an $Al:SO_4^{2-}$ ratio of 1:1 and $[Al_{tot}]$ = 1 M. The mixture is stirred and heated at 70°C until the hydroxide dissolves completely, typically in 24 h. The solution is passed through a 0.4-µm nylon syringe filter into a 20 mL scintillation vial. Crystals grow by slow evaporation in uncapped vials over a period of one to two weeks.

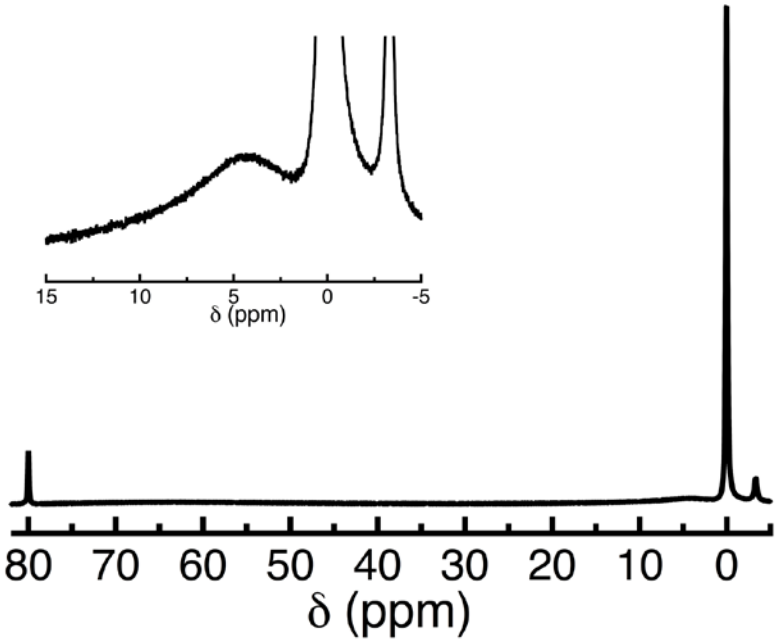

Figure 4.3 ^{27}Al NMR spectrum of the cluster containing solution ($[Al_{tot}]$ = 1 M). The inset highlights the spectral region of six-coordinate aluminum.

We find the Al_8 crystals to be highly twinned, in line with the previous report.[83] We collected diffraction data to confirm that both the unit-cell parameters and the crystal structure (**Figure 4.2**) matched earlier findings. The crystals lose water on removal from the growth solution and convert to an amorphous product. Consequently, partially dehydrated crystals exhibit low solubility in water, which makes the reaction mixtures important for study of the existence and persistence of Al_8 in solution. Previous studies on Al_8 do not describe characterization of these aqueous solutions.

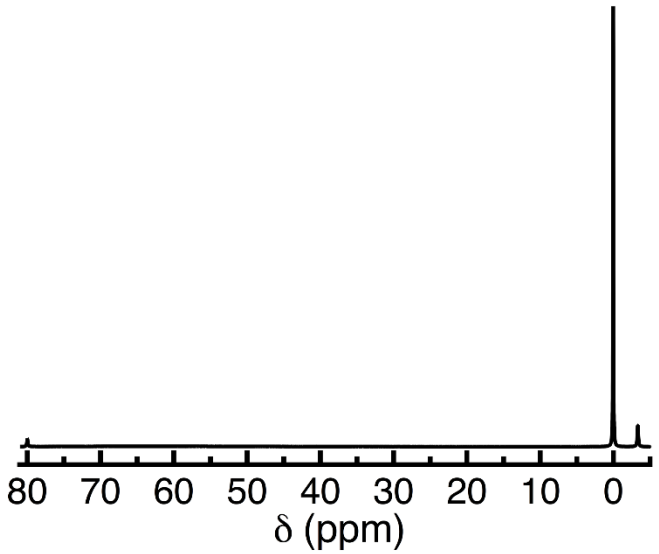

Figure 4.4 ^{27}Al NMR spectrum of 0.5 M $Al_2(SO_4)_3$ solution (1 M Al^{3+})

^{27}Al NMR spectroscopy of a 1 M Al reaction solution shows three separate signals (**Figure 4.3**). We assign the intense signal centered at 0 ppm to $Al(H_2O)_6^{3+}$ and associated monomeric hydrolysis complexes. The signal at -3.3 ppm corresponds to an inner-sphere sulfato species such as $[Al(H_2O)_5(SO_4)]^+$;[72, 89] the spectrum of a 0.5 M $Al_2(SO_4)_3$ solution (**Figure 4.4**), for example, also shows this signal. An electrospray ionization mass spectrum (ESI MS, **Table 4.1**) of the 1 M Al reaction solution also exhibits signals consistent with a monomeric Al-SO_4^{2-} complex.

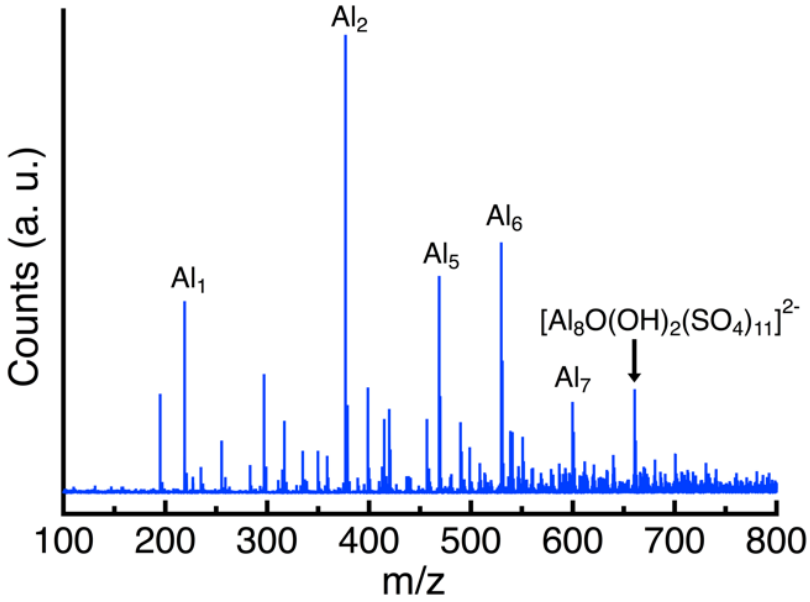

Figure 4.5 ESI-MS spectra of the [Al_{tot}] = 1 M solution. Data are normalized to the strongest peak in each spectrum over the selected range. See ***Table 4.1*** *for detailed peak assignments.*

Table 4.1 List of the assignments on the region of interest of the ESI-MS spectra of the solution with [Al_{tot}] = 1 M

Composition	m/z (measured)	m/z (calculated)	Composition	m/z (measured)	m/z (calculated)
$[H_3(SO_4)_2]^-$	194.9289	194.9275	$[Al_5O(OH)(SO_4)_7(H_2SO_4)]^{2-}$	468.7721	468.768
$[Al(SO_4)_2]^-$	218.8877	218.8855	$[Al_6O(OH)_2(SO_4)_8]^{2-}$	489.7567	489.7523
$[Al_2(OH)_3(SO_4)_2]^-$	296.8776	296.8753	$[Al_6O(OH)_2(SO_4)_8(H_2O)]^{2-}$	498.7605	498.7576
$[Al(SO_4)_2(H_2SO_4)]^-$	316.8567	316.8529	$[Al_5(OH)(SO_4)_8(H_2SO_4)]^{2-}$	508.7532	508.7464
$[H_3Al(OH)(SO_4)_3]^-$	334.8656	334.8635	$[Al_6(OH)_2(SO_4)_9]^{2-}$	529.7346	529.7307
$[Al_4O_2(SO_4)_5(H_2SO_4)]^{2-}$	358.824	358.8216	$[Al_6(OH)_2(SO_4)_9(H_2O)]^{2-}$	538.7425	538.736
$[Al_2(OH)(SO_4)_3(H_2O)]^-$	376.8354	376.8321	$[Al_7O_2(OH)(SO_4)_9]^{2-}$	550.7196	550.715
$[Al_4O(SO_4)_6(H_2SO_4)]^{2-}$	398.8117	398.8	$[Al_7O(OH)_3(SO_4)_9]^{2-}$	559.7241	559.7203
$[Al(SO_4)_2(H_2SO_4)_2]^-$	414.8241	414.8203	$[Al_7O(OH)_3(SO_4)_9(H_2O)]^{2-}$	568.7255	568.7256
$[Al_5O(OH)(SO_4)_7]^{2-}$	419.789	419.7843	$[Al_6(SO_4)_{10}(H_2O)_2]^{2-}$	578.721	578.7144
$[HAl_2(SO_4)_4(H_2O)]^-$	456.7929	456.7889	$[Al_7O(OH)(SO_4)_{10}]^{2-}$	590.7014	590.6934

Its occurrence in the reaction solution likely arises from the excess sulfate added as sulfuric acid, which is required to dissolve solid aluminum hydroxide completely. The third broad signal,

centered at +4 ppm, indicates clusters built from six-coordinate aluminum ions. We and others have yet to assign this signal to specific species.[72, 89] One possibility is the cubane-like unit of $Al_3(\mu_3\text{-}OH)(\mu_2\text{-}OH)_3$, which is found in both Al_8 and *flat*-Al_{13} clusters.[76, 78] Al_8, and the structurally similar *flat*-Al_{13}, present aluminum ions bound only by a total of six aqua and hydroxo ligands, i.e., Al does not directly bind sulfate. In sum, the NMR data suggest the 1 M reaction solution contains a mixture of monomeric and larger hydroxo Al clusters with Al bound exclusively in distorted octahedral environments.

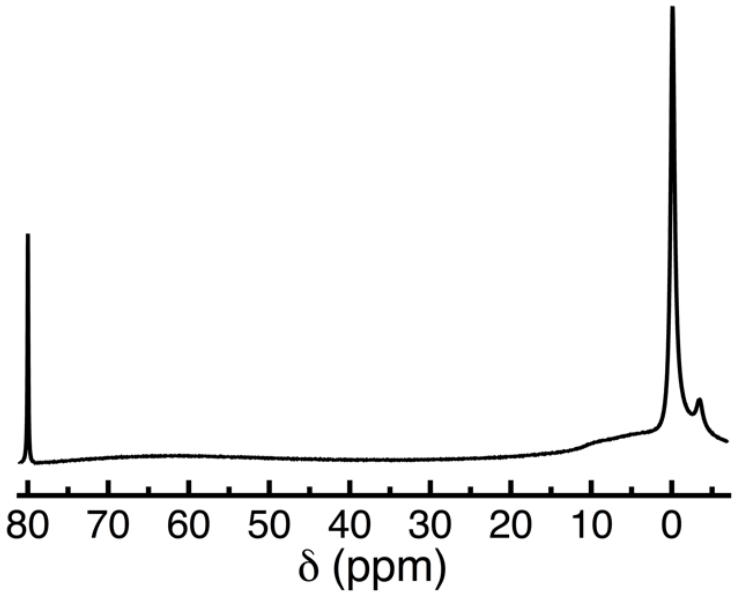

Figure 4.6 ^{27}Al NMR spectrum of 3 M Al solution. The signal at 80 ppm corresponds to the external intensity standard $[Al(OH)_4]^-$.

Figure 4.5 shows the ESI-MS data of the 1 M reaction mixture. The spectrum reveals a parent octameric species and several smaller nuclearity species; some of the smaller species likely derive from Al_8 fragmentation during the ionization process. The presence of small clusters, including aluminum-sulfate dimers, is also reasonable, considering the solution was prepared with excess H_2SO_4 (aq).

To prepare a solution closer to the Al_8 stoichiometry (8:5 ratio of $Al:SO_4^{2-}$), we increased $[Al_{tot}]$ from 1 to 3 M, following the synthesis procedure described above. The solution pH decreased slightly from 3.37 for the 1 M solution to 3.24 for the 3 M solution. Observationally, the 3 M solution was more viscous, but filtration still produced visually clear solutions for NMR and SWAXS (small and wide angle X-ray scattering) studies.

Table 4.2 ^{27}Al NMR signal Intensities divided by the internal standard for three solutions.

Signal (ppm)	1 M Al_8	3 M Al_8	0.5 M $Al_2(SO_4)_3$

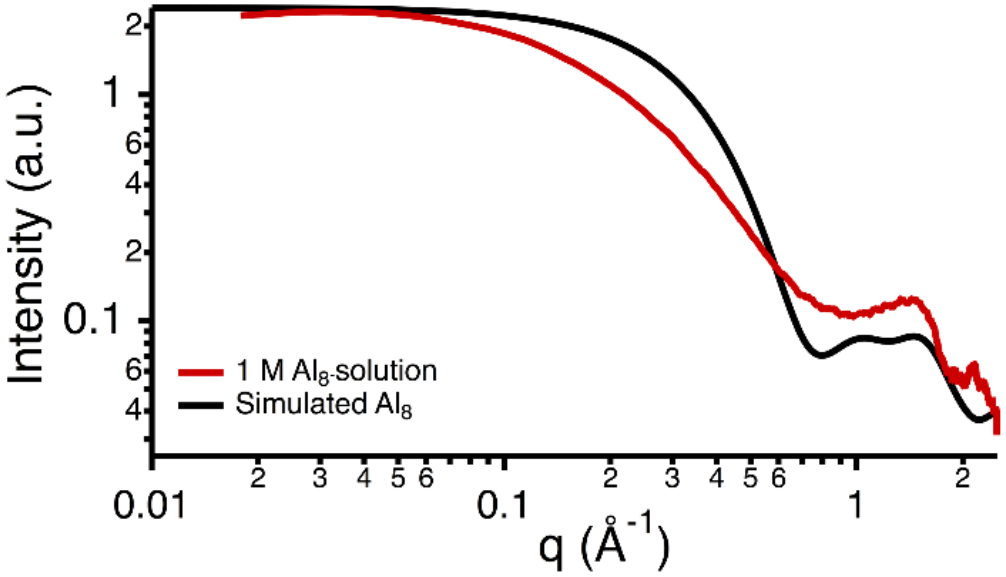

Figure 4.7 SWAXS curve of the as-prepared $[Al_{tot}]$ = 1 M solution containing and simulated Al_8 curve. Data are normalized for ease of comparison.

Figure 4.6 shows the ^{27}Al NMR spectrum of the 3 M solution to be similar to the 1 M solution, although the signals (0 and -3.3 ppm) assigned to monomeric Al are weaker relative to those assigned to the putative clusters (*cf.*, **Table 4.2**). Also, the broad signal or set of overlapping signals in the range 4-12 ppm is much broader in the 3 M solution than in the 1 M solution. The broad resonance marks the higher concentration of cluster species built from six-coordinate Al

in the concentrated solution. Again, this broad signal suggests Al_8 is likely present in the solution. Overall, the NMR data suggest clusters endure at higher solution concentrations.

Despite its capabilities for species characterization, X-ray scattering has been applied infrequently to identify clusters in solution.[67, 90-92] It uniquely complements the molecular-scale structural information derived from NMR. **Figure 4.7** shows scattering data for the 1 M Al reaction solution and a simulated curve for Al_8. The plateau in the experimental curve for $q < 0.7$ indicates the solution contains nearly monodisperse, spherical species. In the Guinier region ($q = 0.06 – 0.5$ $Å^{-1}$), the drop in the solution scattering intensity relative to the simulated curve indicates the presence of scattering species larger than Al_8.

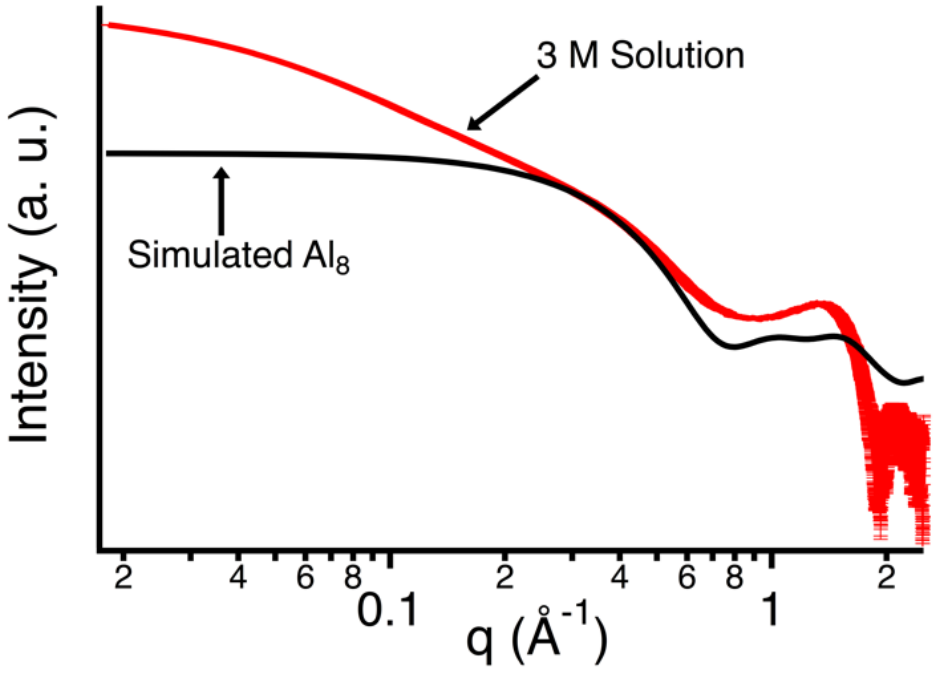

Figure 4.8 SWAXS curve (red) of the 3 M Al solution and simulated curve (black) for Al_8 from the crystal structure file. Data are normalized to the Guinier region to ease comparison.

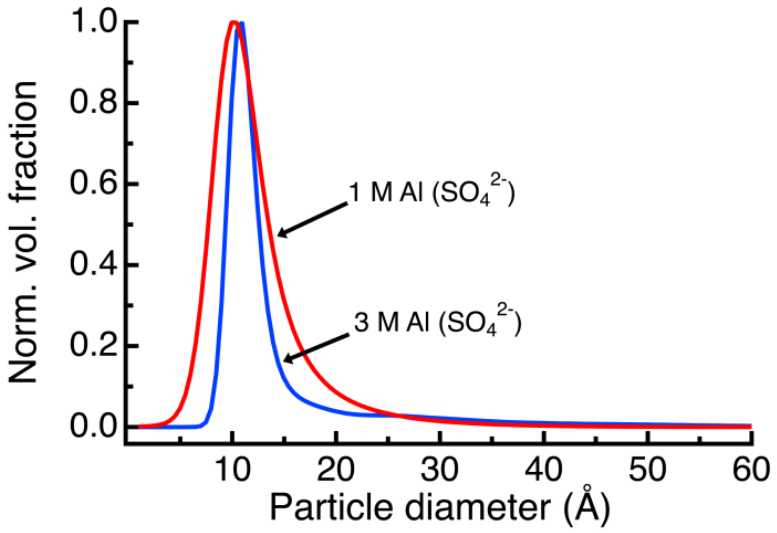

Figure 4.9 Particle size distribution analysis of the SWAXS data of the 1 M (red) and 3 M (blue) reaction mixtures.

Figure 4.8 shows SWAXS data for a concentrated 3 M reaction solution. The negative slope in the region $q = 0 - 0.2$ Å^{-1} indicates a size distribution of species or aggregation arising from the high solution concentration. The Guinier region of the scattering curve ($q = 0.2 - 0.6$ Å^{-1}) matches the simulated scattering for Al_8 reasonably well. Guinier analysis yields a radius of gyration, a shape independent root mean square of the distance of all electrons from the center of a scattering particle. The derived radius, 6.0 Å, compares to the radius of 6.3 Å for Al_8. We performed a size-distribution analysis with the scattering data of the 1 and 3 M solutions. **Figure 4.9** and **Table 4.3** show the dominant species in each solution has an average diameter between 10.1 and 10.7 Å, consistent with the long dimension of Al_8. Secondary species at 14.5-nm

Table 4.3 Gaussian peak fitting of size distribution analysis

Solution	Diameter (Å)	FWHM	Peak area (%)
1 M reaction solution	10.1	5.0	74
	14.5	9.1	36
3 M reaction solution	10.7	2.7	62
	12.8	2.3	22
	20.7	17.3	16

diameter in the 1 M solution and 12.8 nm in the 3 M solution reveals the dilute solution has the greater polydispersity, a result anticipated above from the scattering curve (**Figure 4.7**).

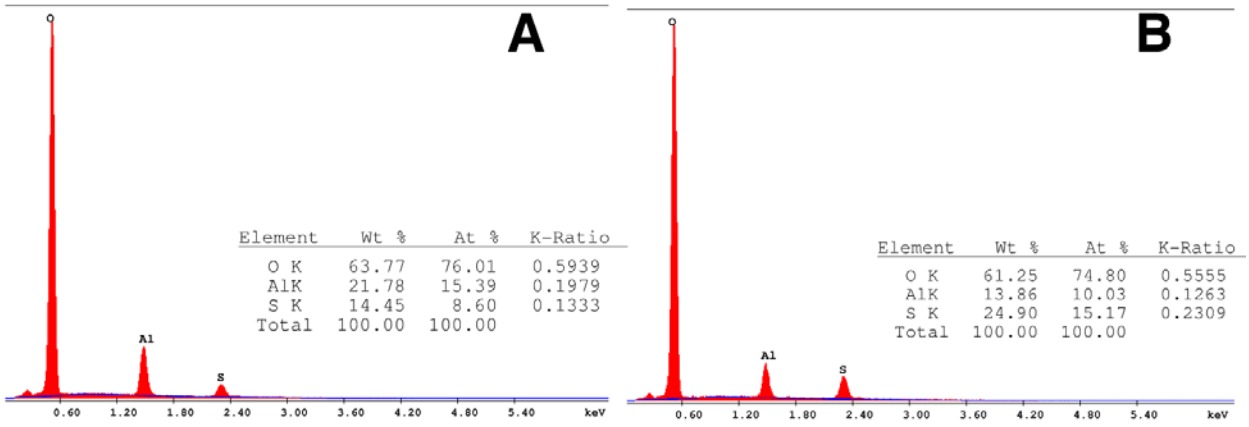

Figure 4.10 EDS data for the bulk solid from the 3 M solution (a) and a $Al_2(SO_4)_3$ control (b)

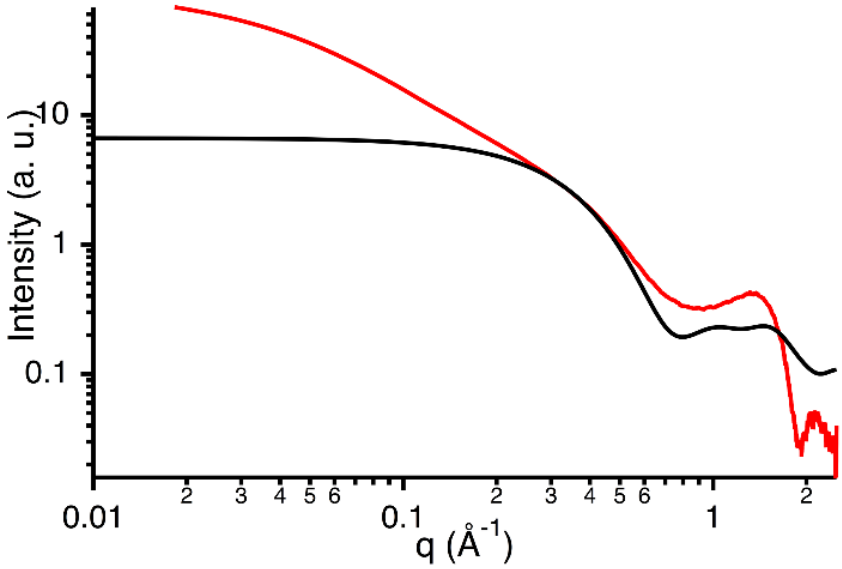

Figure 4.11 SWAXS curve for the as-prepared 3 M Al solution with SeO_4^{2-} counter ions (red) and a simulated curve for an Al_8 cluster with SeO_4^{2-} counterions. These data were normalized to the Guinier region for ease of comparison.

The 3 M solution readily produces Al_8 crystals in high yield - 84% - which further signals the presence of Al_8 in solution. Energy-dispersive X-ray spectroscopy elemental analysis shows elemental ratios for Al_8 crystals of Al:S = 8:4.5 (**Figure 4.10**), close to that of the single-crystal stoichiometry of $Al:SO_4$ = 8:5. From thermogravimetric analysis, we deduce a stoichiometry of

$Al:SO_4$ = 8:5. In this evaluation, we assume evolution of SO_3(g) dominates mass loss above 425 ^oC. We considered ESI-MS analysis to further confirm the crystal composition, but the analysis requires a dilute solution of the cluster. On dilution, however, the solution pH rises, condensation occurs, and a precipitate forms, which obviates the MS analysis. An alternative approach to sample injection must be developed to analyze solutions with the $Al:SO_4$ = 8:5 ratio of the crystal.

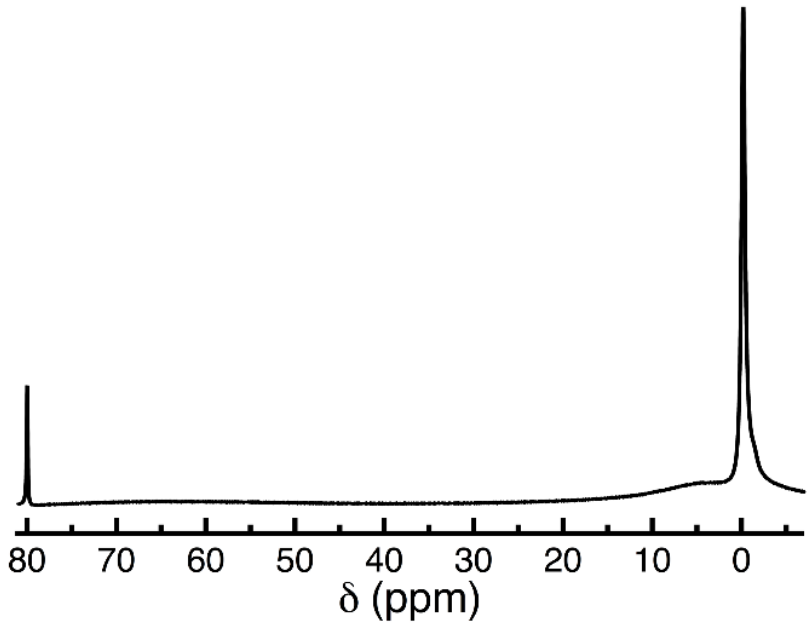

Figure 4.12 ^{27}Al NMR spectrum of 3 M Al^{3+} solution with SeO_4^{2-} counterions.

Because sulfate and selenate are often interchangeable in cluster synthesis,[79, 93] we examined synthesis of the SeO_4^{2-} analogue via dissolution of $Al(OH)_3 \bullet 0.7H_2O$(s) in $H_2SeO_{4(aq)}$. While we were unsuccessful in attempts to crystallize the Al_8 selenate, the ^{27}Al NMR and SWAXS data again suggest clusters exist in the solution (**Figures 4.11 - 4.14**). Additional study should reveal the nature of the dominant species in the solutions and whether they mimic those found with sulfate or with weakly coordinating ligands.

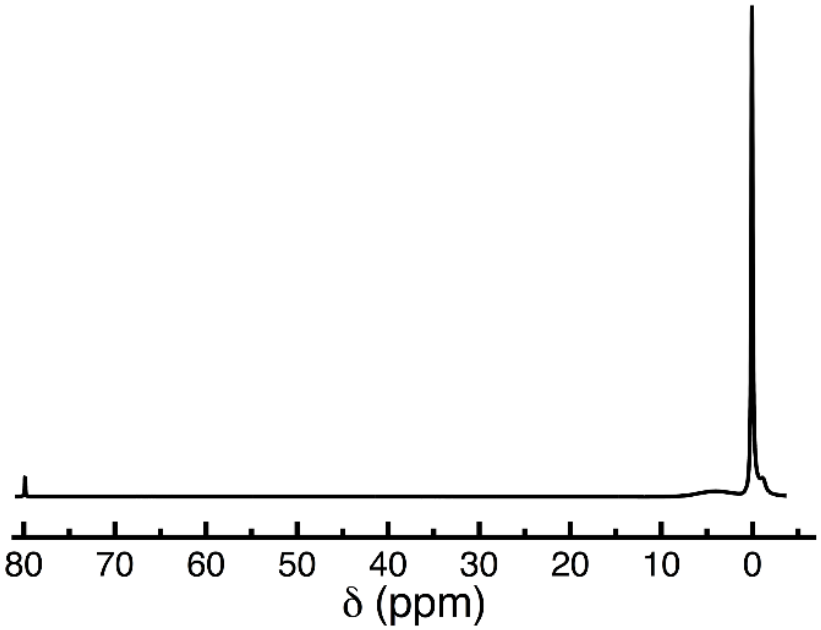

Figure 4.13 ^{27}Al NMR spectrum of a 1 M Al^{3+} solution with SeO_4^{2-} counterions.

We have previously shown the *flat*-Al_{13} cluster serves as a precursor to produce atomically-smooth Al_2O_3 films for both electrical and optical applications.[94-95] Al_8 may be deposited in a similar way to produce an aluminum sulfate film. Electron micrographs (**Figure 4.15**) show a featureless, smooth surface with a continuous, pore-free cross section. The film carries morphological features similar to amorphous Al_2O_3.

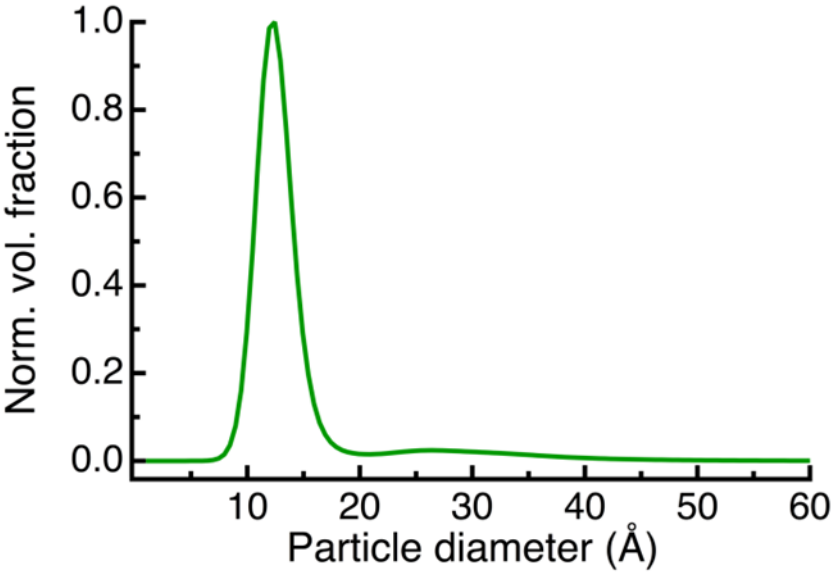

Figure 4.14 Particle size distribution for 3 M solution with SeO_4^{2-} counter ions.

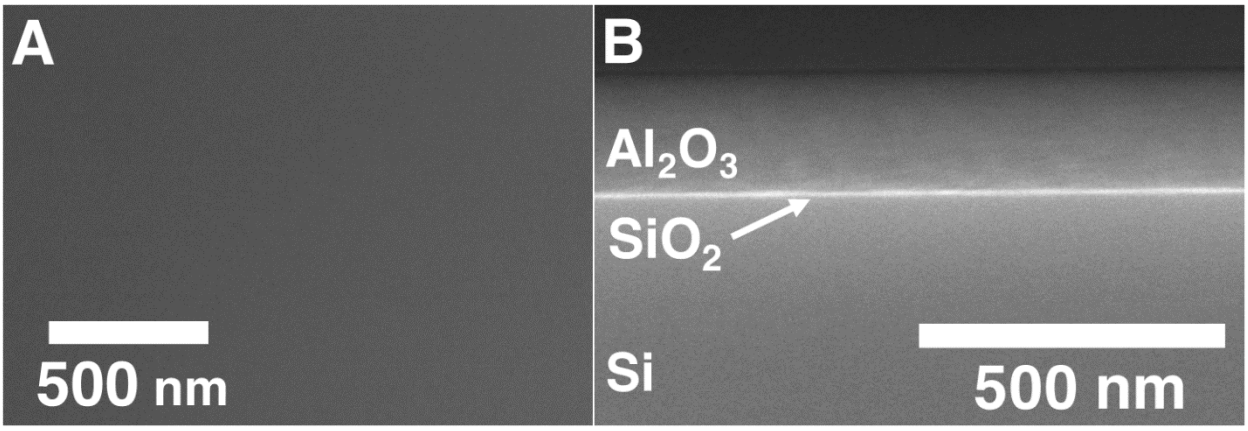

Figure 4.15 Top-down SEM image of a spun-coat film from the Al_8 precursor (a) and the cross-sectional view (b)

4.4 Synthesis and Characterization of the Aluminum Monomer with Selenate

Attempts to isolate the Al_8 cluster with selenate anions were unsuccessful. Spectroscopic evidence does seem to suggest that the Al_8 is present in the Aluminum solutions that utilized dissolution by selenic acid. Interestingly enough, an aluminum monomer $(Al(H_2O)_6)_2(SeO_4)_3 \bullet 4.5\ H_2O$ was isolated as a single crystal instead of the aluminum octamer. **Figure 4.16** shows the thermal ellipsoid diagram representation of the crystal structure obtained from single crystal XRD for this monomer detailing the asymmetric unit. The polyhedral representation (**Figure 4.17**) of this structure is also given, showing the noticeable void spaces that contain solvent (H_2O). This crystal structure has not been isolated previously, despite the analogous sulfate version of this monomer in the same hydration state, $(Al(H_2O)_6)_2(SO_4)_3 \bullet 4.4\ H_2O$.[96-97]. The unit cell of the previously reported aluminum monomer with sulfate has a triclinic cell represented by the unit-cell parameters a = 6.061 Å, b = 7.425 Å, c = 26.975 Å, α = 88.06°, β = 90.03°, γ = 82.34°, and V = 1202.38 Å^3. These results can be compared to the unit cell information, and other selected crystallographic information, and refinement information available in **Table 4.4** for the new $(Al(H_2O)_6)_2(SeO_4)_3 \bullet 4.5\ H_2O$. Additional details regarding the Bond distances (**Table 4.5**), Bond

Angles (**Table 4.6**), and Hydrogen Bonding distances and angles (**Table 4.7**) for $Al(H_2O)_6)_2(SeO_4)_3$

• 4.5 H_2O are also shown here.

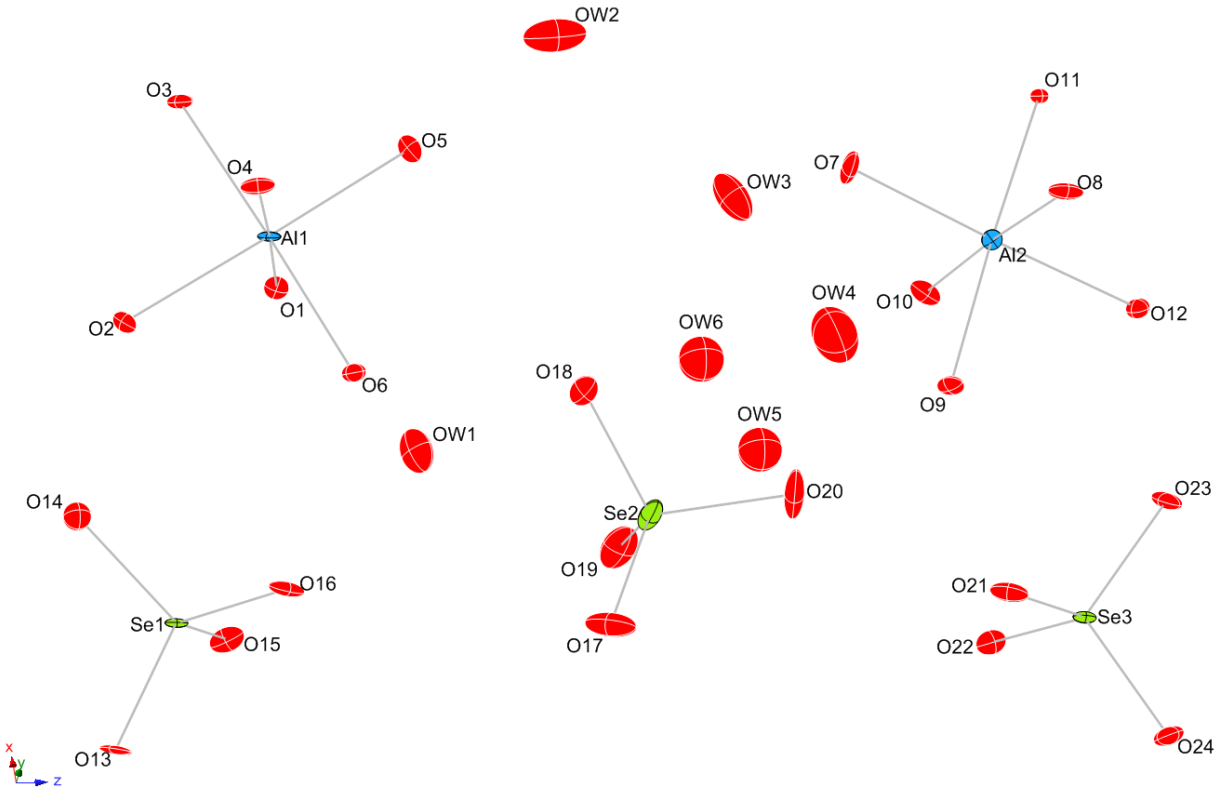

Figure 4.16 Labeled thermal ellipsoid diagram for the asymmetric unit of $(Al(H_2O)_6)_2(SeO_4)_3 \bullet (H_2O)_{4.5}$. H atoms have been removed for clarity. OW4, OW5, and OW6 are each half occupied.

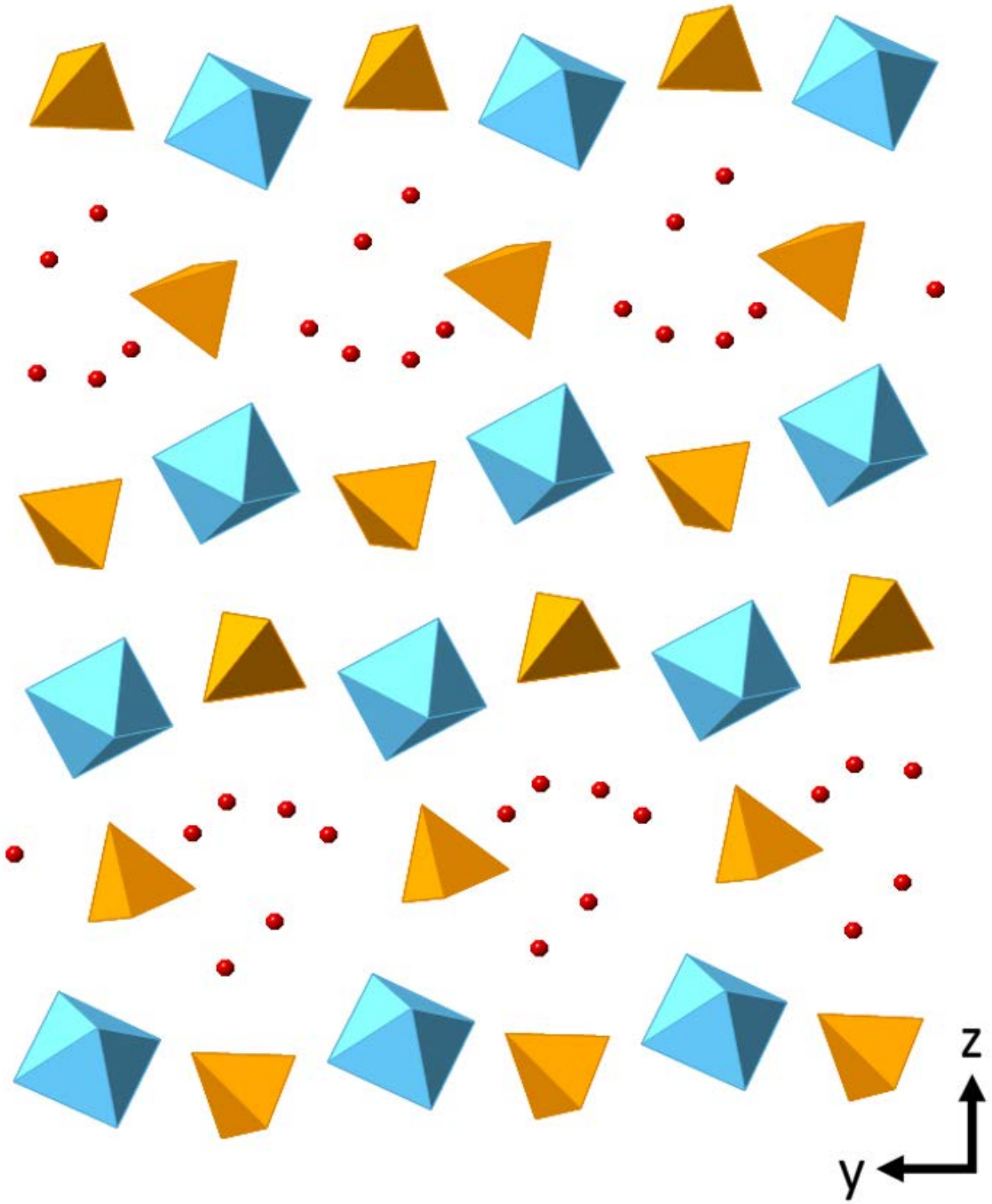

Figure 4.17 Polyhedral representation down the x-axis of $Al(H_2O)_6)_2(SeO_4)_3 \bullet 4.5\ H_2O$ showing interstitial waters as red spheres, Al^{3+} as a blue octahedron, and the selenate as the orange tetrahedron.

Table 4.4 Selected Crystallographic information and Data Refinement Determination for $(Al(H_2O)_6)_2(SeO_4)_3 \bullet 4.5\ H_2O$

Name	Aluminum Selenate Monomer
Formula	$(Al(H_2O)_6)_2(SeO_4)_3 \bullet 4.5\ H_2O$ $Al_3H_{30}O_{28.5}Se_3$
FW (g/mol)	777.08
T (K)	100(2)
Space group	*P-1*
Crystal size (mm)	0.010 x 0.080 x 0.090
a (Å)	6.1114(3)
b (Å)	7.5464(3)
c (Å)	27.5452(12)
α (°)	93.421(2)
β (°)	90.177(2)
γ (°)	97.730(2)
V (Å³)	1256.49
Z	2
*ρ*calc (g/cm^3)	0.1027
F(000)	772
Theta range (°)	2.22 to 26.37
Data collected	$-16 < h < 16$ $-23 < k < 23$ $-24 < l < 24$
Reflections collected/unique	70484/5156 [*Rint* = 0.0901]
GOF on F^2	1.142
Final R indices [I > 2σ(I)]	R1 = 0.0375, wR2 = 0.0684
R indices (all data)	R1 = 0.0491, wR2 = 0.0714
Largest diff. peak and hole (eÅ^{-3})	1.516 and -1.081

Table 4.5 Bond Distances (Å) for $(Al(H_2O)_6)_2(SeO_4)_3 \bullet 4.5\ H_2O$

Se1-O14	1.630(3)	Se1-O16	1.633(3)
Se1-O13	1.639(3)	Se1-O15	1.642(3)
Se2-O17	1.625(3)	Se2-O20	1.633(3)
Se2-O18	1.635(3)	Se2-O19	1.644(3)
Se3-O21	1.627(3)	Se3-O23	1.637(3)
Se3-O24	1.641(3)	Se3-O22	1.641(3)
Al1-O5	1.867(3)	Al1-O1	1.869(3)
Al1-O4	1.879(3)	Al1-O3	1.882(3)
Al1-O6	1.882(3)	Al1-O2	1.889(3)
Al2-O7	1.862(3)	Al2-O11	1.873(3)
Al2-O9	1.873(3)	Al2-O10	1.878(3)
Al2-O12	1.887(3)	Al2-O8	1.888(3)
OW1-H25	0.84(2)	OW1-H26	0.83(2)
OW2-H27	0.83(2)	OW2-H28	0.818(19)
OW3-H29	0.848(19)	OW3-H30	0.84(2)
O1-H1	0.83(2)	O1-H2	0.832(19)
O2-H3	0.842(19)	O2-H4	0.838(19)
O3-H5	0.840(19)	O3-H6	0.83(2)
O4-H7	0.83(2)	O4-H8	0.83(2)
O5-H9	0.827(19)	O5-H10	0.82(2)
O6-H11	0.84(2)	O6-H12	0.829(19)
O7-H13	0.838(19)	O7-H14	0.83(2)
O8-H15	0.83(2)	O8-H16	0.82(2)
O9-H17	0.83(2)	O9-H18	0.830(19)
O10-H19	0.85(2)	O10-H20	0.84(2)
O11-H21	0.84(2)	O11-H22	0.835(19)
O12-H23	0.83(2)	O12-H24	0.84(2)

Table 4.6 Selected Bond Angles (°) for $(Al(H_2O)_6)_2(SeO_4)_3 \bullet 4.5\ H_2O$

O14-Se1-O16	109.22(15)	O14-Se1-O13	110.20(14)
O16-Se1-O13	110.13(15)	O14-Se1-O15	109.71(14)
O16-Se1-O15	109.57(15)	O13-Se1-O15	107.99(14)
O17-Se2-O20	109.31(17)	O17-Se2-O18	111.35(17)
O20-Se2-O18	107.98(18)	O17-Se2-O19	109.42(17)
O20-Se2-O19	109.31(17)	O18-Se2-O19	109.43(17)
O21-Se3-O23	109.45(15)	O21-Se3-O24	109.89(15)
O23-Se3-O24	110.21(15)	O21-Se3-O22	109.45(15)
O23-Se3-O22	109.66(15)	O24-Se3-O22	108.16(15)
O5-Al1-O1	90.69(13)	O5-Al1-O4	90.75(14)
O1-Al1-O4	178.52(15)	O5-Al1-O3	89.60(14)
O1-Al1-O3	89.95(13)	O4-Al1-O3	89.72(13)
O5-Al1-O6	91.94(14)	O1-Al1-O6	90.47(13)
O4-Al1-O6	89.81(13)	O3-Al1-O6	178.39(14)
O5-Al1-O2	177.79(15)	O1-Al1-O2	87.65(13)
O4-Al1-O2	90.90(14)	O3-Al1-O2	88.95(13)
O6-Al1-O2	89.52(13)	O7-Al2-O11	89.54(14)
O7-Al2-O9	92.75(14)	O11-Al2-O9	177.70(14)
O7-Al2-O10	91.92(15)	O11-Al2-O10	90.48(13)
O9-Al2-O10	89.51(14)	O7-Al2-O12	177.96(15)
O11-Al2-O12	88.44(13)	O9-Al2-O12	89.27(14)
O10-Al2-O12	87.77(14)	O7-Al2-O8	90.57(15)
O11-Al2-O8	90.24(14)	O9-Al2-O8	89.67(14)
O10-Al2-O8	177.41(16)	O12-Al2-O8	89.76(14)

Table 4.7 Hydrogen Bond Distances (Å) and Angles (°) for $Al(H_2O)_6)_2(SeO_4)_3 \bullet 4.5\ H_2O$

	Donor-H	Acceptor-H	Donor-Acceptor	Angle
O1-H1···O16	0.83(2)	1.83(2)	2.654(4)	170.(7)
O1-H2···OW1	0.832(19)	1.80(3)	2.610(4)	163.(7)
O2-H3···O14	0.842(19)	1.83(3)	2.658(4)	166.(7)
O2-H4···O13	0.838(19)	1.82(2)	2.654(4)	171.(6)
O3-H5···O14	0.840(19)	1.80(2)	2.637(4)	177.(6)
O3-H6···O15	0.83(2)	1.85(2)	2.679(4)	174.(7)
O4-H7···O13	0.83(2)	1.85(2)	2.668(4)	166.(6)
O4-H8···O15	0.83(2)	1.84(2)	2.665(4)	179.(7)
O5-H9···O17	0.827(19)	1.78(2)	2.603(4)	176.(7)
O5-H10···OW2	0.82(2)	1.83(3)	2.624(5)	162.(6)
O6-H11···O16	0.84(2)	1.85(2)	2.677(4)	170.(6)
O6-H12···O18	0.829(19)	1.76(2)	2.580(4)	170.(7)
O7-H13···OW3	0.838(19)	1.78(2)	2.603(4)	169.(7)
O7-H14···O20	0.83(2)	1.82(2)	2.646(4)	171.(7)
O8-H15···O22	0.83(2)	1.82(2)	2.648(4)	178.(6)
O8-H16···O24	0.82(2)	1.85(2)	2.669(4)	170.(6)
O9-H17···O21	0.83(2)	1.83(2)	2.657(4)	175.(6)
O9-H18···O20	0.830(19)	1.78(3)	2.561(4)	155.(6)
O10-H19···OW5	0.85(2)	1.72(3)	2.551(8)	165.(6)
O10-H19···OW6	0.85(2)	1.90(4)	2.662(8)	150.(6)
O10-H20···O21	0.84(2)	1.86(3)	2.671(4)	162.(6)
O11-H21···O22	0.84(2)	1.80(2)	2.635(4)	176.(6)
O11-H22···O23	0.835(19)	1.83(2)	2.657(4)	171.(6)
O12-H23···O23	0.83(2)	1.80(2)	2.636(4)	177.(7)
O12-H24···O24	0.84(2)	1.81(2)	2.646(4)	175.(6)
OW1-H25···O19	0.84(2)	1.97(3)	2.787(5)	164.(6)
OW1-H26···OW2	0.83(2)	2.03(3)	2.785(5)	151.(6)
OW2-H27···O19	0.83(2)	2.05(3)	2.845(5)	162.(6)
OW2-H28···OW1	0.818(19)	2.02(3)	2.785(5)	156.(7)
OW3-H29···OW4	0.848(19)	2.16(4)	2.885(10)	143.(5)
OW3-H29···OW5	0.848(19)	1.93(3)	2.712(8)	153.(6)
OW3-H29···OW6	0.848(19)	2.63(5)	3.237(8)	130.(5)
OW3-H30···O18	0.84(2)	1.90(2)	2.740(5)	178.(6)

4.5 Experimental

We prepared solutions by dissolving $Al(OH)_3 \bullet 0.7H_2O$ (Alfa Aesar) in $H_2SO_{4(aq)}$ (Mallinckrodt) with an $Al:SO_4^{2-}$ ratio of 1:1. After adding the $Al(OH)_3 \bullet 0.7H_2O$, the slurry was stirred under mild heat (70 ^oC) overnight to produce a colorless solution. Similarly, we prepared a solution by dissolving $Al(OH)_3 \bullet 0.7H_2O$ in an aqueous solution of $Al_2(SO_4)_3 \bullet 18H_2O$ (J. T. Baker), with an $Al:SO_4^{2-}$ ratio of 1:1. We dissolved $Al(OH)_3 \bullet 0.7H_2O$ in 40% wt $H_2SeO_{4(aq)}$ to produce solutions with $Al:SeO_4^{2-}$ ratios of 1:1.4 and 1:1. Solutions of $[Al_{tot}]$ = 3 M were prepared with $Al:SO_4^{2-}$ and $Al:SeO_4^{2-}$ ratios of 8:5 and 8:6, respectively; the $Al(OH)_3 \bullet 0.7H_2O$ starting material was less soluble in $H_2SeO_{4(aq)}$ than in $H_2SO_{4(aq)}$.

Single crystals grew via slow evaporation in open scintillation vials, typically forming within 2 weeks. They were isolated from the mother liquor, immediately coated in oil, and placed on a Bruker D8 Quest X-ray diffractometer equipped with Mo Kα radiation (λ = 0.71017 Å), a CMOS detector, and an Oxford Cryosystems Cryostream 800 low-temperature attachment. Data were collected at 100 K. Crystals from dissolution in $Al_2(SO_4)_3 \bullet 18H_2O$ and $H_2SO_{4(aq)}$ have triclinic cells represented by the unit-cell parameters a = 9.218(2) Å, b = 12.002(2) Å, c =14.618(3) Å, α = 99.878(7)°, β = 102.863(6)°, γ = 110.204(5)°, and V = 1424.1(4) $Å^3$. These parameters, as well as refined atomic parameters, match the crystallographic results reported previously for $[Al_8(\mu_3\text{-}OH)_2(\mu_2\text{-}OH)_{12}(H_2O)_{18}](SO_4)_5 \bullet 16\ H_2O$.[83] Crystals isolated from $H_2SeO_{4(aq)}$ were determined to be $Al(H_2O)_6)_2(SeO_4)_3 \bullet 4.5\ H_2O$, a structure that has not previously been reported.

Crystals were imaged using a FEI QUANTA 600F environmental scanning electron microscope (SEM) and analyzed using X-ray energy dispersive spectroscopy (EDS).

Prior to thin-film deposition, substrates were treated in a low-energy O_2 plasma to create a clean, hydrophilic surface. The films were deposited onto 100-nm thermally grown SiO_2/Si. Films were deposited by spin coating the aqueous Al_8 precursor at 3000 rpm for 30 s. After deposition, the films were baked at 300 °C for 1 min and then annealed to 500 °C. Top-down and cross-sectional SEM images of thin films were collected on a FEI Helios 650 dual beam SEM.

^{27}Al NMR spectra were collected on a Bruker 400-MHz DPX-400 Spectrometer with samples in a 90% H_2O-10% D_2O solution. An insert containing $NaAl(OH)_4$ (0.04 M) served as an internal standard in an external coaxial glass NMR insert for determination of chemical shifts and intensities.

Small and wide angle X-ray scattering data were collected on an Anton Paar SAXSess with Cu-Kα radiation (λ =1.54 Å) and a 2-D image plate detector with a sample-to-image-plate distance of 26.1 cm. Data were collected with line collimation over the q range 0.018-2.5 $Å^{-1}$. Solutions were contained in 1.5-mm borosilicate glass capillaries and exposed to X-rays for 30 min. Data were collected and initially process with the SAXSquant software package. Data were analyzed with Igor Pro software and Irena macros. SolX software produced simulated scattering curves from the structural data described above.

ESI-MS measurements were made with an Agilent 6230 ESI-MS system comprising a Time-of-Flight (TOF) mass spectrometer coupled to an electrospray ionizer. 10-µL volumes of the as-prepared solutions ($[Al^{3+}]$ = 0.1-0.2 M) were first mixed with water, then injected into the ESI-MS system with an Agilent 1260 Infinity quaternary pump at a flow rate of 0.4 mL min^{-1}. Solutions were nebulized with the aid of heated N_2(g) (325°C) flowing under a pressure of 35 psig (241 kPa) at 8 L min^{-1}. Voltages of the capillary, skimmer, and RT octopole were set at 3500, 65 and 750 V,

respectively, while the voltage of the fragmenter was set at 100 V. The data were collected in negative ion mode.

4.6 Conclusions

In summary, this study shows the Al_8 aluminum cluster forms readily by simple dissolution of aluminum hydroxide in sulfuric acid; an observation that mirrors natural processes, namely, the effects of acid rain on soil. The combination of NMR, ESI-MS, and SAXS data reveals Al_8 persists in both dilute and concentrated solutions. X-ray diffraction results show it readily crystallizes from these solutions in high yield. Together, the solution and crystal-growth findings clarify speciation in an environmentally and technologically important aqueous system, while also confirming the unique structure-directing role of sulfate in aluminum hydroxide cluster chemistry. The study removes potentially confounding effects on speciation from cations introduced via conventional base titrations. The acid-dissolution method enables the first top-down preparation of a simple aluminum hydroxide cluster. The results highlight its efficacy and growing and general applicability.[98-101] The method supports scale-up needs for high-purity film precursors in materials science. Notably, the isolation and study of simple and novel hydroxyl-Al clusters can enable more effective study of Al in the environment and then be utilized in Al-containing wastes.

4.7 Acknowledgments

This material is based on work in the Center for Sustainable Materials Chemistry, which is supported by the U.S. National Science Foundation under Grant CHE-1606982. We thank Shawn R. Decker for EDX analysis and Ryan H. Mansergh for the electron micrographs of the thin film.

CHAPTER 5. SYNTHESIS AND CHARACTERIZATION OF NOVEL Al_{30} CLUSTERS FORMED THROUGH DISSOLUTION OF AN AMORPHOUS ALUMINUM HYDROXIDE PRECURSOR: RELATIONSHIPS TO HANFORD TANK WASTE

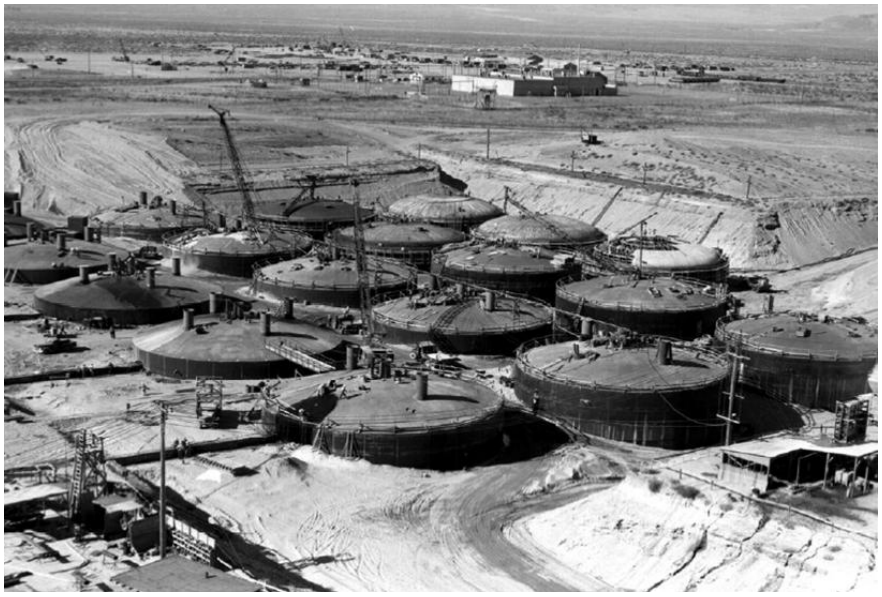

The research in this chapter was completed with help from Mackenzie Cole and Cyrus Mansouri. TOC image is a historical photo of the Hanford Tank Farm, courtesy of the U.S. Department of Energy.[102]

5.1 Abstract

Aluminum clusters may be important in environmental systems as possible vehicles for particle transport of contaminants and a key component of technical problems at the Hanford site. Detailed investigations of these systems can elucidate adsorption sites and provide mechanisms of contaminant transport at the atomistic level. Herein, we describe an approach for synthesizing and isolating clusters from simple starting materials. Aluminum hydroxide gel was used as the pure cluster precursor and can be dissolved using both organic and inorganic acids. In this study, the gel was dissolved in formic acid to mimic small organic acids found both in environmental systems and the Hanford waste site. From these solutions, the Al_{30} polyaluminum oxy-hydroxy clusters were characterized using single crystal X-ray diffraction studies, FTIR, and additional ^{1}H and ^{13}C solution NMR studies. Additional complexity was added to the system in the form of Cu^{2+} cations and other small organic molecules (glycine) to investigate how competing adsorbates behaved within the aluminum hydroxide system.

5.2 Introduction

The Hanford Site is a decommissioned plutonium nuclear production complex in Washington State that currently houses significant amounts of nuclear waste. The original plutonium production facility, reactor B, was completed in 1944 and crucial to the success of the Manhattan project.[103] Plutonium produced at this site was used in the development of the first nuclear weapons, including “fat man”, which was detonated over Nagasaki, Japan in 1945.

Production of this nuclear material for weapons creates a significant amount of waste and the Hanford site currently houses approximately two-thirds of the United States' high level radioactive waste volume.[104] This waste stream includes 53 million US gallons stored in 177 storage tanks and 25 million cubic feet of solid radioactive waste. In more recent years, aging and corrosion of the steel tanks has led to the release of the liquid waste into the surrounding soil and groundwater. In fact, leaks were discovered in at least 14 of the 149 the single-shell tanks,[103] including one tank that had been releasing approximately 640 US gallons per year into the subsurface environment since about 2010 and threatening the nearby Columbia River.[103]

Cleanup of the Hanford Site has been a high priority for the Department of Energy (DOE) due to the high radioactivity and large volumes of waste. A Waste Treatment Plant was developed on-site to assist in the disposal of the liquid wastes stored in these tanks (Chapter 5 TOC image). Unfortunately, persistent problems with legacy undocumented waste and significant leaks have slowed the overall remediation progress. In 2011, the DOE designed a short-term solution for the leaking tanks whereby they removed the liquid waste forms from the 149 single-shell tanks and pumped them into 28 newer double-shell tanks. The new double-shelled tanks have also experienced problems because there is additional release due to construction flaws and/or corrosion. Due to the large amounts of liquid waste and difficulties in storage, it is critical that the waste be properly processed and disposed of in a suitable waste form.

Processing the liquid tank waste is problematic not only because it is radioactive, but also due to its extraordinary chemical complexity.(**Table 5.1**)[105] These wastes are a mix of radionuclides, stable metals, inorganic anions, and organic chelators that were used during the manufacture and separation of Pu for nuclear weapons. The organic molecules present in the

waste streams are chelators designed to complex with various metals for separation techniques.[106] Among these are common chelating agents, like EDTA (Ethylenediaminetetraacetic acid), gluconate, glycolate, citrate and N-(2-hydroxyethyl)-ethylenediaminetriacetic acid (HEDTA)[107] which tend to form aqueous soluble complexes with most metals.[106] Radiolysis of these larger organic molecules occurs within these high radiation fields creating numerous byproducts that exhibit different chemistries and complexes. The major degradation products include formate, acetate, glycolate, glycine, and iminodiacetate.[108]

Table 5.1 Final equilibrium state for SX-108 Hanford tank.[104]

Primary Species	Molarity	Complex	Molarity
$Al(OH)_4^-$	3.19	$NaNO_{3(aq)}$	5.28
$Fe(OH)_4^-$	8.34E−09	$NaNO_{2(aq)}$	2.82
Ca^{2+}	8.33E−06	HCO_3^-	9.92E−08
Ni^{2+}	4.10E−15	$H_3SiO_4^-$	2.33E−08
K^+	7.39E−02	$CaCO_{3(aq)}$	2.38E−09
Na^+	10.98	$SiO_{2(aq)}$	1.36E−12
OH^-	5.23	$NH_{3(aq)}$	1.27E−13
NO_3^-	1.53E−01	H^+	1.18E−14
NO_2^-	1.20	$CO_{2(aq)}$	1.65E−15
Cl^-	3.40E−01	HSO_4^-	8.14E−17
CO_3^{2-}	3.25E−02	$O_{2(aq)}$	1.25E−25
SO_4^{2-}	2.77E−02	Al^{3+}	1.51E−27
CrO_4^{2-}	4.13E−01	Fe^{3+}	7.15E−35
$H_2SiO_4^{2-}$	3.19E−07		
Cs^+	6.51E−05		
H_2O	35.4		

As shown in **Table 5.1**, Al^{3+} is a major inorganic constituent in the tank waste and represents a major barrier to reprocessing. There is approximately 8700 metric tons of aluminum present in the Hanford waste for a total of $3.2x10^8$ moles.[46] The large quantity of Al^{3+} in the tank waste is due to the prevalence in aluminum nitrate as a component of the separation processes and the inclusion of aluminum metal in early uranium fuel cladding materials (1956-1972).[46] For

disposal s in the underground storage tanks, a neutralization reaction was utilized to create soluble aluminate:[46]

$$Al(NO_3)_{3(aq)} + 3\ NaOH_{(aq)} \rightarrow Al(OH)_{3(s)} + 3\ NaNO_{3(aq)}\ Al(OH)_{3(s)} + NaOH_{(aq)} \rightarrow NaAl(OH)_{4(aq)}$$

$$Al^{3+}_{(aq)} + 3\ NaOH_{(aq)} \rightarrow Al(OH)_{3(s)} + 3\ Na^{+}_{(aq)}$$

The precipitation reaction is complete between ~pH 4 and 12.

$$Al(OH)_{3(s)} + NaOH_{(aq)} \rightarrow Al(OH)_4^-{}_{(aq)} + Na^{+}_{(aq)}$$

The $Al(OH)_3$ solid begins dissolving above ~pH 12 to form soluble aluminate ($Al(OH)_4^-$). Some of these tanks have a total concentration of 3 M aluminum, presumably mostly in the form of aluminate, as the pH resides around pH 12.[46] The large quantities of organics and metals, including Al, create a more complex mixed radioactive waste system that is not easily reprocessed due to the behavior of the aluminum hydrolysis products found in the solution.

In the process of transferring the waste from one tank to another, hydrolysis and condensation of the Al^{3+} resulted in the formation of amorphous aluminum hydroxides and clogging the transfer pipes. Due to the complexity of the waste stream, it unclear what exact constituent drove the precipitation process or how the chemical complexity influences the speciation and solubility of Al^{3+} in this system. Factors such as ionic strength and the presence of organic molecules could significantly change the overall rate of the hydrolysis reaction or the resulting species.

Advancing our understanding of aluminum chemistry in complex environments is, therefore, critical for enhancing the reprocessing of the Hanford tank waste. Our work focuses on a molecular-level understanding of these processes, including their mechanism of formation, aggregation, complexation, formation of phases, and nucleation of aluminum hydroxide in aqueous systems. Developing a working knowledge of the factors that influence speciation in

aqueous systems is needed, particularly in complex matrices that contain small organic acids and other metals.

5.3 Basics of Aluminum Hydrolysis in Aqueous Solutions

The chemistry and speciation of Al^{3+} in waste environments is complex because of its amphoteric nature and ability to hydrolyze in aqueous solutions. At low pH values, the hexaaqua coordination complex, with the formula $[Al(H_2O)_6]^{3+}$ dominates in solution. With increasing alkalinity, a water group can become deprotonated to a hydroxo group with a pKa of ~4.70 - 4.85.

$$[Al(H_2O)_6]^{3+} \rightleftharpoons [Al(H_2O)_5OH]^{2+} + H^+$$

This mechanism can continue, forming other hydrated oxy-hydroxy species.[109]

$$[Al(H_2O)_6]^{3+} + (OH^-)_n \rightleftharpoons [Al(H_2O)_{6-n}(OH)_n]^{(3-n)+}$$

At higher concentrations, Al^{3+} dimers form through the mechanism of formation called an olation reaction, which is initiated when a water molecule on hexaaqua complex is displaced by a hydroxo complex, forming a bridging hydroxo between two metal cations.

$$[(H_2O)_5OH]^{2+} + [Al(H_2O)_6]^{3+} \rightleftharpoons [Al(H_2O)_5(\mu\text{-}OH)Al(H_2O)_5]^{5+} + H_2O$$

Figure 5.1 Photo of insoluble amorphous aluminum hydroxide precipitate upon hydrolysis of Al^{3+}, forming a semi-solid with a relatively unknown structure.

Continued hydrolysis and condensation of Al^{3+} occurs throughout neutral region of the pH scale, resulting in the formation of an insoluble amorphous aluminum hydroxide precipitate (**Figure 5.1**). Upon a continued increase in alkalinity the insoluble phase can re-dissolve whereby the ($Al(OH)_4^-$) aluminate anion becomes dominant. Specifics of this transition has undoubtedly been oversimplified and the exact speciation present in this region is likely much more complex than simple aluminate. General aluminum speciation diagrams have been conceived showing a fairly simple scenario, with the initial soluble product identified as the various cationic Al species

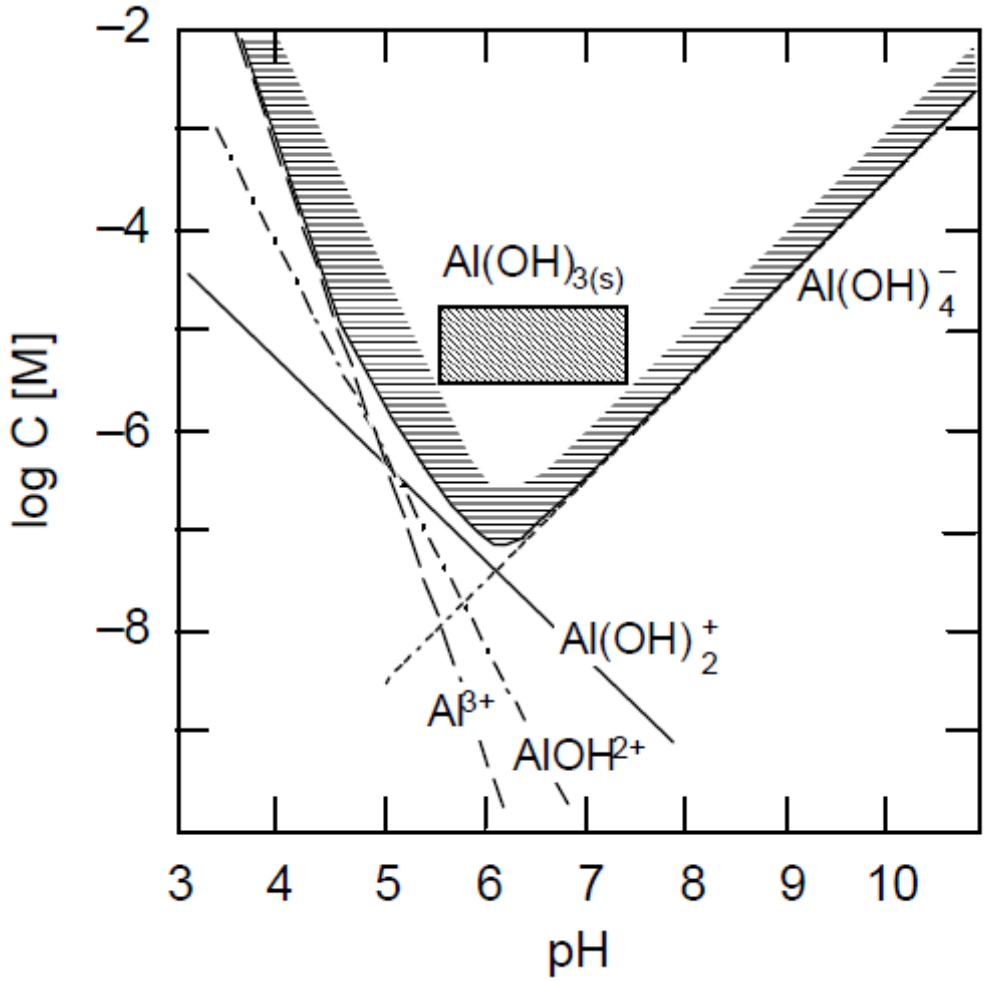

Figure 5.2 LogC – pH diagram for $Al^{3+}_{(aq)}$

followed by the soluble aluminate anion with insoluble aluminum hydroxide present at an intermediate pH. (**Figure 5.2**) These trends can also be represented in a Pourbaix diagram, which again shows seemingly simple Al chemistry. This diagram indicates a transition around pH 4 from cationic Al^{3+} to the insoluble $Al(OH)_3$ and another transition around pH 9 to aluminate. (**Figure 5.3**)[110] This is considered an oversimplified due to the exclusion of polyaluminum clusters under these acidic conditions, specifically from the pH region between about 3 and 5. Perhaps other aluminum clusters are present in the "basic transition" around pH 8-10 in which the diagram indicates a straightforward conversion to aluminate. It should be noted that this is also the way the "acidic transition" was denoted in the literature for years before a more complex and complete understanding emerged showing more complex cationic polyaluminum oxyhydroxy

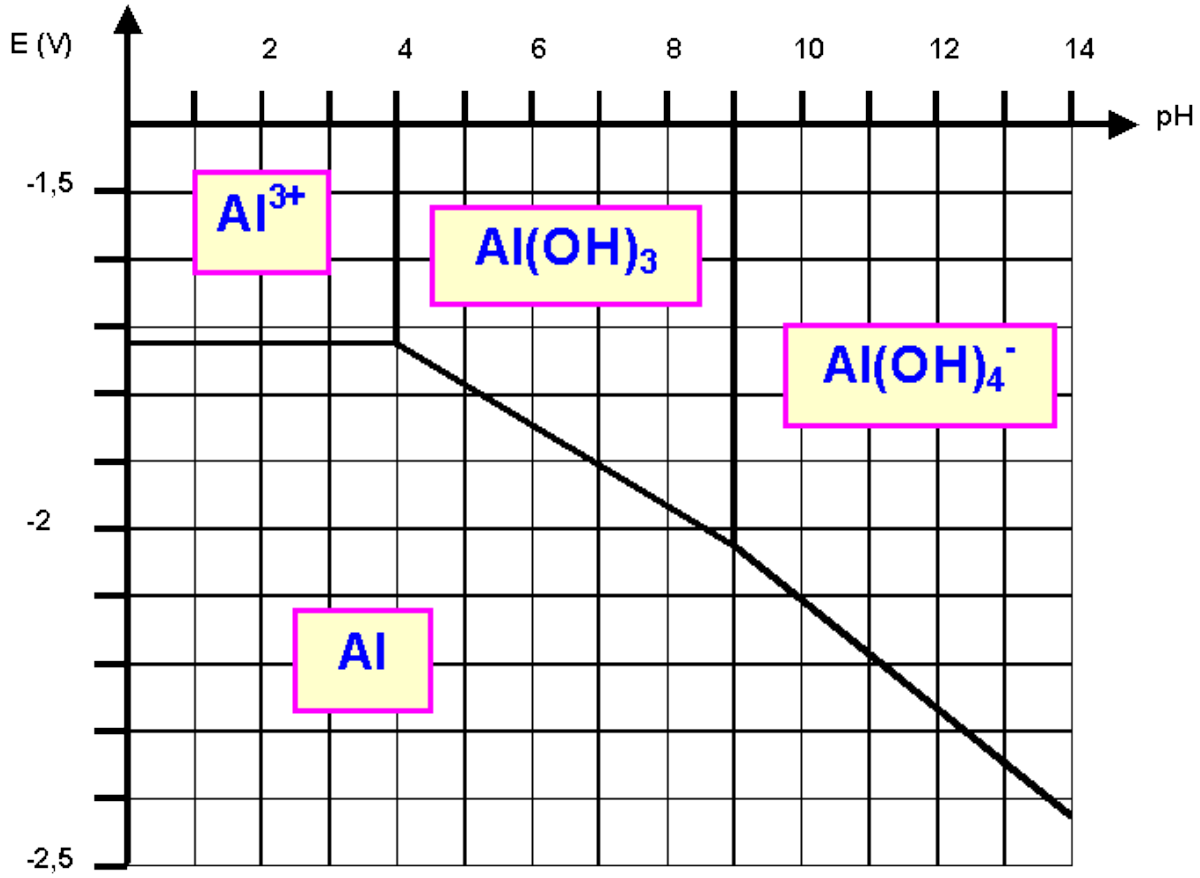

Figure 5.3 Pourbaix diagram for aluminum.[110]

compounds. Perhaps anionic polyaluminum complexes are also present, but currently neglected by our limited understanding of this system.

Aluminum speciation has traditionally shown a simplified speciation diagram that excludes oligomeric species. The exception to that is the diagram created by Baes & Mesmer in 1976, indicating the existence of the tridecameric aluminum species. (**Figure 5.4**).[109]

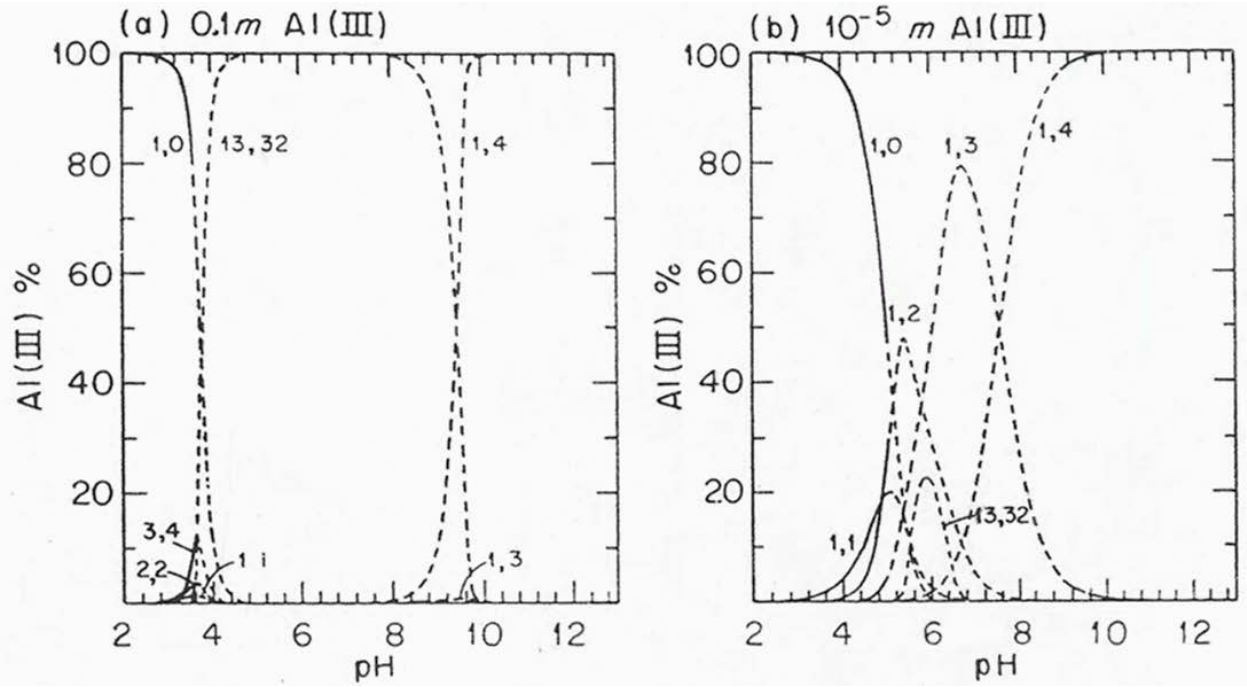

Figure 5.4 Distribution of hydrolysis products (x,y where x = Al, y = OH) at 25°C in (a) 0.1 m Al(III) (b) 10^{-5} m Al(III) x = Al, y = OH [109]

One of the early, and more notable, oligomeric aluminum species isolated was the Al_{13} Keggin (Al_{13}^{k}) discovered in 1960 by Johansson.[79, 111] The Keggin moiety is a common unit observed, notably in polyoxometalate chemistry.[80, 112-126] The Al_{13}^{k} has a central, tetrahedral coordinated Al (**Figure 5.5**)[127] surrounded by 12 octahedrally coordinated aluminum (**Figure 5.6 A**). These octahedrally coordinated aluminum are arranged as four trimers $[Al_3(\mu_2\text{-}OH)_6(H_2O)_3]$ through edge-sharing of hydroxyl groups ($\varepsilon\text{-}Al_{13}^{k}$). There are five Keggin isomers (α, β, γ, δ, and ε) that are distinguished based upon the number of edges shared between the trimeric units. Each

isomer can also be formed by turning each of the trimers by 60°, whereby turning one trimer from the α-isomer creates the β-isomer. By turning all 4 trimers 60°, you can change the clusters from all shared vertices to all shared edges and create the α- through ε-isomers.[128]

The ε-Keggin was the first to be crystallized using sulfate and selenate counterions.[79, 111] With additional heating the δ-Keggin can also be stabilized in the presence of a sodium cap and the β- and γ- isomers were also potentially identified under various conditions.[68, 80, 82] The α-isomer has yet to be isolated, but occurs in nature in the presence of silicates as a mineral zunyite.[75] There has been literature precedence for the formation and identification of the α-isomer in an aqueous solution, but it has not been isolated in a solid crystalline lattice.[70]

The transition between the Al_{13}^{k} and the Al_{30} Keggin in aqueous solutions and the relative abundance of these two nanoscale clusters are important to understanding the chemistry of

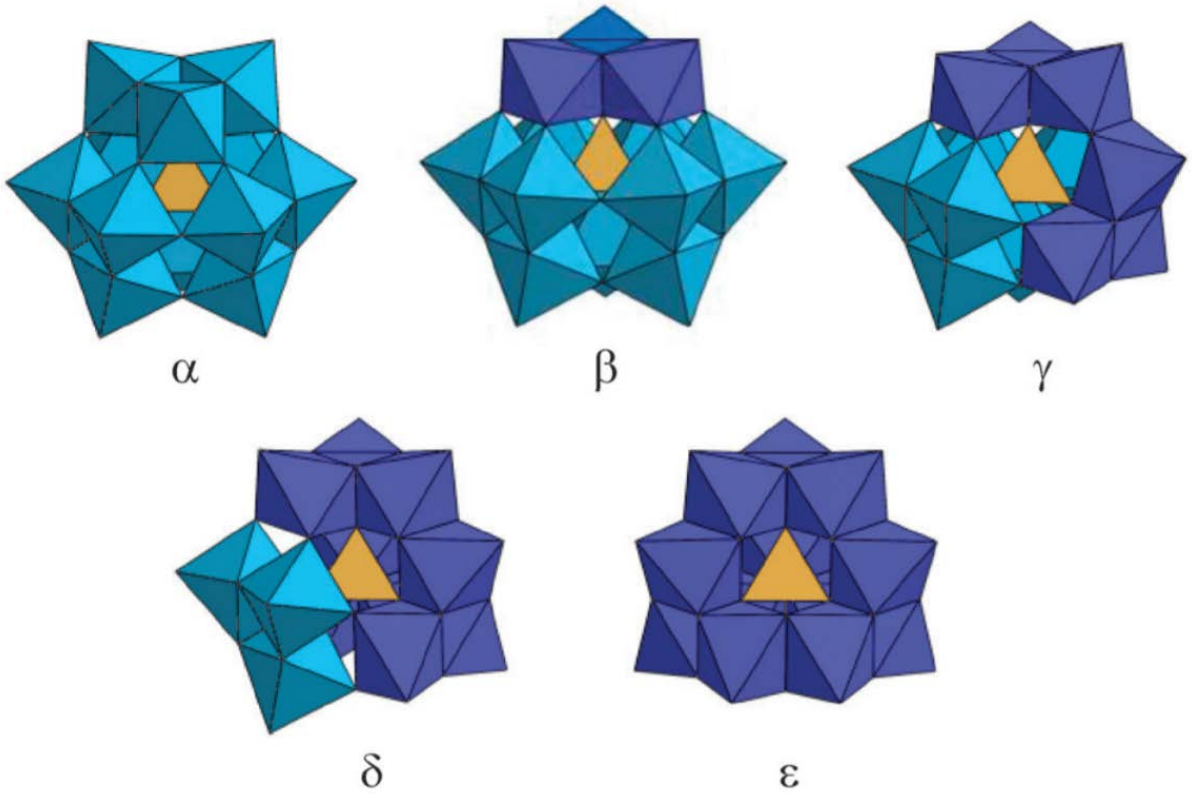

Figure 5.5 Keggin-Baker-Figgins Isomers.[127]

aluminum in aqueous systems. The Al_{30} Keggin is the result of condensation of the δ-Al_{13} Keggin clusters and free Al^{3+} monomers and, therefore, the formation of the Al_{30} requires the Al_{13} Keggin precursors in solution. This has traditionally been completed with additional hydrolysis, notably by heating. For example, Oliveri at al. demonstrated that aging of the initial solution leads to the isomerization of the Al_{13}^{k} and these results were represented in a new speciation diagram that considers the aging process (**Figure 5.7**). Al_{30} has also been found to represent 50% of the Al

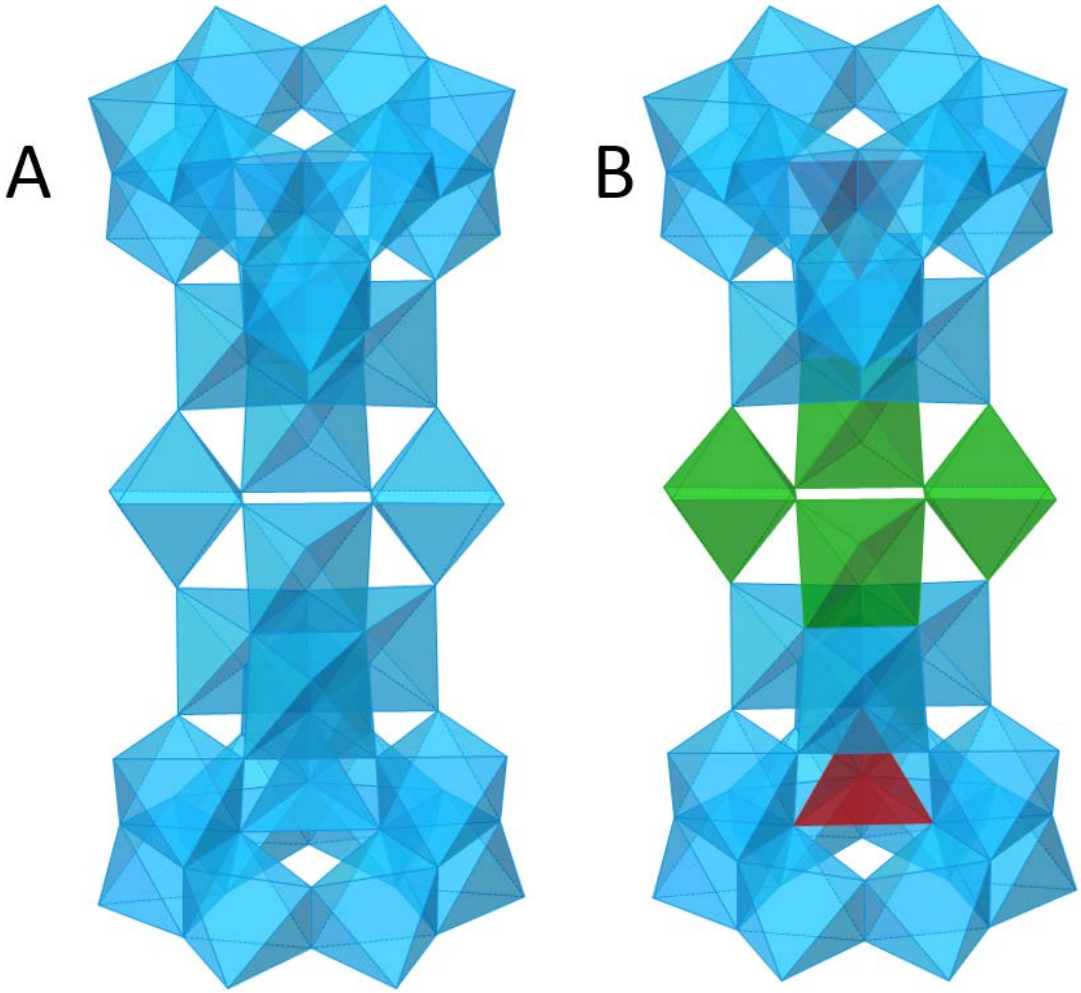

Figure 5.6 Translucent polyhedron representation of the Aluminum-30 Cluster. A: Blue polyhedrons represent Aluminum at the center with oxygens in the form of oxo, hydroxo, or aqua at each vertices. The Al_{30} polyaluminum cluster has 2 tetrahedrally coordinated aluminum and 28 octahedrally coordinated aluminum B: The two red polyhedrons represent the tetrahedrally coordinated aluminums in the "keggin-like" Al_{30} "dimer". The green polyhedron are the four octahedrally coordinated aluminum that comprise the "belt" of the Al_{30} that are not part of the two keggin moieties on either side of the belt. The remaining blue polyhedrons are the octahedrally coordinated aluminum that are in the "δ-keggins" of the dimer, along with the red tetrahedral aluminum centers.

species present in specific partially hydrolyzed aluminum bearing solutions and is also assumed to be an important precursor in the formation of the amorphous precipitate.[68] Upon aging, Oliveri, et al. showed an increased concentration of Al_{30} Keggin molecules and the formation of a gel-like precipitate upon aging that could be the result of Al_{30} aggregation (**Figure 5.1**).[70]

Aluminum Keggin molecules have also been utilized in water treatment facilities as a coagulant that adsorbs a wide array of contaminant molecules.[129-130] Furrer et al., investigated coagulates that contained Al salts, Al_{13} Keggin molecules and Al_{30} clusters and found that the larger Al_{30} cluster were more effective at removing arsenate from aqueous solutions.[131] Other transition metals and small polycarboxylate ligands can also interact with the surface of the Al_{30} molecule.[74, 132]

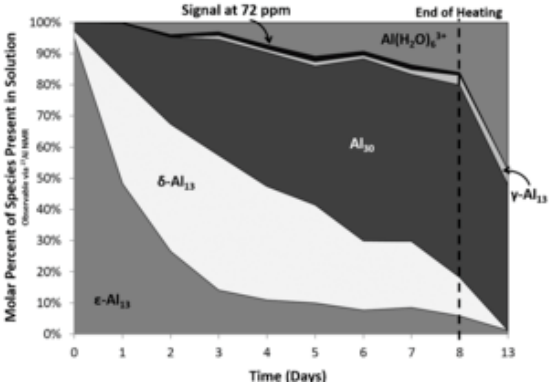

Figure 5.7 Relative dominance based on ^{27}Al NMR data of each Aluminum molecular species in solution is a function of time upon aging an Al_{13}^{k}/Glycine/Ca^{2+} 1:1:1 solution (0.026 M) at 90 ^{o}C for 13 days.

Density functional theory calculation have indicated a preferred binding site associated with the beltway region and that the counterions present in solution influences the adsorption process. The "active site" (denoted by the pink aluminum polyhedra) in the beltway region on Al_{30} preferentially adsorbs various inorganic cations and anions (**Figure 5.8 B**).[74, 82, 132] The active site consists of two Al^{3+} octahedral that allows the various species to bind in a bridging bidentate fashion. Rustad utilized computational methods to show that the active site on the bare Al_{30}

molecule consists of one terminal H_2O and one OH group, which will deprotonate or exchange upon binding to form a stable Al_{30}^{16+} molecule.[133] Both transition metal cations (Al^{3+} and Cu^{2+}) and inorganic anions (PO_4^{3-}, AsO_4^{3-}) have been shown both experimentally and computationally to bind to the Al_{30} cation through an inner sphere interaction. One thing to note is the importance of additional outer sphere interactions and the cooperative effect between cations and anions during the adsorption process is crucial for a stable complex to form. This is highlighted in the "Al_{30}-Cu_2" previously reported by Samangi et al, where the Cu^{2+} cation coordinates in a bridging bidentate fashion to the active site, but DFT calculations find that this complex only forms when it is stabilized by outer sphere sulfate anions.[74]

Competition between metals and small organic acids adsorption on the surface of these aluminum hydroxide clusters has significance in nuclear waste and can potential of environmental transport of heavy metals and radionuclides within groundwater. Understanding aluminum hydrolysis and potential interaction of these species with the complex matrix may contribute to enhanced reprocessing efforts and a better understanding of the environmental transport process. These complexes can be influenced by a variety of factors, including pH, Ionic strength, temperature, identity and concentrations of the anions and cations in the solution. Thus, it is critical to explore these variables to provide a well-defined insight into their function and speciation in the environment.

This chapter explores competitive adsorption for the Al_{30} Keggin molecules in a more complex matrix as a first step to explore interactions between aluminum hydroxide species and small organic molecules and metal ions that are abundant in the Hanford tank waste. Three Al_{30} molecules were isolated (Al_{30}-F, Al_{30}-F-Cu, and Al_{30}-F-Cu-Gly) utilizing a dissolution approach that

used formic acid and aluminum hydroxide starting materials. Soluble clusters were crystallized into a solid-state material to provide structural characterization by single-crystal X-ray diffraction. The solutions were further characterized by FTIR and NMR spectroscopy to provide a more complete understanding of the system.

5.4 Synthesis of the Al_{30} Keggin Molecules

5.4.1 Isolation Using a Supramolecular Approach to Crystallization

Previous studies have utilized sulfate and selenate and naphthalene disulfonate to isolate Keggin and Keggin-like polyaluminum oxy-hydroxy clusters.[74, 82, 132] The disulfonate anions, particularly 2,6-napthalene disulfonate (2,6-NDS), provides precise control over the crystallization of the Keggin phases and even isolation of a new intermediate cluster, Al_{26}.[82] Due to the high charge of the Al_{30} molecules, charge separation and supramolecular interactions perhaps becomes an important factor to encourage crystallization. The large disulfonate anions provides greater intermolecular distances and the addition of intermolecular forces (like π-π interaction, H-bonding) aid in crystallization. These NDS molecules have been utilized previously for soft metal-organic frameworks and rely heavily on supramolecular interactions to aid in lattice ordering and crystallization of the final product.[134-137]

5.4.2 General Synthesis Methodology

All reagents used were ACS grade equivalent or higher and used without any additional purification: Aluminum hydroxide dried gel ($Al(OH)_3$•0.8 H_2O (FW 92.4 g/mol), 99%, Strem Chemicals, USA), Sodium 2,6-Napthalenedisulfonate ($C_{10}H_6Na_2O_6S_2$ (FW 332.26 g/mol), 97%, Aldrich Chemistry, USA), Sodium 2,7-Napthalenedisulfonate ($C_{10}H_6Na_2O_6S_2$, >98%, Tokyo Chemical Industry, Japan), Formic Acid (HCOOH, 88%, Mallinckrodt Chemicals, USA), Copper (II)

Chloride ($CuCl_2$, 99%+, Acros Organics, USA), Glycine ($C_2H_5NO_2$, 99%, Amresco, USA), All syntheses were performed using ultrapure deionized Milli-Q water (18.2 $M\Omega \cdot cm^{-1}$ resistivity at 25 °C, Millipore Corporation, USA) in 20 mL glass liquid scintillation vials.

Each of the Al_{30} compounds were synthesized by dissolving the amorphous aluminum hydroxide gel with formic acid with either at 0.85:1, or 2:1 Formic acid:$Al(OH)_3 \bullet 0.8\ H_2O$ molar ratio. The 0.85 equivalents of formic acid required the addition of moderate heat on a hot plate to completely dissolve the Al starting material. Upon complete dissolution, an aliquot of the solution was added to a crystallization plate and complexing species (Cu(II) or glycine) and crystallizing agents (napthalenedisulfonate (NDS)) were carefully added in various ratios to individual wells. These solutions underwent slow evaporation for several days to weeks to yield single crystals in yields of approximately 10 – 50% for single-crystal XRD.

5.4.3 Synthesis of Al_{30}-Formate (Al_{30}-F)

$[(HCO_2)_2Al_2O_8Al_{28}(OH)_{56}(H_2O)_{22})(2,7NDS)_8(H_2O)_{\mathbf{52}}]$

Aluminum hydroxide dried gel (1.85 g, 20 mmol) was added to a 20 ml liquid scintillation vial with 8 ml of ultrapure deionized Milli-Q water and 1.72 mL formic Acid (1.72 ml, 40 mmol). An additional 12 mL of water was added to the vial and the solution was heated on a hot plate set at 150 °C (~80 °C internal temperature) until solid starting materials completely dissolved (approximately 2 hours). The 2:1 formate:Al stock solution (100 µL) was added to a crystallization plate with 3.5 ml wells, followed by 50 µl of 2M glycine (1 eq, 0.1 mmol) and 2.5 ml of 0.1M 2,7 naphthalene disulfonate, disodium (2,7-NDS, 2.5 eq, 0.25 mmol). A small amount of precipitate formed upon addition of the 2,7-NDS and additional opaque small single crystals plates of Al_{30}-F formed after 3-5 days of slow evaporation in low yields estimated at 10% with respect to

Aluminum. The water content was calculated based on the electrons squeezed out of the modeled structure in Platon.

5.4.4 Synthesis of Al_{30}-Formate-Copper (Al_{30}-F-Cu)

$[Cu(H_2O)_2(HCO_2)Al_2O_8Al_{28}(OH)_{59}(H_2O)_{24})(2,6NDS)_8(H_2O)_{48}]$

Similar methodology was used to create a 0.85:1 Formate:Al stock solution (1.85 g of aluminum hydroxide dried gel 20 mmol; 0.73 mL, concentrated formic acid 17 mmol). In a 3.5 ml well plate, 900 µl of milli-Q H_2O was added, followed by 100 µl of the 0.85:1 Formate:Al stock solution, 50 µl of 2M $CuCl_2$ (1 eq, 0.1 mmol), and 0.5 ml of 0.1M 2,6 naphthalene disulfonate, disodium (2,6-NDS, 0.5 eq, 0.05 mmol). The solution was allowed to slowly evaporate for two days before small light blue single crystal with a plate-like morphology formed on the bottom of the well and the surface of the solution in approximate yields of 20% based upon Al.

5.4.5 Synthesis of Al_{30}-Formate-Copper-Glycine (Al_{30}-F-Cu-Gly)

$[Cu(H_2O)_2(HCO_2)_2(NH_3CH_2CO_2)Al_2O_8Al_{28}(OH)_{58}(H_2O)_{23})(2,6NDS)_8(H_2O)_{48}]$

The 0.85:1 Formate:Al stock solution (100 µL) was added with 900 µL of milli-Q H_2O was added to a 3.5 mL well plate. Complexing and crystallization agents (50 µl of 2M $CuCl_2$ (1 eq, 0.1 mmol), and 1.5 ml of 0.1M 2,6-NDS (1.5 eq, 0.15 mmol)) were added and a small amount of precipitate was observed in the bottom of the well. Small light blue single crystal plates were isolated of Al_{30}-F-Cu-Gly after 3-5 days of slow evaporation in yields estimated at 20% based upon Al. The chemical formula presented here is an estimation of the actual formula and more research is needed to assure that this is the correct formulation.

5.5 Single Crystal X-Ray Diffraction and structure determination

Single Crystal X-ray diffraction (XRD) is a technique that is used to structurally characterize crystalline materials, giving a 3D, spatial arrangement of the atoms. Crystal Structure determination can yield valuable information regarding bond distances and bond angles as well as supramolecular information regarding confirmation and orientation.

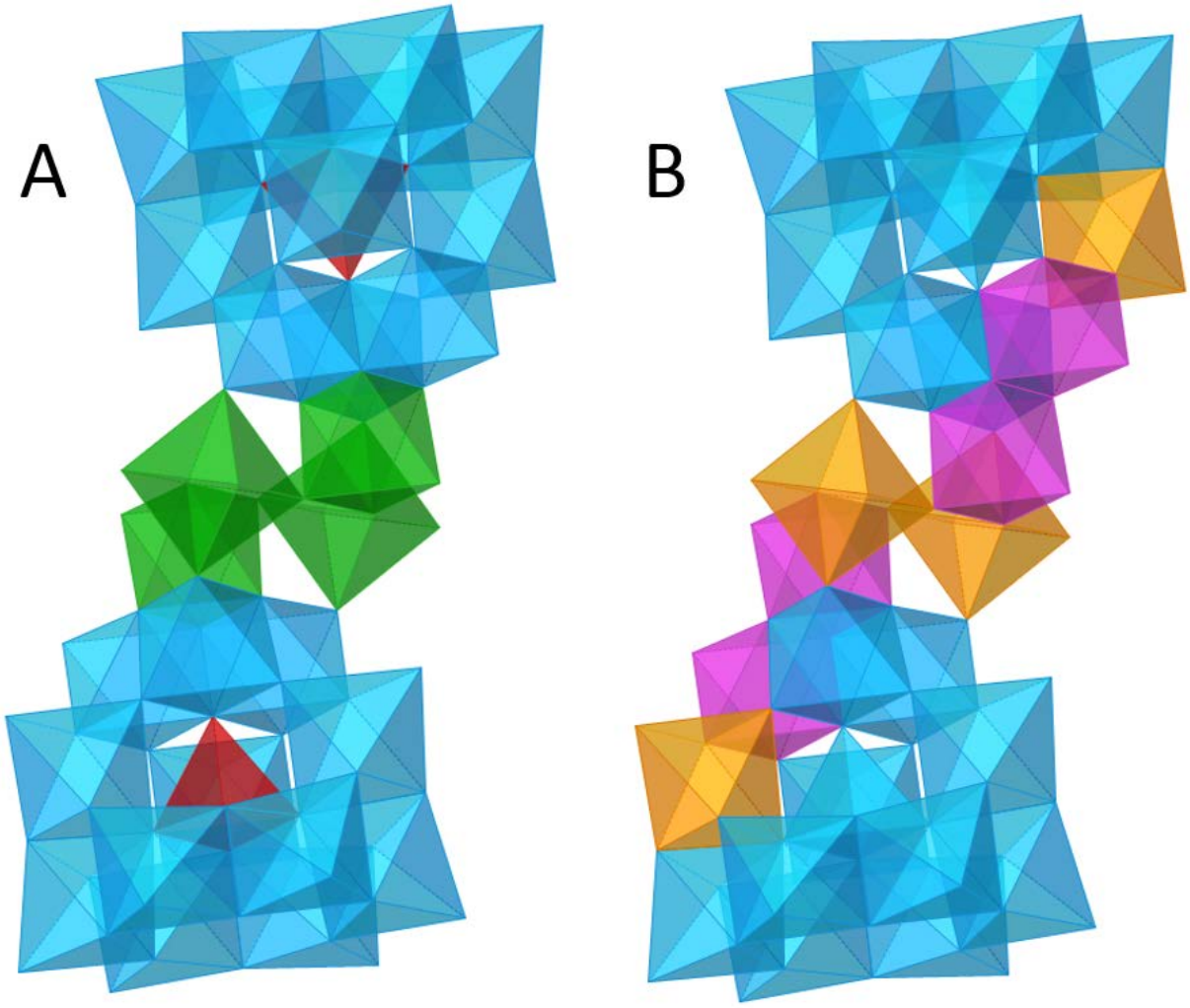

Figure 5.8 Translucent polyhedron representation of the Aluminum-30 Cluster. A: The two red polyhedrons represent the tetrahedrally coordinated aluminums in the "keggin-like" Al_{30} "dimer". The green polyhedron are the four octahedrally coordinated aluminum that comprise the "belt" of the Al_{30} that are not part of the two keggin moieties on either side of the belt. The remaining blue polyhedrons are the octahedrally coordinated aluminum that are in the "δ-keggins" of the dimer, along with the red tetrahedral aluminum centers. B: pink polyhedron aluminums are representative of the "active site". The orange polyhedron aluminums are representative of the aluminums that have terminal η-H_2O that engage in hydrogen bonding interactions with the NDS molecules.

Crystals synthesized by the methods described above were isolated from the mother liquor, coated in paratone-n oil (Hampton Research, Aliso Viejo, CA), and mounted on a Bruker-D8 Quest single crystal X-ray diffractometer (Mo Kα radiation, λ = 0.7107 Å) equipped with a CMOS detector and a low temperature cryostream 800 (Oxford Cryosystems, Oxford, UK) set at 100K. Data collection, cell refinement, data integration, and absorption corrections were performed using APEX3 v2016.1-0 with SHELXTL software.[138] All compounds crystallized in the triclinic space-group, *P*-1, and each structure was solved using the intrinsic phasing method. The Al, S, and O atoms were identified in the initial structure solution and other atoms were located in the subsequent least-squares refinement using SHELXTL software.

In each of the structural models, there is significant disorder of the O and C atoms within NDS molecules. Disorder was either modeled as two crystallographic sites with partial occupancy or as single isotropic atoms. The naphthalene rings were refined using SADI restraints to appropriately model the C-C bond distances and geometries. When possible, H-atoms were added to the naphthalene rings using a riding model.

5.6 Structural Information

Due to the size of these clusters, there is also significant void spaces which is occupied by disordered water molecules. Relatively well ordered water molecules were included in the structural model, although H-atoms were not located for these molecules. The SQUEEZE[139] command in the Platon software was used on the void spaces containing disordered solvent (H_2O). The resulting void spaces modeled this way were as follows: Al_{30}-F: 25% void, Al_{30}-F-Cu: 29% void, Al_{30}-F-Cu-Gly: 27% void. The interstitial waters were also calculated and included in the

formula based on the electrons found by the SQUEEZE function. Selected crystallographic information and data collection parameters are shown in **Tables 5.2 - 5.4**.

Table 5.2 Selected crystallographic and refinement information for Al_{30}-F

Name	Al_{30}-Formate (Al_{30}-F)
Formula	$[(HCO_2)_2Al_2O_8Al_{28}(OH)_{56}(H_2O)_{22})(2,7NDS)_8(H_2O)_{\mathbf{52}}]$ or $(Al_{30}O_{190}S_{16}C_{82}H_{286})$
FW (g/mol)	5635.51
T (K)	100(2)
Space group	*P-1*
Crystal size (mm)	0.010 x 0.050 x 0.090
a (Å)	13.7829(8)
b (Å)	19.3660(9)
c (Å)	20.4063(10)
α (°)	109.418(3)
β (°)	98.480(4)
γ (°)	92.174(4)
V (Å^3)	5058.7(5)
Z	1
*ρ*calc (g/cm^3)	1.850
Absorption coefficient (mm^{-1})	0.428
F(000)	2450
Theta range (°)	2.13 to 25.50
Data collected	-16 < *h* < 16 -23 < *k* < 23 -24 < *l* < 24
Reflections collected/unique	125279/ 18673 [*Rint* = 0.3302]
GOF on F^2	1.113
Final R indices [I > 2σ(I)]	R1 = 0.1222, wR2 = 0.3177
R indices (all data)	R1 = 0.2338, wR2 = 0.3856
Largest diff. peak and hole (eÅ^{-3})	1.882 and -0.840

Table 5.3 Selected crystallographic and refinement information for Al_{30}-F-Cu

Name	Al_{30}-Formate-Copper (Al_{30}-F-Cu)
Formula	$[Cu(H_2O)_2(HCO_2)Al_2O_8Al_{28}(OH)_{59}(H_2O)_{24})(2,6NDS)_8(H_2O)_{48}]$ or $(CuAl_{30}O_{191}S_{16}C_{81}H_{288})$
FW (g/mol)	5705.06
T (K)	100(2)
Space group	*P-1*
Crystal size (mm)	0.010 x 0.050 x 0.080
a (Å)	14.5754(7)
b (Å)	18.4281(8)
c (Å)	20.2488(9)
α (°)	85.626(2)
β (°)	74.620(2)
γ (°)	76.157(2)
V (Å^3)	5091.2(4)
Z	2
*ρ*calc (g/cm^3)	1.861
Absorption coefficient (mm^{-1})	0.484
F(000)	2139
Theta range (°)	2.02 to 26.02
Data collected	-17 < *h* < 17 -22 < *k* < 19 -24 < *l* < 24
Reflections collected/unique	185812/ 20031 [*Rint* = 0.1017]
GOF on F^2	1.035
Final R indices [I > 2σ(I)]	R1 = 0.0923, wR2 = 0.2711
R indices (all data)	R1 = 0.1268, wR2 = 0.3053
Largest diff. peak and hole (eÅ^{-3})	4.444 and -1.019

Table 5.4 Selected crystallographic and refinement information for Al_{30}-F-Cu-Gly

Name	Al_{30}-Formate-Copper-Glycine (Al_{30}-F-Cu-Gly)
Formula	$[Cu(H_2O)_2(HCO_2)_2(NH_3CH_2CO_2)Al_2O_8Al_{28}(OH)_{58}(H_2O)_{23})(2,6NDS)_8(H_2O)_{48}]$ or $(CuAl_{30}O_{193}S_{16}C_{83}NH_{291})$
FW (g/mol)	5778.11
T (K)	100(2)
Space group	*P-1*
Crystal size (mm)	0.010 x 0.030 x 0.070
a (Å)	13.338(13)
b (Å)	18.404(17)
c (Å)	20.226(19)
α (°)	109.418(3)
β (°)	81.307(15)°
γ (°)	79.679(15)
V (Å^3)	4602.(8)
Z	2
*ρ*calc (g/cm^3)	2.085
Absorption coefficient (mm^{-1})	0.852
F(000)	2909
Theta range (°)	2.11 to 25.35
Data collected	-16 < *h* < 16 -22 < *k* < 18 -24 < *l* < 24
Reflections collected/unique	156328/ 16839 [*Rint* = 0.1028]
GOF on F^2	1.051
Final R indices [I > 2σ(I)]	R1 = 0.0981, wR2 = 0.2642
R indices (all data)	R1 = 0.1472, wR2 = 0.3239
Largest diff. peak and hole (eÅ^{-3})	2.447 and -1.430

5.7 Bond Valence Calculations

Bond valence calculations were performed to validate the crystal structure analysis by confirming the oxygen group identities. Bond valence is a method that helps quantify the bonding interaction between atoms based on previously refined crystal structures. For many elements, empirical data is isolated from these well-refined crystal structures, for a given oxidation state and coordination geometry, to determine empirical values r_o and B, which can be used to determine the bond valence (s) for a specific bond. These values have been determined by various sources and are subject to the quality and similarity of an elements chemical environment to what is most commonly observed for the element.[140]

Bond Valence:

$$s = exp((ro-r)/B)$$

s = bond valence

r = bond distance

r_o = parameter based on "ideal" bond distance

B = empirical constant, typically 0.37 Å

This bond valence is performed *per bond*, with s indicating the charge of the atom due to a specific bond. By summing each of these bond valence (s) values for a certain atom, a total bond valence sum (V) is calculated.

$$\sum_{i} s_i = V$$

i = index for all bonds on a certain atom

V = bond valence sum

s = bond valence

The bond valence sum is expected to be approximately the oxidation state of the atom. For example, aluminum is a trivalent atom, so upon the summation of all of the bond valence contributions (*s*) to the bond valence sum (*V*), a value of 3 would be expected. The bond valence calculations are presented as tables and were calculated using the bond valence parameters outlined by Allmann in 1975 where, for Al^{3+} in an octahedral coordination, B = 0.38 Å and r_o = 1.644 Å.[141] (**Tables 5.5 – 5.7**) Copper, formate, and glycine were excluded for clarity to compare the various Al_{30} clusters. These results were derived from the bond distances (**Tables 5.8 – 5.10**).

Bond Valence calculations for the Al^{3+} in these clusters does show a summation to near +3. It should be noted that geometry (including molecular strain) may play a critical role in the determination of the bond valence. The tendency to underestimate the bond valence here may also be due to the overall charge of the cluster being +16 or +18, which is atypical of the structural database that the bond valence parameters are empirically derived. This model is only as good as the similarity of the structure analyzed and the average Al structure used in the parameter determination. Also, it is clearly not effective for the tetrahedral aluminum center, which had B.V. calculations averaging around +2.5.

*Table 5.5 Bond valence (B.V.) calculations for Al_{30}-F from bond distances (**Table 5.8**) obtained from crystallography. The Orange highlighted Al cells indicate the "sulfate hydrogen-bonding" Al (**Figure 5.10**). The purple highlighted Al cells indicate the "active site" Al (**Figure 5.10**), the red oxygens are the mu3-OH groups, the green oxygens are the "active site" oxygens, the blue Al is the tetrahedral Al.*

Al_{30}-F	Al1	Al2	Al3	Al4	Al5	Al6	Al7	Al8	Al9
O1	0.399								
O2	0.534	0.498							
O3	0.521						0.502		
O4	0.528					0.547			
O5	0.552					0.476			
O6	0.345	0.349					0.393		
O7		0.435							
O8		0.565	0.537						
O9		0.524	0.531						
O10			0.434						
O11			0.454					0.481	
O12			0.340	0.339				0.389	
O13			0.514	0.530					
O14				0.435					
O15				0.505				0.512	
O16				0.543	0.578				
O17				0.465	0.487				
O18					0.425				
O19					0.325	0.339			0.423
O20					0.537				0.517
O21					0.502	0.528			
O22						0.514			0.479
O23						0.446			
O24							0.458		
O25							0.472		
O26							0.503		
O27		0.540					0.490		
O28									
O29									0.463
O30									0.431
O31									0.482
O32								0.495	
O33								0.462	
O34								0.514	
O35									
O36									
O37									
O38									
O39									
O40									
O41									
O42									
O43									
O44									
O45									
B.V.	2.8795	2.9119	2.8109	2.8171	2.8535	2.8506	2.8174	2.8529	2.7964

Table 5.5 – continued.

Al_{30}-F	Al10	Al11	Al12	Al13	Al14	*Al15	B.V.	Identity
O1							0.40	H_2O
O2							1.03	μ_2-OH
O3							1.02	μ_2-OH
O4							1.08	μ_2-OH
O5							1.03	μ_2-OH
O6						0.640	1.73	μ_4-O
O7							0.43	H_2O
O8							1.10	μ_2-OH
O9							1.06	μ_2-OH
O10							0.43	H_2O
O11							0.93	μ_2-OH
O12						0.635	1.70	μ_4-O
O13							1.04	μ_2-OH
O14							0.43	H_2O
O15							1.02	μ_2-OH
O16							1.12	μ_2-OH
O17							0.95	μ_2-OH
O18							0.42	H_2O
O19						0.611	1.70	μ_4-O
O20							1.05	μ_2-OH
O21							1.03	μ_2-OH
O22							0.99	μ_2-OH
O23							0.45	H_2O
O24							0.46	H_2O
O25	0.578						1.05	μ_2-OH
O26					0.558		1.06	μ_2-OH
O27							1.03	μ_2-OH
O28	0.401	0.362			0.354	0.576	1.69	μ_4-O
O29	0.567						1.03	μ_2-OH
O30							0.43	H_2O
O31		0.595					1.08	μ_2-OH
O32		0.578					1.07	μ_2-OH
O33							0.46	H_2O
O34					0.537		1.05	μ_2-OH
O35	0.395			0.451	0.454		1.30	μ_3-OH
O36			0.520		0.524		1.04	μ_2-OH
O37		0.405		0.414	0.384		1.20	μ_3-OH
O38	0.410	0.402		0.426			1.24	μ_3-OH
O39	0.452						0.45	*Formate*
O40				0.547			0.55	*Formate*
O41			0.486	0.543			1.03	μ_2-OH
O42		0.546	0.479				1.03	μ_2-OH
O43			0.489	0.510			1.00	μ_2-OH
O44			0.417				0.42	H_2O
O45			0.419				0.42	H_2O
B.V.	2.8020	2.8884	2.8094	2.8910	2.8116	2.4629		

*Table 5.6 Bond valence (B.V.) calculations for Al_{30}-F-Cu from bond distances (**Table 5.9**) obtained from crystallography. The Orange highlighted Al cells indicate the "sulfate hydrogen-bonding" Al (**Figure 5.12**). The purple highlighted Al cells indicate the "active site" Al (**Figure 5.12**), the red oxygens are the mu3-OH groups, the green oxygens are the "active site" oxygens, the blue Al is the tetrahedral Al.*

Al_{30}-F-Cu	Al1	Al2	Al3	Al4	Al5	Al6	Al7	Al8	Al9
O1				0.320	0.342				
O2				0.491					
O3				0.572	0.541				
O4				0.521					0.490
O5				0.559					0.555
O6				0.447					
O7							0.299		0.352
O8									0.449
O9							0.549		0.558
O10									0.510
O11							0.528		
O12							0.435		
O13		0.528					0.514		
O14		0.558					0.547		
O15		0.302	0.366					0.409	
O16		0.431							
O17		0.531						0.507	
O18		0.541	0.530						
O19			0.502					0.487	
O20			0.441						
O21			0.509		0.514				
O22			0.534		0.549				
O23					0.437				
O24					0.506				
O25									
O26						0.575			
O27									
O28						0.567			
O29									
O30								0.437	
O31								0.502	
O32						0.396			
O33	0.410					0.441			
O34									
O35	0.427								
O36	0.437					0.417			
O37						0.494			
O38	0.555								
O39	0.549								
O40									
O41									
O42	0.533								
O43									
O44								0.505	
O45									
B.V.	2.9104	2.8924	2.8816	2.9100	2.8900	2.8886	2.8727	2.8475	2.9143

Table 5.6 – continued.

Al_{30}-F-Cu	Al10	Al11	*Al12	Al13	Al14	Al15	B.V.	Identity
O1	0.433		0.625				1.72	μ_4-O
O2	0.476						0.97	μ_2-OH
O3							1.11	μ_2-OH
O4							1.01	μ_2-OH
O5							1.11	μ_2-OH
O6							0.45	$Formate_{cap}$
O7			0.665		0.415		1.73	μ_4-O
O8							0.45	H_2O
O9							1.11	μ_2-OH
O10					0.519		1.03	μ_2-OH
O11					0.494		1.02	μ_2-OH
O12							0.43	H_2O
O13							1.04	μ_2-OH
O14							1.11	μ_2-OH
O15			0.649				1.73	μ_4-O
O16							0.43	H_2O
O17							1.04	μ_2-OH
O18							1.07	μ_2-OH
O19							0.99	μ_2-OH
O20							0.44	H_2O
O21							1.02	μ_2-OH
O22							1.08	μ_2-OH
O23							0.44	H_2O
O24	0.497						1.00	μ_2-OH
O25	0.442						0.44	H_2O
O26	0.502						1.08	μ_2-OH
O27					0.439		0.44	H_2O
O28					0.483		1.05	μ_2-OH
O29				0.565	0.513		1.08	μ_2-OH
O30							0.44	H_2O
O31				0.565			1.07	μ_2-OH
O32			0.555	0.347		0.399	1.70	μ_4-O
O33				0.436			1.29	μ_3-OH
O34		0.487		0.507			0.99	μ_2-OH
O35				0.419		0.395	1.24	μ_3-OH
O36						0.426	1.28	μ_3-OH
O37							0.49	*Formate/Cu*
O38							0.55	*Formate/Cu*
O39		0.490					1.04	μ_2-OH
O40		0.423					0.42	H_2O
O41		0.411					0.41	H_2O
O42		0.485					1.02	μ_2-OH
O43		0.497				0.533	1.03	μ_2-OH
O44						0.565	1.07	μ_2-OH
O45	0.479					0.564	1.04	μ_2-OH
B.V.	2.8283	2.7928	2.4934	2.8398	2.8627	2.8813		

*Table 5.7 Bond valence (B.V.) calculations for Al_{30}-F-Cu-Gly from bond distances (**Table 5.10**) obtained from crystallography. The Orange highlighted Al cells indicate the "sulfate hydrogen-bonding" Al (**Figure 5.14**). The purple highlighted Al cells indicate the "active site" Al (**Figure 5.14**), the red oxygens are the mu3-OH groups, the green oxygens are the "active site" oxygens, the blue Al is the tetrahedral Al.*

Al_{30}FCuGly	*Al1	Al2	Al3	Al4	Al5	Al6	Al7	Al8	Al9
O1	0.685	0.335					0.300	0.419	
O2	0.670				0.359	0.300			
O3	0.625		0.316	0.377					0.423
O4	0.570								
O5				0.540	0.534				
O6				0.489	0.498				
O7		0.498	0.530						
O8					0.457				
O9		0.478							
O10			0.434						
O11					0.482				
O12			0.526						0.505
O13						0.524	0.520		
O14				0.505					0.489
O15				0.429					
O16			0.528	0.516					
O17									0.436
O18									0.505
O19									
O20									
O21									
O22									
O23									
O24						0.507			
O25					0.544	0.536			
O26						0.437			
O27						0.567	0.552		
O28							0.431		
O29		0.550					0.561		
O30		0.549	0.562						
O31		0.503						0.487	
O32								0.429	
O33							0.530	0.498	
O34								0.521	
O35									
O36									
O37									
O38									
O39									
O40									
O41									
O42								0.503	
O43									0.498
O44									
O45									
B.V.	2.5501	2.9132	2.8962	2.8551	2.8742	2.8719	2.8942	2.8579	2.8555

Table 5.7 – continued.

$Al_{30}FCuGly$	Al10	Al11	Al12	Al13	Al14	Al15	B.V.	Identity
O1							1.74	μ_4-O
O2	0.413						1.74	μ_4-O
O3							1.74	μ_4-O
O4		0.399	0.353			0.395	1.72	μ_4-O
O5							1.07	μ_2-OH
O6							0.99	μ_2-OH
O7							1.03	μ_2-OH
O8							0.46	*Glycine*
O9							0.48	$Formate_{cap}$
O10							0.43	H_2O
O11	0.497						0.98	μ_2-OH
O12							1.03	μ_2-OH
O13							1.04	μ_2-OH
O14							0.99	μ_2-OH
O15							0.43	H_2O
O16							1.04	μ_2-OH
O17							0.44	H_2O
O18		0.567					1.07	μ_2-OH
O19		0.512					0.51	*Formate/Cu*
O20	0.491	0.547					1.04	μ_2-OH
O21	0.415						0.42	H_2O
O22		0.442	0.420		0.408		1.27	μ_3-OH
O23	0.519		0.584				1.10	μ_2-OH
O24	0.490						1.00	μ_2-OH
O25							1.08	μ_2-OH
O26							0.44	H_2O
O27							1.12	μ_2-OH
O28							0.43	H_2O
O29							1.11	μ_2-OH
O30							1.11	μ_2-OH
O31							0.99	μ_2-OH
O32							0.43	H_2O
O33							1.03	μ_2-OH
O34			0.552				1.07	μ_2-OH
O35			0.423		0.421	0.403	1.25	μ_3-OH
O36			0.527	0.487			1.01	μ_2-OH
O37				0.478	0.549		1.03	μ_2-OH
O38				0.495	0.536		1.03	μ_2-OH
O39				0.433			0.43	H_2O
O40				0.426			0.43	H_2O
O41				0.499		0.541	1.04	μ_2-OH
O42						0.570	1.07	μ_2-OH
O43						0.572	1.07	μ_2-OH
O44		0.436			0.451	0.407	1.29	μ_3-OH
O45					0.556		0.56	*Formate/Cu*
B.V.	2.8250	2.9030	2.8594	2.8183	2.9200	2.8875		

*Table 5.8 Bond distances (Å) for Al_{30}-F obtained from crystallography. The Orange highlighted Al cells indicate the "sulfate hydrogen-bonding" Al (**Figure 5.10**). The purple highlighted Al cells indicate the "active site" Al (**Figure 5.10**), the red oxygens are the mu3-OH groups, the green oxygens are the "active site" oxygens, the blue Al is the tetrahedral Al. The Copper in Figure 5.9 is a placeholder for the formate.*

Al_{30}-F	Al1	Al2	Al3	Al4	Al5	Al6	Al7	Al8	Al9
O1	1.960(9)								
O2	1.852(8)	1.878(8)							
O3	1.861(8)						1.875(8)		
O4	1.856(9)					1.843(8)			
O5	1.840(8)					1.895(9)			
O6	2.014(7)	2.009(8)					1.966(7)		
O7		1.928(8)							
O8		1.831(8)	1.850(8)						
O9		1.859(8)	1.854(8)						
O10			1.929(9)						
O11			1.912(8)					1.891(8)	
O12			2.019(8)	2.020(7)				1.969(8)	
O13			1.866(8)	1.855(8)					
O14				1.928(8)					
O15				1.873(9)				1.868(8)	
O16				1.846(9)	1.823(9)				
O17				1.903(9)	1.886(9)				
O18					1.937(8)				
O19					2.036(7)	2.020(8)			1.938(8)
O20					1.850(9)				1.864(8)
O21					1.875(9)	1.856(9)			
O22						1.866(9)			1.892(9)
O23						1.919(9)			
O24							1.909(8)		
O25							1.898(8)		
O26							1.874(8)		
O27		1.848(8)					1.884(8)		
O28									
O29									1.905(8)
O30									1.931(9)
O31									1.890(8)
O32								1.880(8)	
O33								1.906(8)	
O34								1.866(7)	
O35									
O36									
O37									
O38									
O39									
O40									
O41									
O42									
O43									
O44									
O45									
AVERAGE	1.897(9)	1.892(8)	1.905(9)	1.904(9)	1.901(9)	1.900(9)	1.901(8)	1.897(8)	1.903(9)
BONDS	6	6	6	6	6	6	6	6	6

Table 5.8 – continued.

Al_{30}-F	Al10	Al11	Al12	Al13	Al14	*Al15	Identity
O1							H_2O
O2							μ_2-OH
O3							μ_2-OH
O4							μ_2-OH
O5							μ_2-OH
O6						1.785(7)	μ_4-O
O7							H_2O
O8							μ_2-OH
O9							μ_2-OH
O10							H_2O
O11							μ_2-OH
O12						1.788(8)	μ_4-O
O13							μ_2-OH
O14							H_2O
O15							μ_2-OH
O16							μ_2-OH
O17							μ_2-OH
O18							H_2O
O19						1.802(8)	μ_4-O
O20							μ_2-OH
O21							μ_2-OH
O22							μ_2-OH
O23							H_2O
O24							H_2O
O25	1.823(7)						μ_2-OH
O26					1.836(7)		μ_2-OH
O27							μ_2-OH
O28	1.958(8)	1.996(7)			2.004(7)	1.824(7)	μ_4-O
O29	1.830(8)						μ_2-OH
O30							H_2O
O31		1.812(8)					μ_2-OH
O32		1.823(8)					μ_2-OH
O33							H_2O
O34					1.850(8)		μ_2-OH
O35	1.964(8)			1.915(7)	1.912(8)		μ_3-OH
O36			1.862(7)		1.859(8)		μ_2-OH
O37		1.954(7)		1.946(8)	1.974(7)		μ_3-OH
O38	1.950(7)	1.957(8)		1.936(8)			μ_3-OH
O39	1.914(9)						*Formate*
O40				1.843(8)			*Formate*
O41			1.887(7)	1.846(7)			μ_2-OH
O42		1.844(7)	1.892(7)				μ_2-OH
O43			1.885(8)	1.869(7)			μ_2-OH
O44			1.944(8)				H_2O
O45			1.942(7)				H_2O
AVERAGE	1.907(8)	1.898(8)	1.902(8)	1.893(8)	1.906(8)	1.800(8)	
BONDS	6	6	6	6	6	4	

*Table 5.9 Bond distances (Å) for Al_{30}-F-Cu obtained from crystallography. The Orange highlighted Al cells indicate the "sulfate hydrogen-bonding" Al (**Figure 5.12**). The purple highlighted Al cells indicate the "active site" Al (**Figure 5.12**), the red oxygens are the mu3-OH groups, the green oxygens are the "active site" oxygens, the blue Al is the tetrahedral Al.*

Al_{30}-F-Cu	Al1	Al2	Al3	Al4	Al5	Al6	Al7	Al8	Al9
O1				2.042(6)	2.017(6)				
O2				1.883(6)					
O3				1.827(8)	1.847(8)				
O4				1.861(8)					1.884(6)
O5				1.835(6)					1.838(7)
O6				1.918(7)					
O7							2.067(5)		2.006(5)
O8									1.916(6)
O9							1.842(6)		1.836(6)
O10									1.869(7)
O11							1.856(6)		
O12							1.928(6)		
O13		1.856(6)					1.866(6)		
O14		1.836(6)					1.843(6)		
O15		2.063(6)	1.992(6)					1.951(6)	
O16		1.931(7)							
O17		1.854(6)						1.871(6)	
O18		1.847(7)	1.855(7)						
O19			1.875(8)					1.886(7)	
O20			1.923(8)						
O21			1.870(8)		1.866(8)				
O22			1.852(8)		1.842(8)				
O23					1.926(8)				
O24					1.872(7)				
O25									
O26						1.825(6)			
O27									
O28						1.830(5)			
O29									
O30								1.926(6)	
O31								1.875(6)	
O32						1.963(5)			
O33	1.950(5)					1.923(5)			
O34									
O35	1.935(5)								
O36	1.926(5)					1.944(5)			
O37						1.881(6)			
O38	1.838(6)								
O39	1.842(5)								
O40									
O41									
O42	1.853(5)								
O43									
O44								1.873(5)	
O45									
AVERAGE	1.891(6)	1.898(7)	1.895(8)	1.894(8)	1.895(8)	1.894(6)	1.900(6)	1.897(7)	1.892(7)
BONDS	6	6	6	6	6	6	6	6	6

Table 5.9 – continued.

Al_{30}-F-Cu	Al10	Al11	*Al12	Al13	Al14	Al15	Identity
O1	1.930(6)		1.794(6)				μ_4-O
O2	1.895(6)						μ_2-OH
O3							μ_2-OH
O4							μ_2-OH
O5							μ_2-OH
O6							*Formate$_{cap}$*
O7			1.771(5)		1.945(6)		μ_4-O
O8							H_2O
O9							μ_2-OH
O10					1.863(6)		μ_2-OH
O11					1.881(6)		μ_2-OH
O12							H_2O
O13							μ_2-OH
O14							μ_2-OH
O15			1.780(6)				μ_4-O
O16							H_2O
O17							μ_2-OH
O18							μ_2-OH
O19							μ_2-OH
O20							H_2O
O21							μ_2-OH
O22							μ_2-OH
O23							H_2O
O24	1.879(7)						μ_2-OH
O25	1.922(6)						H_2O
O26	1.875(7)						μ_2-OH
O27					1.925(6)		H_2O
O28					1.889(5)		μ_2-OH
O29				1.831(5)	1.867(5)		μ_2-OH
O30							H_2O
O31				1.831(5)			μ_2-OH
O32			1.838(5)	2.012(5)		1.960(5)	μ_4-O
O33				1.927(5)			μ_3-OH
O34		1.886(5)		1.871(5)			μ_2-OH
O35				1.942(5)		1.964(5)	μ_3-OH
O36						1.936(5)	μ_3-OH
O37							*Formate/Cu*
O38							*Formate/Cu*
O39		1.884(5)					μ_2-OH
O40		1.938(6)					H_2O
O41		1.949(5)					H_2O
O42		1.888(5)					μ_2-OH
O43		1.879(5)				1.853(5)	μ_2-OH
O44						1.831(6)	μ_2-OH
O45	1.892(6)					1.832(5)	μ_2-OH
AVERAGE	1.899(7)	1.904(6)	1.796(6)	1.902(5)	1.895(6)	1.896(6)	
BONDS	6	6	4	6	6	6	

*Table 5.10 Bond distances (Å) for Al_{30}-F-Cu-Gly obtained from crystallography. The Orange highlighted Al cells indicate the "sulfate hydrogen-bonding" Al (**Figure 5.14**). The purple highlighted Al cells indicate the "active site" Al (**Figure 5.14**). the red oxygens are the mu3-OH groups, the green oxygens are the "active site" oxygens, the blue Al is the tetrahedral Al.*

Al_{30}FCuGly	*Al1	Al2	Al3	Al4	Al5	Al6	Al7	Al8	Al9
O1	1.760(6)	2.025(6)					2.065(6)	1.942(5)	
O2	1.768(6)				1.999(6)	2.065(6)			
O3	1.794(6)		2.046(6)	1.981(6)					1.938(6)
O4	1.828(5)								
O5				1.848(6)	1.852(7)				
O6				1.885(7)	1.878(7)				
O7		1.878(6)	1.855(7)						
O8					1.910(7)				
O9		1.893(7)							
O10			1.929(7)						
O11					1.890(7)				
O12			1.858(7)						1.873(7)
O13						1.859(6)	1.862(6)		
O14				1.873(7)					1.885(6)
O15				1.933(7)					
O16			1.856(7)	1.865(7)					
O17									1.927(6)
O18									1.873(7)
O19									
O20									
O21									
O22									
O23									
O24						1.871(6)			
O25					1.845(6)	1.851(6)			
O26						1.926(6)			
O27						1.830(6)	1.840(6)		
O28							1.931(6)		
O29		1.841(6)					1.834(6)		
O30		1.842(6)	1.833(7)						
O31		1.874(6)						1.886(6)	
O32								1.933(6)	
O33							1.855(6)	1.878(6)	
O34								1.861(5)	
O35									
O36									
O37									
O38									
O39									
O40									
O41									
O42								1.874(6)	
O43									1.878(6)
O44									
O45									
AVERAGE	1.788(6)	1.892(7)	1.896(7)	1.898(7)	1.896(7)	1.900(6)	1.898(6)	1.896(6)	1.896(6)
BONDS	4	6	6	6	6	6	6	6	6

Table 5.10 – continued.

$Al_{30}FCuGly$	Al10	Al11	Al12	Al13	Al14	Al15	Identity
O1							μ_4-O
O2	1.947(6)						μ_4-O
O3							μ_4-O
O4		1.960(6)	2.005(5)			1.964(5)	μ_4-O
O5							μ_2-OH
O6							μ_2-OH
O7							μ_2-OH
O8							*Glycine*
O9							*Formate$_{cap}$*
O10							H_2O
O11	1.879(6)						μ_2-OH
O12							μ_2-OH
O13							μ_2-OH
O14							μ_2-OH
O15							H_2O
O16							μ_2-OH
O17							H_2O
O18		1.830(6)					μ_2-OH
O19		1.868(6)					*Formate/Cu*
O20	1.883(6)	1.843(6)					μ_2-OH
O21	1.945(7)						H_2O
O22		1.922(6)	1.941(6)		1.952(5)		μ_3-OH
O23	1.863(6)		1.819(5)				μ_2-OH
O24	1.884(6)						μ_2-OH
O25							μ_2-OH
O26							H_2O
O27							μ_2-OH
O28							H_2O
O29							μ_2-OH
O30							μ_2-OH
O31							μ_2-OH
O32							H_2O
O33							μ_2-OH
O34			1.840(5)				μ_2-OH
O35			1.938(5)		1.940(5)	1.956(5)	μ_3-OH
O36			1.857(5)	1.886(5)			μ_2-OH
O37				1.893(5)	1.842(5)		μ_2-OH
O38				1.880(6)	1.851(5)		μ_2-OH
O39				1.930(6)			H_2O
O40				1.936(6)			H_2O
O41				1.877(5)		1.847(5)	μ_2-OH
O42						1.828(6)	μ_2-OH
O43						1.827(5)	μ_2-OH
O44		1.927(6)			1.915(5)	1.953(6)	μ_3-OH
O45					1.837(6)		*Formate/Cu*
AVERAGE	1.900(6)	1.892(6)	1.900(6)	1.900(6)	1.900(6)	1.896(6)	
BONDS	6	6	6	6	6	6	

Bond valence calculations do show aluminum as a trivalent cation, which confirms what would be expected from aluminum. Bond valence is not just useful for metal centers, but also for nonmetals, including oxygen. Depending on the nature of the oxygen in the compound, a variety of bond valence sums can occur. If the oxygen is attributed to have a more formal -2

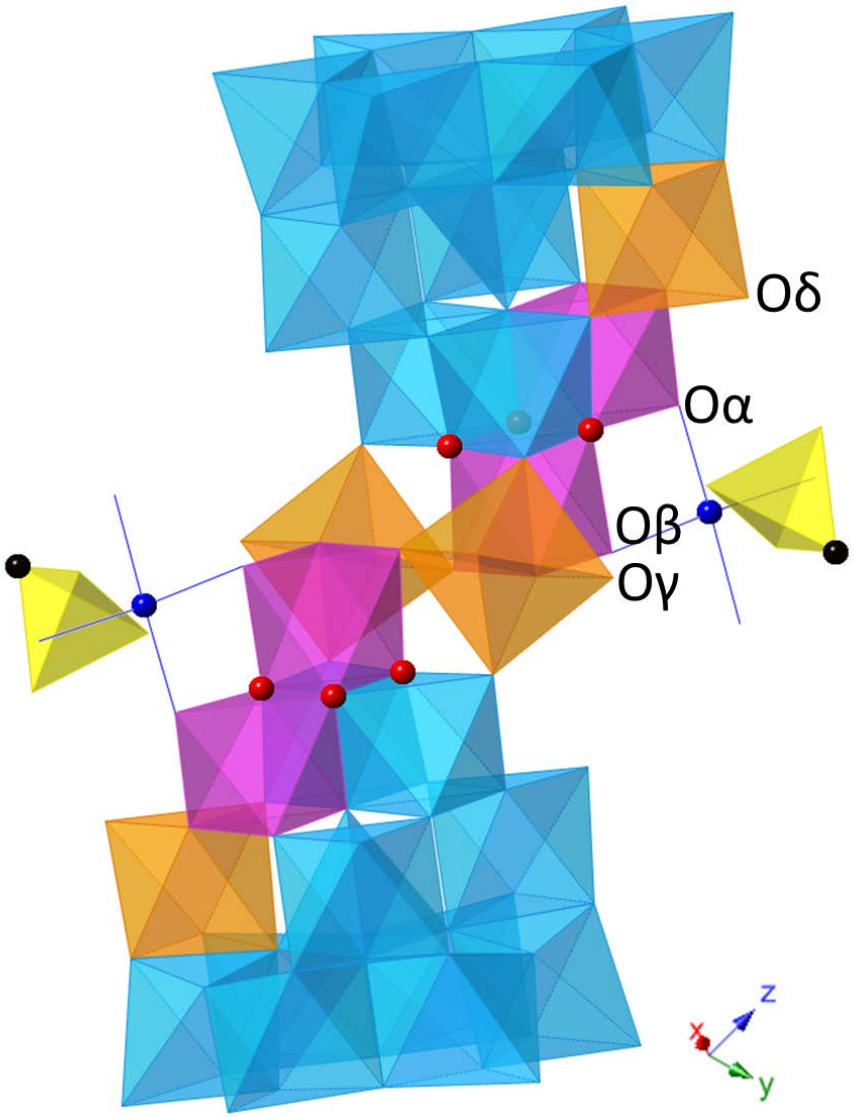

Figure 5.9 Representative Al_{30} polyhedron representation. Pink polyhedron aluminums are representative of the "active site", where the blue atom (Cu) can be seen bonding. The red spheres are indicating the oxygens that are μ_3-OH groups. All oxygens are left out for clarity. The orange polyhedron aluminums are representative of the aluminums that have terminal η-H_2O that engage in hydrogen bonding interactions with the NDS molecules. The yellow tetrahedral is a representative sulfate corresponding to an NDS molecule with the black sphere (carbon) denoting the naphthalene ring's connectivity. The terminal oxygen-containing groups of the pink and orange aluminums are labeled as Oδ, Oα, Oβ, & Oγ. Each of the bonded aluminums are labeled Alδ, Alα, Alβ, & Alγ, respectively.

charge, indicative of an oxo (O^{2-}) group, then the bond valence sum would be closer to -2. Similarly, hydroxo groups (HO^{-}) have bond valence sums closer to -1. Water groups observe bond valence sums somewhere between 0 and -1.

There are limitations in the use of bond valence calculations. First, there is an assumption of complete iconic bond character. Since covalency within a bond occurs along a spectrum, some slight variation in the bond valence sum can occur based on difference in bonding character. Secondly, the structural parameters are based on the specific data sets within a database and there may be differences in the data quality and chosen structural parameters. Lastly, this method may not be refined or sensitive enough to determine slight variations in bond valence, which could be indicative of variations in reactivity, electrostatics, and/or bonding capabilities.

5.8 Structural Descriptions of Al_{30} Clusters

Three Al_{30} clusters have been synthesized and characterized by single crystal XRD: Al_{30}-F, Al_{30}-F-Cu, Al_{30}-F-Cu-Gly. As previously described, the structure of these polyaluminum structures are composed of two δ-Al_{13}^{k} structures linked by four bridging octahedrally coordinated Al cations. (**Figure 5.8 A**) This structure can be described in more detail by denoting specific important regions of the cluster. One region is considered the "beltway" which is located about the four "bridging" Al that connects the δ-Al_{13}^{k} clusters. Another region is denoted as the "cap" which is the terminal ends of the cluster located at the base of the Keggin molecule (**Figure 5.8 B**, blue polyhedra). The "beltway" has previously been identified as the most likely place on the cluster for surface binding. This "active site" has previously bound Cu^{2+}, Zn^{2+}, Al^{3+}, and phosphonate groups through a bridging bidentate bonding coordination between two adjacent aluminum octahedra (**Figure 5.8 B**, pink polyhedra).[74, 82, 132] Similarly, sulfonate groups (from the

NDS molecules) have been previously shown to stabilize the cations in the active site as they participate in inner and outer sphere coordination with the metal centers and hydrogen bonding interactions with the terminal η-H_2O groups on the clusters that adjacent to the active site. (**Figure 5.8 B**, orange polyhedra). Slight variations at these regions of the Al_{30} clusters can be observed in the three new structures presented here.

The reactivity of the Al_{30} cluster has been associated with the general shape,[142] yet that physical attribute may not be the sole reason for the coordination of cations and oxyanions in that particular region of the cluster. A notable aspect of the active site is that these two Al polyhedra are edge-sharing and, therefore, have two sharing bridging-μ_3-OH groups. This allows a situation where the two terminal η-H_2O waters of these aluminum cations to be sufficiently close to allow bidentate binding of a ligand. (**Figure 5.9**) The "active site" aluminum octahedra are some of the few aluminum cations in the Al_{30} cluster that have μ_3-OH bridging ligands (**Figure 5.9,** red spheres), which also may play a role in this reactivity. Likewise, these aluminum cations in the active site not only have multiple μ_3-OH groups, but they also have adjacent aluminums (the only two) that have *no* η-H_2O groups. This, undoubtedly, affects the reactivity of the terminal oxygen groups on these active site aluminum octahedra due to η-H_2O groups contributing little charge to the metal center as opposed to oxy or hydroxy groups which contribute more due to their charge. This trend can be yet another factor, beyond shape of the Al_{30}, which helps determine the reason for reactivity at this active site and bidentate ligand binding. This bidentate binding tendency of the Al_{30} at the active site may play a crucial role in the adsorption of metal or organic contaminants in complex nuclear wastes.

5.8.1 Al-O Bond Distances

In the bare Al_{30} molecule, the Al-O bond lengths associated with the active site are 1.911(6) and 1.816(7) Å.[82] (**Table 5.11**) This distance changes when the Cu^{2+} cation coordinates in a bridging bidentate fashion within the active site as observed in Al_{30}-Cu_2, which previously reported by Samangi et al. with Al-O bonds distances of 1.841(13) and 1.811(12) Å. Complexation by the Cu^{2+} cation most notably changes the bond distances for Alβ-Oβ, which is on the beltway side of the active site. Shortening of the Alβ-Oβ bond is noted with other complexants as well, including in the presence of formate and glycine ligands. The Alβ-Oβ bond distances shorten in the order: Al_{30}-F (1.843(8) Å), Al_{30}-F-Cu(1.826(6) Å), Al_{30}-Cu_2(1.811(12) Å). The Al_{30}-F-Cu is modeled as partial occupancy with 50% Cu and 50% formate; therefore, the bond distance trends agree with this assessment. However, the longest bond for the Alβ-Oβ site is associated with Al_{30}-F-Cu-Gly (1.847(6) Å), but could be related to the disorder present in this compound.

While the active site Alα-Oα bond remained relatively unchanged from Al_{30} to the Al_{30}-Cu_2, there are observable differences in the three new structures that also follow the trends related to occupancy of the site. The Al_{30}-F and Al_{30} structures have a similar Alα-Oα bond distances, 1.914(9) and 1.911(6) Å, respectively. This is followed by progressively shorter bonds of Al_{30}-F-Cu, Al_{30}-F-Cu-Gly, and Al_{30}-Cu_2: 1.887(6), 1.876(6), and 1.841(13) Å, respectively. This trend is the same as the alpha site and shows that with more Cu and less formate, the Alα-Oα bond decreases in length. Again, providing an indication that the Al_{30}-F-Cu occupancy at the active site lies somewhere between the Al_{30}-Cu_2 and Al_{30}-F. Despite there being some uncertainties in the site occupancy for the active site within the Al_{30}-F-Cu-Gly compound, the bond distances falls into a similar observable range as the Al_{30}-F-Cu compound. These trends do

help determine if the modeled occupancy for these compounds is a correct interpretation of the X-ray diffraction data.

*Table 5.11 Bond distances corresponding to **Figure 5.9** (Å) for each cluster (Cu being a place-holder). The greek symbols refer to the respective oxygens (or the aluminums they are attached to) from **Figure 5.9**. The Al_{30}-Cu_2 is a structure from the publication:[74] The Al_{30} is a structure from the publication:[82]*

Active Site		Al_{30}-F(Å)	Al_{30}-F-Cu(Å)	Al_{30}-F-Cu-Gly(Å)	Al_{30}-Cu_2(Å)	Al_{30}(Å)
Alδ	Oδ	1.909(8)	1.919(6)	1.941(7)	1.927(8)	1.903(8)
Alα	Oα	1.914(9)	1.887(6)	1.876(6)	1.841(13)	1.911(6)
Alβ	Oβ	1.843(8)	1.826(6)	1.847(6)	1.811(12)	1.816(7)
Alγ	Oγ	1.942(7)	1.953(7)	1.956(7)	1.946(9)	1.935(7)

5.8.2 Al_{30}-F Active Site Description

The site along the "beltway" region of the Al_{30} polycation that typically engages in binding interactions has a variety of different structures between the Al_{30} clusters. The first structure, Al_{30}-F, may contain a formate anion bridging in a bidentate fashion through the adjacent aluminum octahedra, though this cannot be conclusively determined with single crystal XRD. This finding, however, would not be too dissimilar to previous observations regarding the Al_{30} moiety. Previous work has reported the presence of Cu^{2+}, Al^{3+}, tert-butylphosphonate bridging in a bidentate fashion at what is denoted as the "active site".[74, 82, 132] The Al_{30}-F compound does support these previous observations and shows the formate fully occupied yet undergoing considerable strain due to the bending needed to achieve this bidentate binding mode. (**Figure 5.11**) The bridging distance may be too long for a small organic carboxylate to effectively bridge that distance and further computational analysis is necessary to determine the correct binding mode. Despite this uncertainty, the figures all portray the formate bridging. (**Figure 5.10**) The sulfate positioned to engage in hydrogen bonding interactions with the surface η-H_2O's on the

orange polyhedral for the Alδ and Alγ atoms. Similarly, there is sufficient void space surrounding the active site which is not observed in all three of these of Al_{30} structures. (**Figure 5.11**)

5.8.3 Al_{30}-F-Cu Active Site Description

The Al_{30}-F-Cu is thought to be similar to the Al_{30}-F due to evidence that there is still a formate bridging in a bidentate fashion across the active site, yet this time modeled at 50% occupancy. (**Figure 5.12**) The other 50% occupation is Cu, which has previously been observed by Samangi et al.[74] This is thought to be due to the method of formation, utilizing formic acid with the later addition of Cu. Due to significant disorder in this site, it is difficult to discern the exact coordination and bonding within this region. Similarly, there is sufficient void space surrounding the active site that is not observed in the Al_{30}-F-Cu-Gly structure and is best seen with **Figure 5.13 B – C**.

5.8.4 Al_{30}-F-Cu-Gly Active Site Description

Based on the current crystallography of Al_{30}-F-Cu-Gly and despite the disorder observed at the active site, the data suggests that the Cu^{2+} cation is present in the active site to roughly a 50% occupation. (**Figure 5.14**) The inability to observe the terminal waters that are commonly seen on the copper could be due to disorder of the electron density associated with those oxygen atoms.[74] This may be due to the presence of the formate ligand on an adjacent Al_{30} cluster's cap that resides near the "active site" (**Figure 5.15 C, Figure 5.16**) and may cause disorder in the active site. The lack of void space surrounding this active site is a notable difference as compared to the Al_{30}-F-Cu and Al_{30}-F compounds.

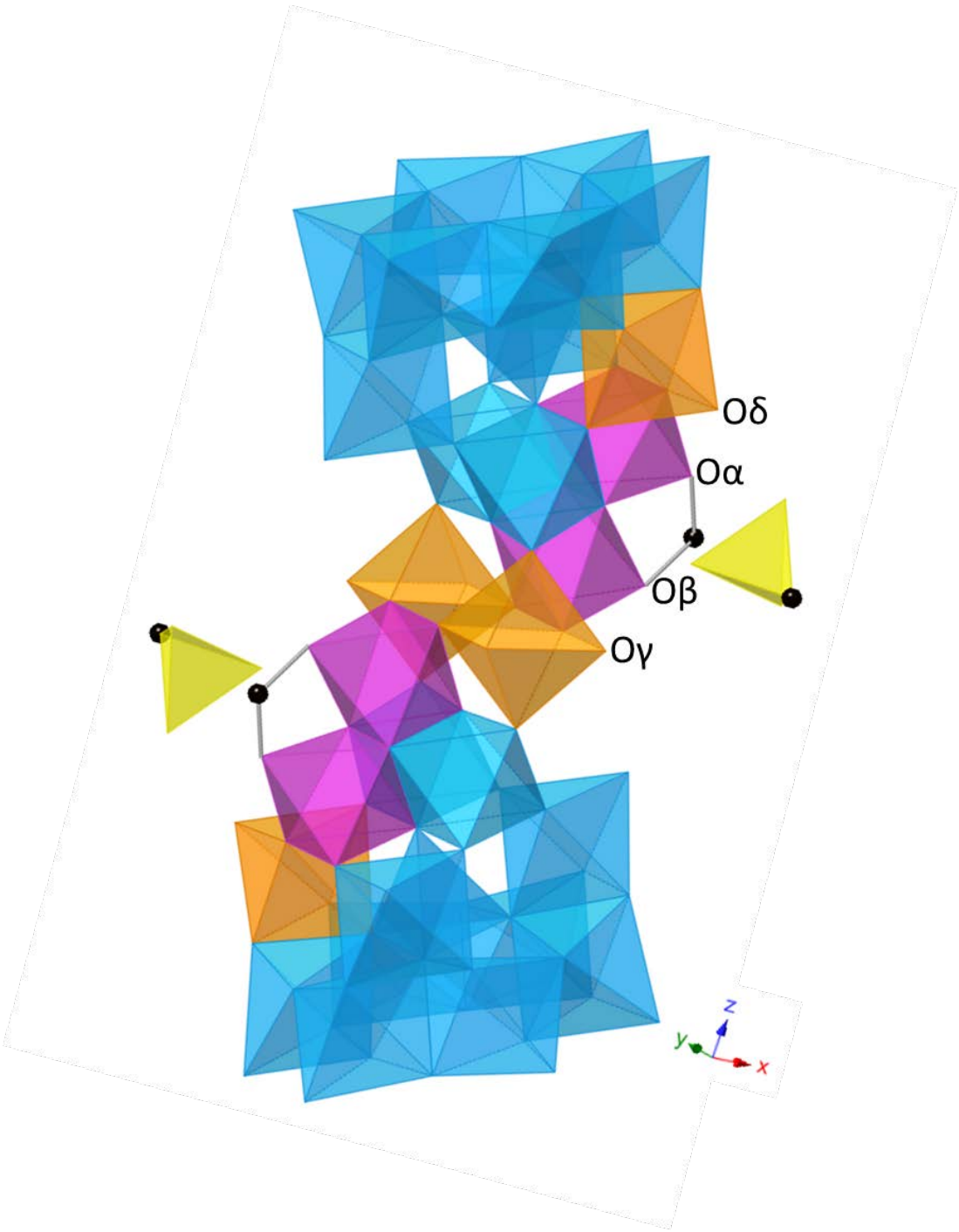

Figure 5.10 Al_{30}-F as a polyhedron representation. Pink polyhedron aluminums are representative of the "active site", where the blue atom (Cu) can be seen bonding. The black spheres are carbons. All oxygens are left out for clarity. The orange polyhedron aluminums are representative of the aluminums that have terminal η-H_2O that engage in hydrogen bonding interactions with the NDS molecules. The yellow tetrahedral is a representative sulfate corresponding to an NDS molecule with the black sphere (carbon) denoting the naphthalene ring's connectivity. The terminal oxygen-containing groups of the pink and orange aluminums are labeled as Oδ, Oα, Oβ, & Oγ. Each of the bonded aluminums are labeled Alδ, Alα, Alβ, & Alγ, respectively.

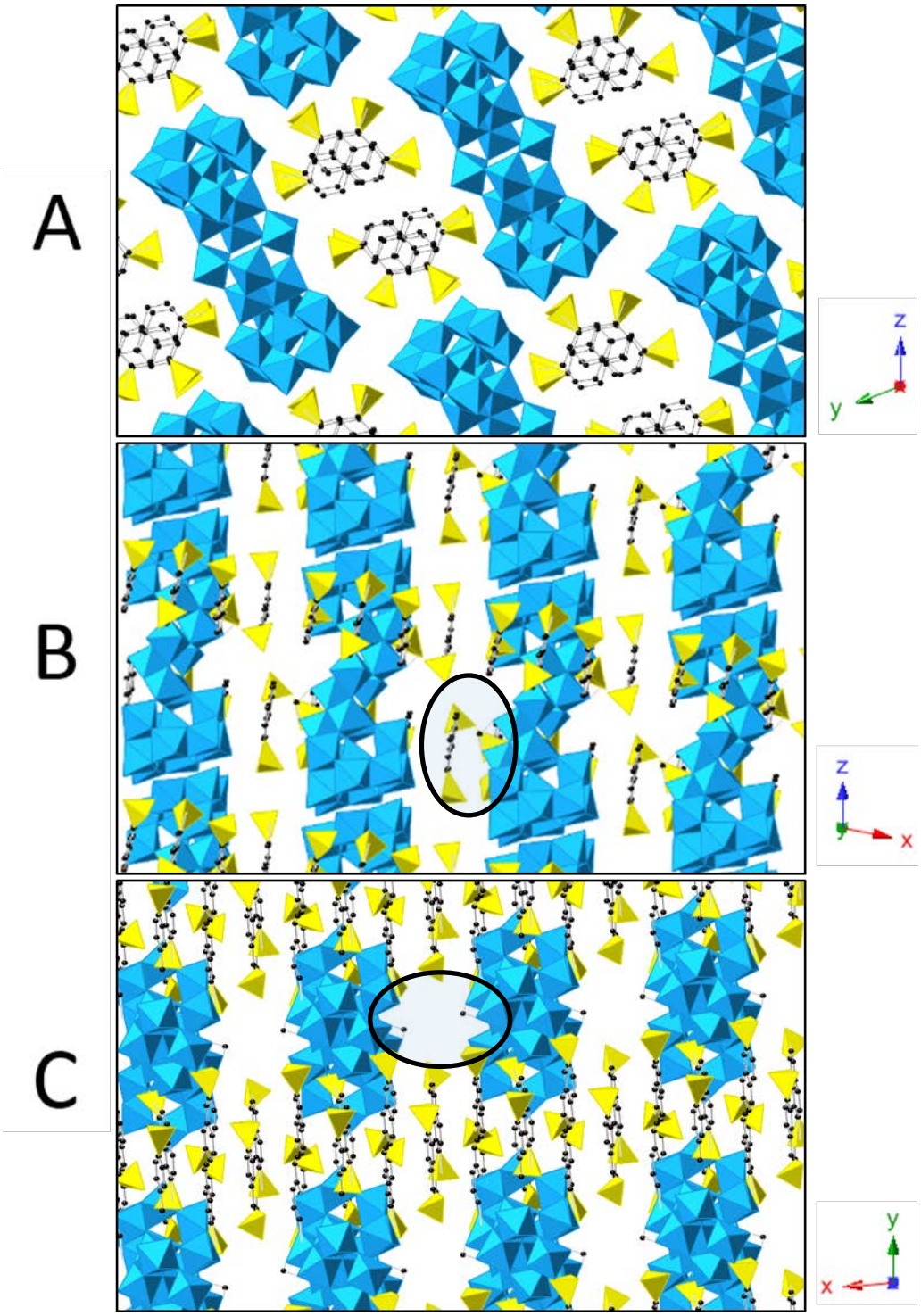

Figure 5.11 Polyhedron representation of Al_{30}-F showing aluminum as blue polyhedrons, sulfates on the NDS molecules as yellow polyhedron, carbon as Hydrogens, oxygens and interstitial waters are left out for clarity. (A) view down a (x-axis). (B) view down b (y-axis). (C) view down c (z-axis). Circles identify the active site.

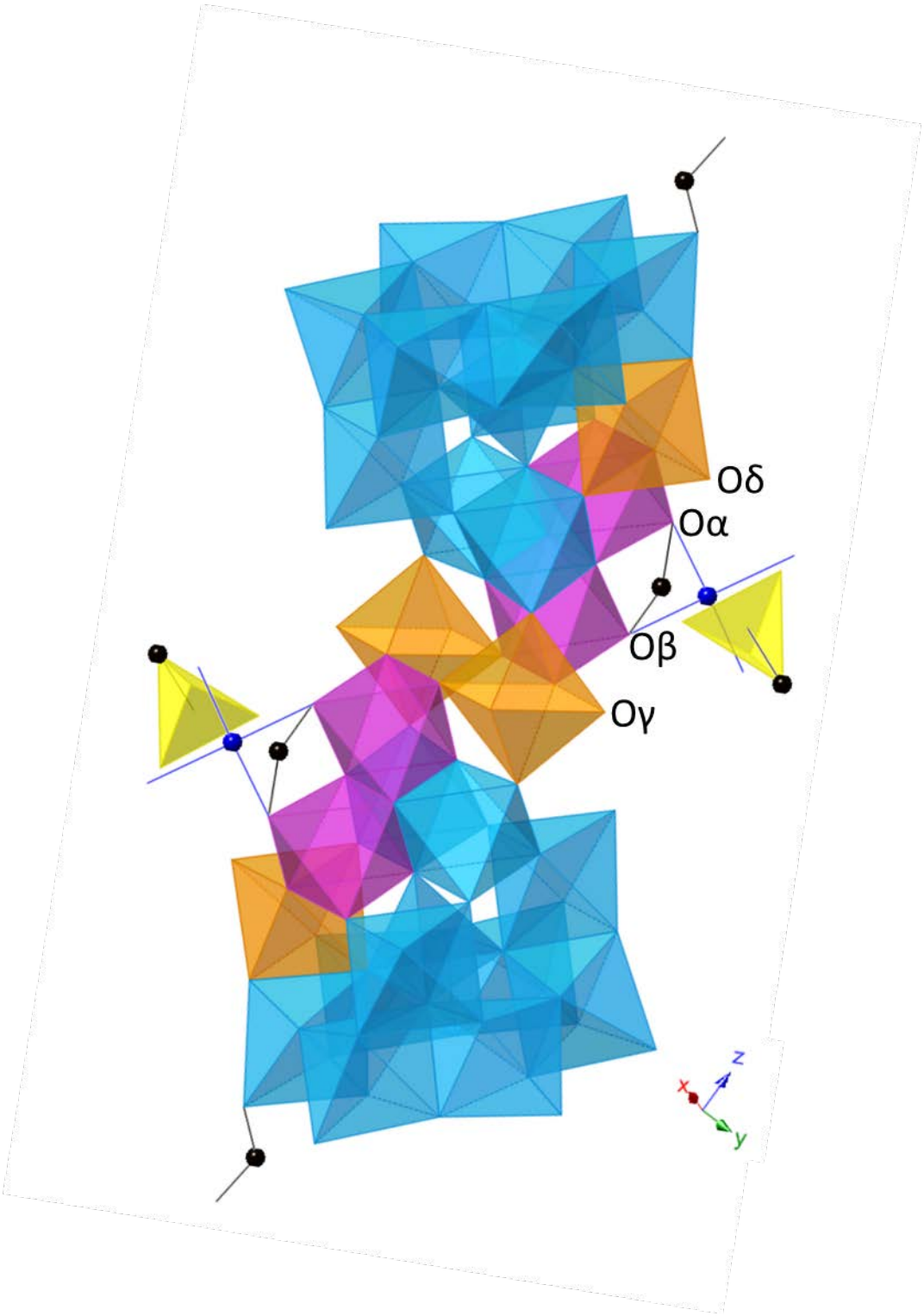

Figure 5.12 Al_{30}-F-Cu as a polyhedron representation. Pink polyhedron aluminums are representative of the "active site", where the blue atom (Cu) can be seen bonding. The black spheres are carbons, the orange polyhedron aluminums are representative of the aluminums that have terminal η-H_2O that engage in hydrogen bonding interactions with the NDS molecules. The yellow tetrahedral is a representative sulfate corresponding to an NDS molecule with the black sphere (carbon) denoting the naphthalene ring's connectivity. The terminal oxygen-containing groups of the pink and orange aluminums are labeled as Oδ, Oα, Oβ, & Oγ. Each of the bonded aluminums are labeled Alδ, Alα, Alβ, & Alγ, respectively.

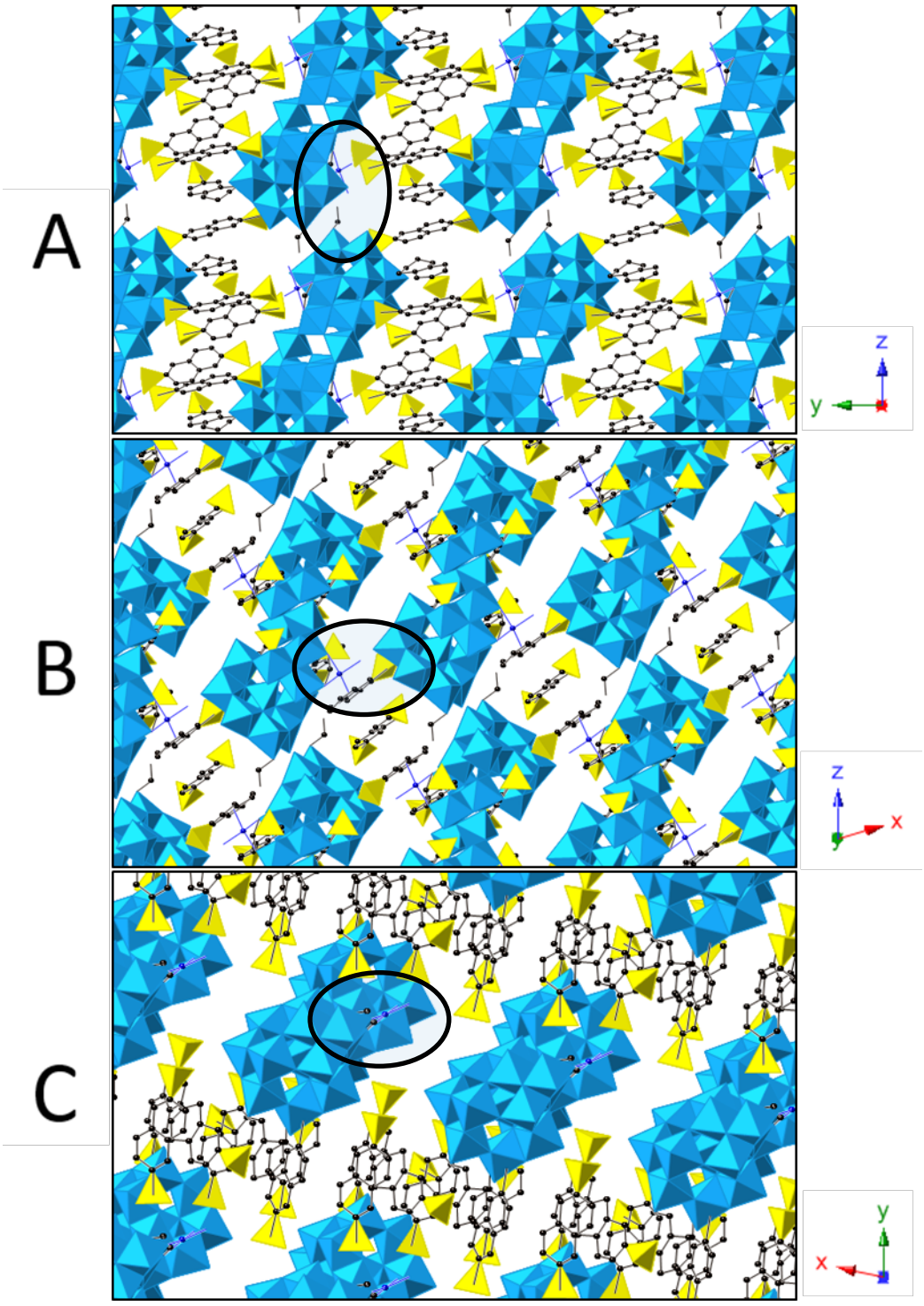

Figure 5.13 Polyhedron representation of Al_{30}-F-Cu showing aluminum as blue polyhedrons, sulfates on the NDS molecules as yellow polyhedron, carbon as black spheres, and copper as blue spheres. Hydrogens, oxygens, some sulfates and interstitial waters are left out for clarity. (A) view down a (x-axis). (B) view down b (y-axis). (C) view down c (z-axis). Circles identify the active site.

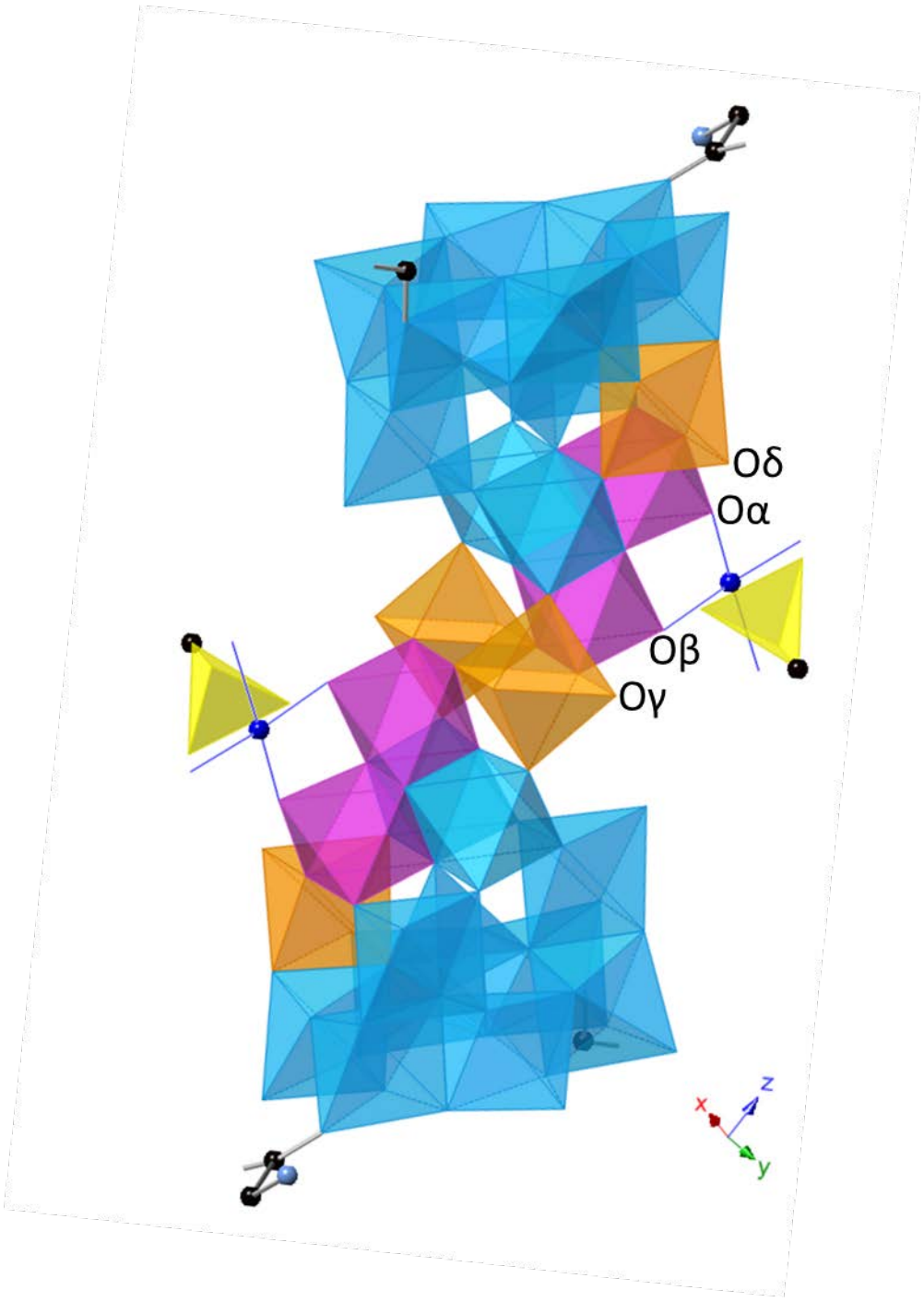

Figure 5.14 Al_{30}-F-Cu as a polyhedron representation. Pink polyhedron aluminums are representative of the "active site", where the blue atom (Cu) can be seen bonding. The black spheres are carbons, light blue spheres are nitrogen of the glycine. All oxygens are left out for clarity. The orange polyhedron aluminums are representative of the aluminums that have terminal η-H_2O that engage in hydrogen bonding interactions with the NDS molecules. The yellow tetrahedral is a representative sulfate corresponding to an NDS molecule with the black sphere (carbon) denoting the naphthalene ring's connectivity. The terminal oxygen-containing groups of the pink and orange aluminums are labeled as Oδ, Oα, Oβ, & Oγ. Each of the bonded aluminums are labeled Alδ, Alα, Alβ, & Alγ, respectively.

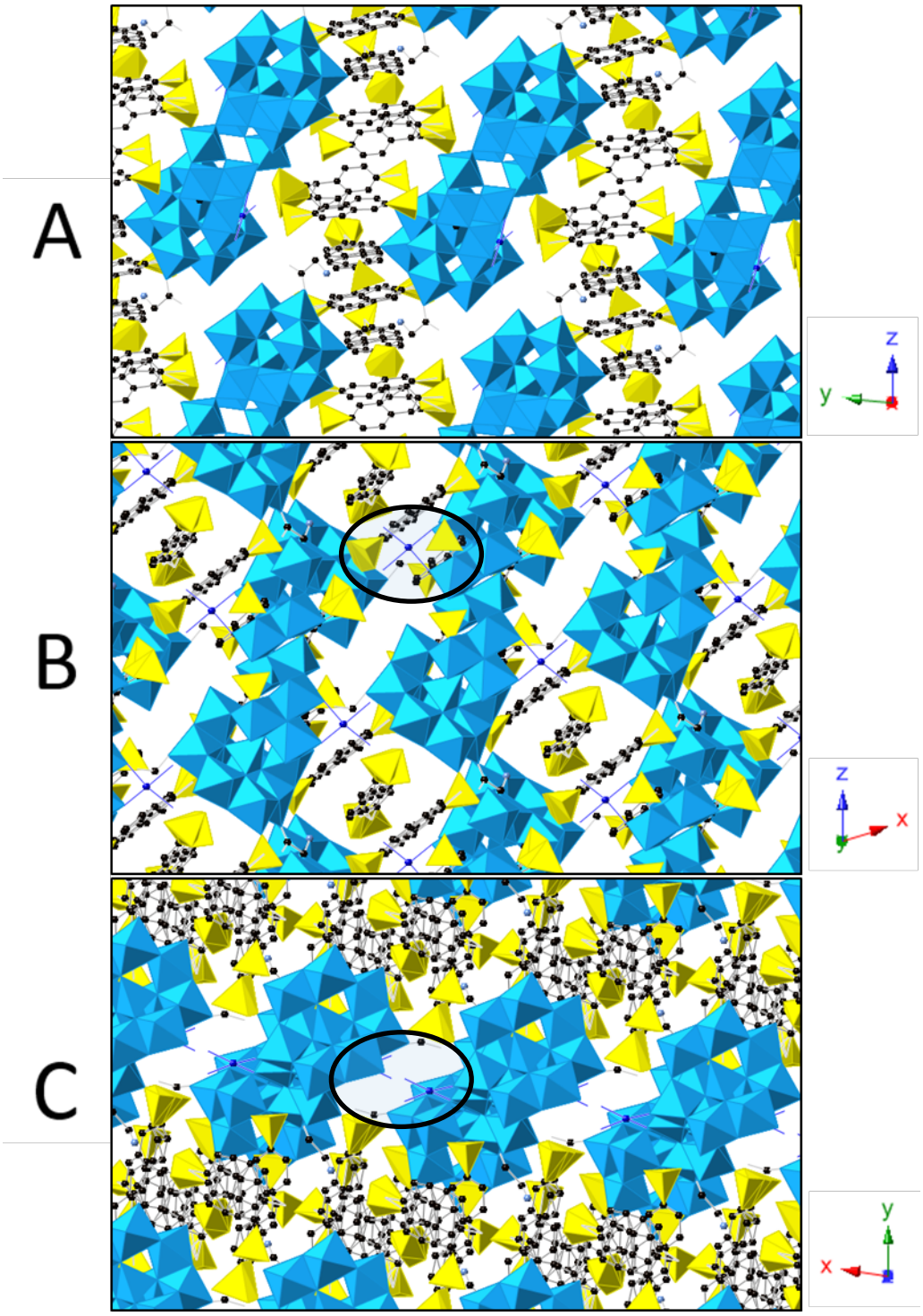

Figure 5.15 Polyhedron representation of Al_{30}-F-Cu-Gly showing aluminum as blue polyhedrons, sulfates on the NDS molecules as yellow polyhedron, carbon as black spheres, copper as blue spheres, and the nitrogen on the glycine as a light blue sphere. Hydrogens, oxygens and interstitial waters are left out for clarity. All disordered NDS molecules are shown. (A) view down a (x-axis). (B) view down b (y-axis). (C) view down c (z-axis). Circles identify the active site.

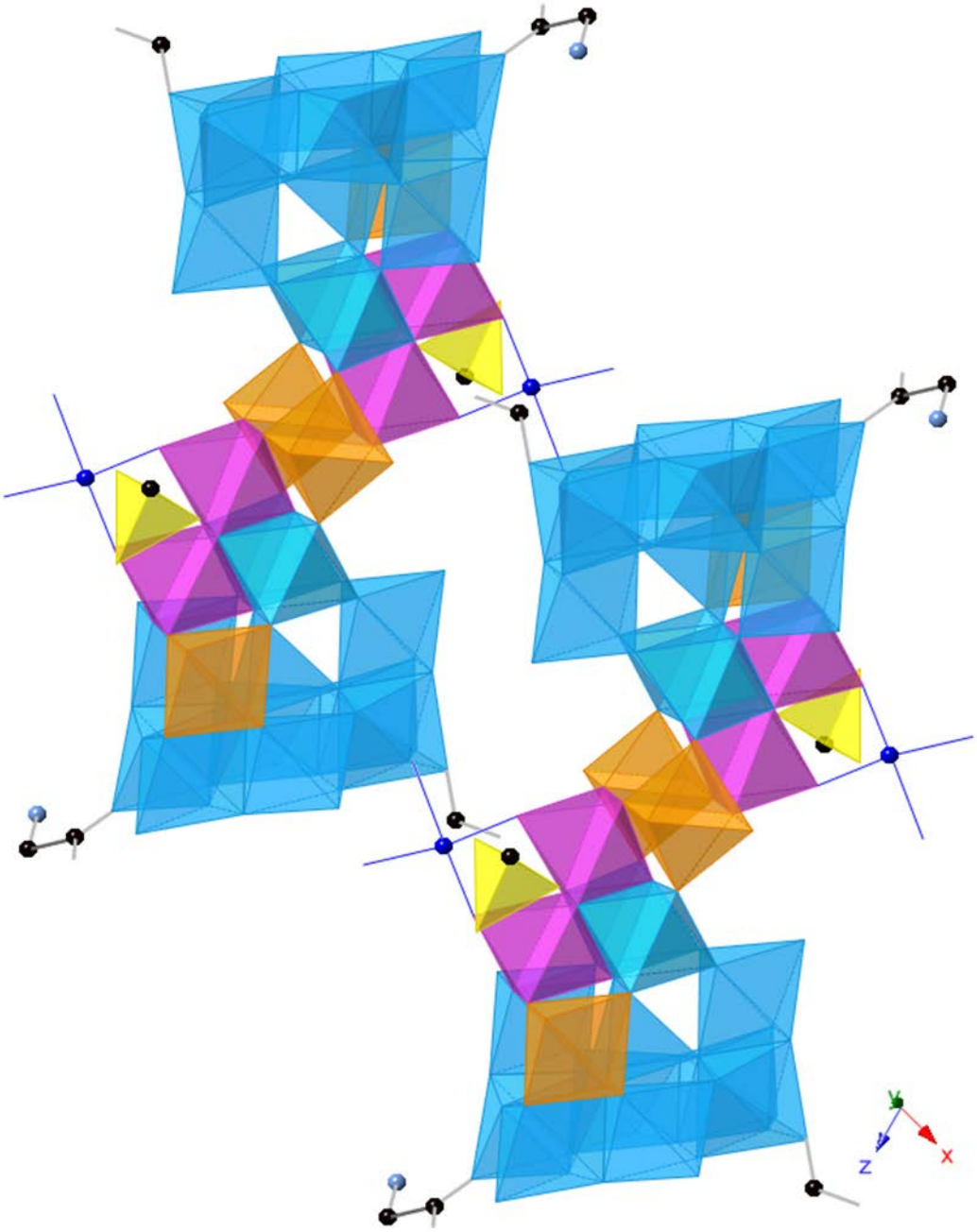

Figure 5.16 Two Al_{30}-F-Cu as a polyhedron representation focusing on the close proximity of the formate on the cap and the disordered active site. Pink polyhedron aluminums are representative of the "active site", where the blue atom (Cu) can be seen bonding. The black spheres are carbons, light blue spheres are nitrogen of the glycine. All oxygens are left out for clarity. The orange polyhedron aluminums are representative of the aluminums that have terminal η-H_2O that engage in hydrogen bonding interactions with the NDS molecules. The yellow tetrahedral is a representative sulfate corresponding to an NDS molecule with the black sphere (carbon) denoting the naphthalene ring's connectivity.

It has been observed that the sulfate anion, whether as an NDS molecule or simply sulfate, is important in the isolation of these Al_{30} clusters (as well as many other polyaluminum clusters).[68, 74, 79, 81-83, 111, 132, 143] This is an important additive for stabilizing the active site to allow adsorption of various cations and oxoanions.[74, 142] Sulfate interactions with the isolated Al_{30} clusters, with and without adsorbates in the active region, were explored to a means to understand the differences observed in this system. More specifically, we compared the interatomic distances from the sulfate to η-H_2O groups (Oγ and Oδ) of Alγ and Alδ and the Cu site. (**Figure 5.10, 5.12, 5.14**, **Table 5.12**)

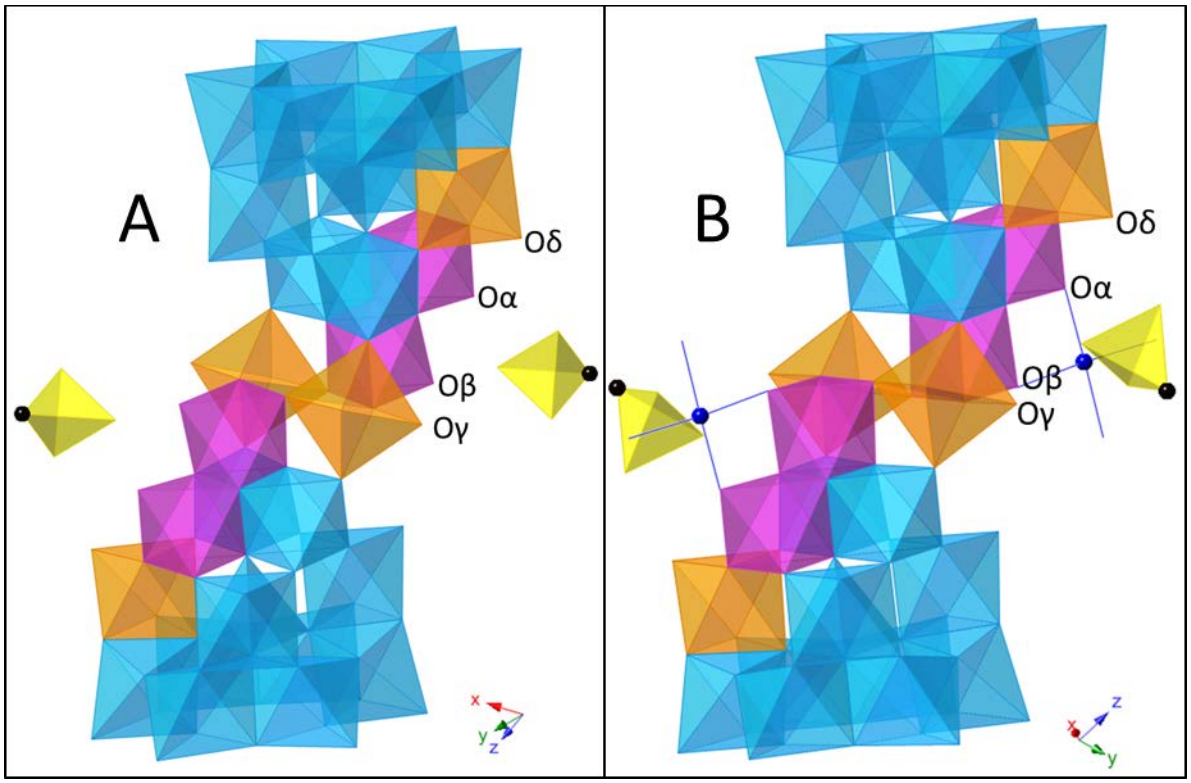

Figure 5.17 (A) Al_{30} (B) Al_{30}-Cu_2. Both A and B are a polyhedron representation focusing on the close proximity of the formate on the cap and the disordered active site. Pink polyhedron aluminums are representative of the "active site", where the blue atom (Cu) can be seen bonding. The black spheres are carbons, light blue spheres are nitrogen of the glycine. All oxygens are left out for clarity. The orange polyhedron aluminums are representative of the aluminums that have terminal η-H_2O that engage in hydrogen bonding interactions with the NDS molecules. The yellow tetrahedral is a representative sulfate corresponding to an NDS molecule with the black sphere (carbon) denoting the naphthalene ring's connectivity.

It is challenging to discern a trend within these sulfate interaction distances, yet it does seem as though the sulfate anions exhibit weaker interactions with the Al_{30} molecule and potentially explaining the disorder on the active site of Al_{30}-F-Cu-Gly. These weaker interactions are suggested by the longer hydrogen donor to acceptor (D-A) distances between the sulfate oxygen atoms and Oγ and Oδ hydroxo groups of Al_{30}-F-Cu-Gly as compared to the other structures. Al_{30}-F-Cu-Gly has the longer average D-A distance (Oδ/γ - O_{sulf}) of 2.746 Å as compared to 2.685, 2.728, and 2.730 Å for Al_{30}-F, Al_{30}-F-Cu, and Al_{30}-Cu_2, respectively. These distances are similar and can then be compared to the other distances of 2.761 Å and 2.59 Å for the other two Cu-containing structures. This is a notable difference and could either be the result of the formate from the adjacent Al_{30} cap interfering with this interaction to create more disorder, or this could be the result of a disordered Cu at the active site.

Just measuring the interatomic distances does not provide the complete picture because the angles of the interactions could also be dramatically different which would likewise exhibit a change in the chemical environment of the site. (**Table 5.13**) The angles observed here seems to be similar amongst each group, indicating that the position of the sulfonate anion is similar across all of the reported structures. The Al_{30}-F-Cu-Gly does have the most obtuse angle listed at 111.9°, which would potentially indicate that the actual sulfur atom associated with the sulfate is located slightly farther from the Al_{30} cluster than the other structures.

*Table 5.12 Bond distances corresponding to **Figure 5.10** (Al_{30}-F), **Figure 5.12** (Al_{30}-F-Cu), **Figure 5.14** (Al_{30}-F-Cu-Gly), **Figure 5.17 A** (Al_{30}) **& 5.17 B** (Al_{30}-Cu_2), (Å) for each cluster. The greek symbols refer to the respective oxygens (or the aluminums they are attached to) from these figures. O_{sulf} refers to the oxygen on the sulfate of an NDS molecule. The Cu used for the Al_{30}-F-Cu-Gly bond distances was the closest of the split sites to the atom listed. The Al_{30}-Cu_2 is a structure from the publication:[74] The Al_{30} is a structure from the publication:[82]*

Active Site (Å)		Al_{30}-F	Al_{30}-F-Cu	Al_{30}-F-Cu-Gly	Al_{30}-Cu_2	Al_{30}
Oδ	S	3.539	3.625	3.576	3.576	3.663
Oγ	S	3.863	3.787	3.798	3.798	3.672
Oδ	O_{sulf}	2.652	2.807	2.777	2.777	2.683
Oγ	O_{sulf}	2.718	2.649	2.715	2.715	2.815
Cu	O_{sulf}	--	2.590	2.761	2.761	--

*Table 5.13 Angles from the sulfur of the sulfate, through atoms O_{sulf} (referring to the oxygen on the sulfate), to the oxygen denoted with Greek symbols ((**Figure 5.10** (Al_{30}-F), **Figure 5.12** (Al_{30}-F-Cu), **Figure 5.14** (Al_{30}-F-Cu-Gly), **Figure 5.17 A** (Al_{30}) **& 5.17 B** (Al_{30}-Cu_2)). The Greek symbols refer to the respective oxygen from these figures The Al_{30}-Cu_2 is a structure from the publication:[74] The Al_{30} is a structure from the publication:[82]*

		Al_{30}-F	Al_{30}-F-Cu	Al_{30}-F-Cu-Gly	Al_{30}-Cu_2	Al_{30}
Oδ	O_{sulf}	116.3°	113.1°	111.9°	114.9°	121.6°
Oγ	O_{sulf}	132.6°	128.7°	128.8°	131.4°	113.5°

5.8.5 Al_{30} Cap Description

As discussed in above, organic molecules can be observed binding to the "cap" of the Al_{30}. This includes the formate anion, which is present in large quantities during the synthesis of the Al_{30} clusters (Al_{30}-F, Al_{30}-F-Cu, Al_{30}-F-Cu-Gly). The formate anion within Al_{30}-F-Cu binds to the same cap location as the glycine ligand in Al_{30}-F-Cu-Gly. (**Figures 5.12, 5.14**) The glycine on Al_{30}-F-Cu-Gly is binding on the end of the cap three Al atoms away from the formate. (**Figure 5.14**) The bonding of any adsorbate to the cap of the Al_{30} molecule has not previously been reported in the literature. This trend could help inform how we decide to treat Al in nuclear waste

scenarios with the new understanding that these polyaluminum clusters can bind with carboxylate groups in numerous capacities.

5.9 Chemical Characterization

5.9.1 Fourier Transform Infrared Spectroscopy (FTIR)

Other spectroscopic techniques for the identification of aluminum hydroxide clusters include vibrational spectroscopy (i.e. Raman and Infrared (IR) spectroscopy). IR spectroscopy can often give information regarding the functional groups present, along with Raman spectroscopy. Raman experiences very low background yet has high limits of detection. A major advantage is the simple sample preparation and the non-destructive nature of these analytical techniques. FT-IR was performed on a Nicolet iS5 with a potassium bromide (KBr) pellet for a total of 512 scans.

Table 5.14 Aluminum formate ($Al(O_2CH)_3$) IR shifts (cm^{-1})[144]

Units: (cm^{-1})	υ (O−H)	υ (C−H)	υ_{as} (OCO)	υ_{as}, d_{ef} (OCO)	υ_{s} (OCO)	$\upsilon\ d_{ef}$ (C−H)	υ_{s}, d_{ef} (OCO)
$Al(O_2CH)_3$	3600–2300	2907	1620	1400	1375	1080	800

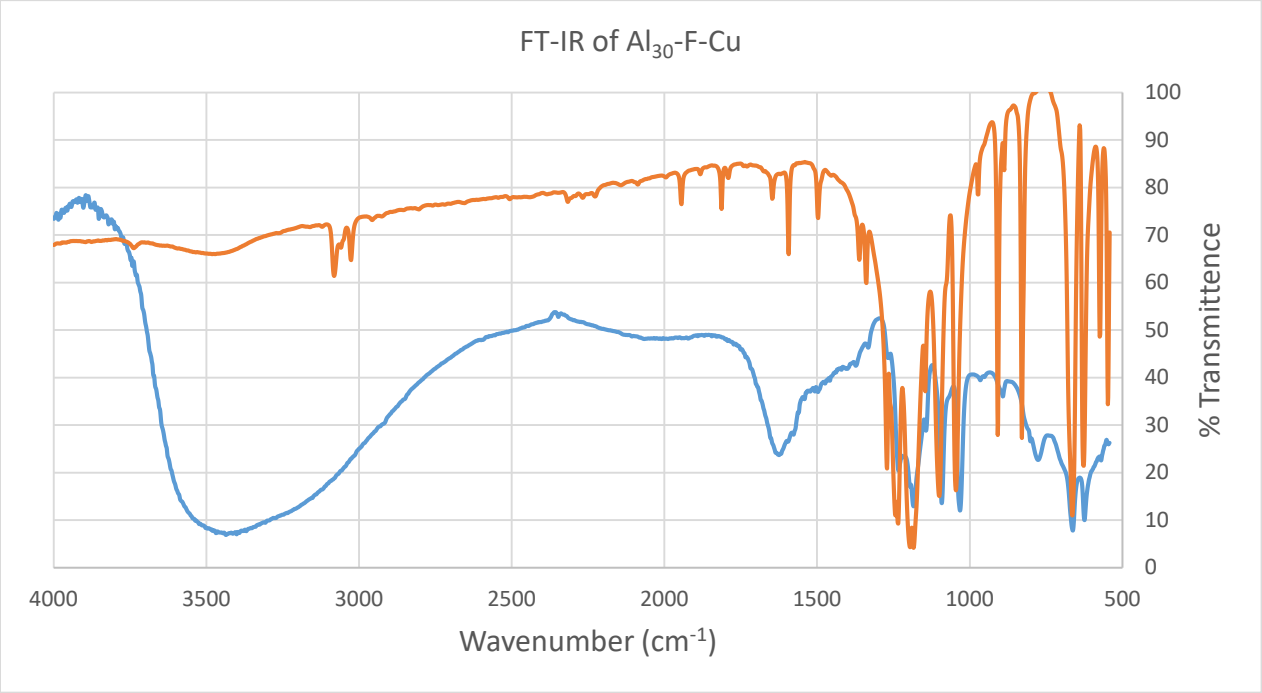

Figure 5.18 FT-IR of Al_{30}-F-Cu, KBr pellet, 512 scans (blue) along with the FT-IR of 2,6-NDS (orange).

Aluminum formate ($Al(O_2CH)_3$) has previously been reported to have IR active stretches, and their respective IR shift, as shown in **Table 5.13**.[144] The broad peak centered around 3400 cm^{-1} indicates the presence of water, which is the solvating the Al_{30} cluster in the crystal structure in significant quantities. Several other peaks below 1250 cm^{-1} correspond bands associated with the 2,6-NDS anion (**Figure 5.18**, orange). The remaining prominent peak(s) at 1622 cm^{-1} with shouldering at 1577 cm^{-1} can be assigned to the antisymmetric COO- stretching mode for a bridging-type formate complex.[145] These results indicate that there is formate inner sphere coordinating with Aluminum in the Al_{30}-F-Cu structure, which is supported by the crystallographic data.

5.9.2 ^{1}H and ^{13}C NMR of the Formate:Aluminum Solutions

Nuclear Magnetic Resonance (NMR) techniques can also be used to get a structural understanding of these clusters in both the solid-state and in solution. Single Crystal XRD is by nature only in the solid-state and can have scenarios where disorder does not allow precise determination of atom location or bond distances. NMR shifts can help determine some of these features like bond angles from molecular geometries as well as interactions between atoms due to their electronic environment (i.e. electronegativity of nearby atoms). Quadrupolar nuclei (nuclear spin quantum number, I > ½) can also be probed by NMR for nuclei of interest, including ^{27}Al.[68-69] This is hindered by typical peak-broadening, yet can sometimes be circumvented by the advent of very high magnetic fields as well as ultra-fast magic-angle spinning (MAS) NMR. Characteristic ^{27}Al NMR peaks can be seen due to the tetrahedral Al centers in Keggins and Al_{30} clusters. For example, the well-known ε-Keggin of aluminum has a characteristic ^{27}Al peak at 63 ppm that can be easily observed. Recent ventures have utilized ^{27}Al techniques to even help distinguish the various Keggin isomers due to this tetrahedral peak's chemical shift.[70, 146-148] NMR techniques have proven a useful addition in the characterization and speciation of cluster chemistry in solution.

Due to the introduction of organic molecules in these aluminum oxyhydroxy systems, traditional NMR techniques for organic molecules can be useful, including ^{1}H and ^{13}C NMR. These techniques can give information regarding the electronic (i.e. chemical) environment around these nuclei. For example, formate is a well characterized simple organic molecule that has distinct chemical environments for the hydrogen and carbon in the molecule. Upon coordination or other bonding interactions, a change in chemical shift can be expected due to this change in

chemical environments. These changes can be observed utilizing NMR and even verified using computational techniques to appropriately assign the changing peak with a new chemical environment.

^{1}H and ^{13}C NMR of the Formate:Aluminum stock solutions (0.85:1 and 2:1) was performed using a Bruker AvanceIII 500 MHz NMR with a gradient capable 4.0mm HR-MAS $^{1}H/^{13}C$ double-resonance probe. The probe was initially calibrated to the deuterium signal from deuterium oxide (D_2O). The samples were not spun and the ^{1}H NMR was run with 16 scans while the reported ^{13}C NMR was run with 512 scans.

To explore how the solutions change upon aging, 720 µl of each respective stock solution (2:1 & 0.85:1 formic:Al) was combined with 80 µl deuterium oxide (D_2O) in two separate NMR tubes. ^{1}H and ^{13}C NMR spectra were collected immediately and then each NMR tube was placed in an oil bath at 90^{o}C overnight. Solution NMRs were performed once a day for the 2:1 Formate:Al solution NMR. The 0.85:1 Formate:Al solution NMR was not able to be performed each day because after 24 hours, the solution had turned to a white gel. The formation of these white gels is not uncommon for these solutions as they hydrolyze with heat and precipitate as insoluble polyaluminum polymeric species.

There is a combination of three distinct peaks around 8.1 to 8.3 ppm in ^{1}H NMR, corresponding to the hydrogen of the formate.[144] This report indicates the ^{13}C NMR of aluminum formate ($Al(O_2CH)_3$) to be 169 ppm (**Figure 5.19**) and the ^{1}H NMR of the hydrogen of the formate to be 8.3 ppm.[144] For simplicity, the peak farthest downfield is excluded from analysis due to its low and seemingly unchanging intensity upon aging. The other two peaks, indicated as peak F1 and peak F2 have intensities that are seemingly changing as aging occurs. (**Figure 5.20**) After day

six, no further changes were observed in the peak morphology. More precise determination of the relative intensities with peak-fitting software was not deemed necessary due to the uncertainty of the precise identity of these peaks.

Peaks shown for ^{1}H NMR can be attributed to a changing formate environment in this aging aluminum solution. This could be explained in two ways: 1) The formate is changing its coordination location or mode with the surface of the aluminum cluster in solution; or 2) The aluminum clusters in solution are changing and thus the formate chemical environment is

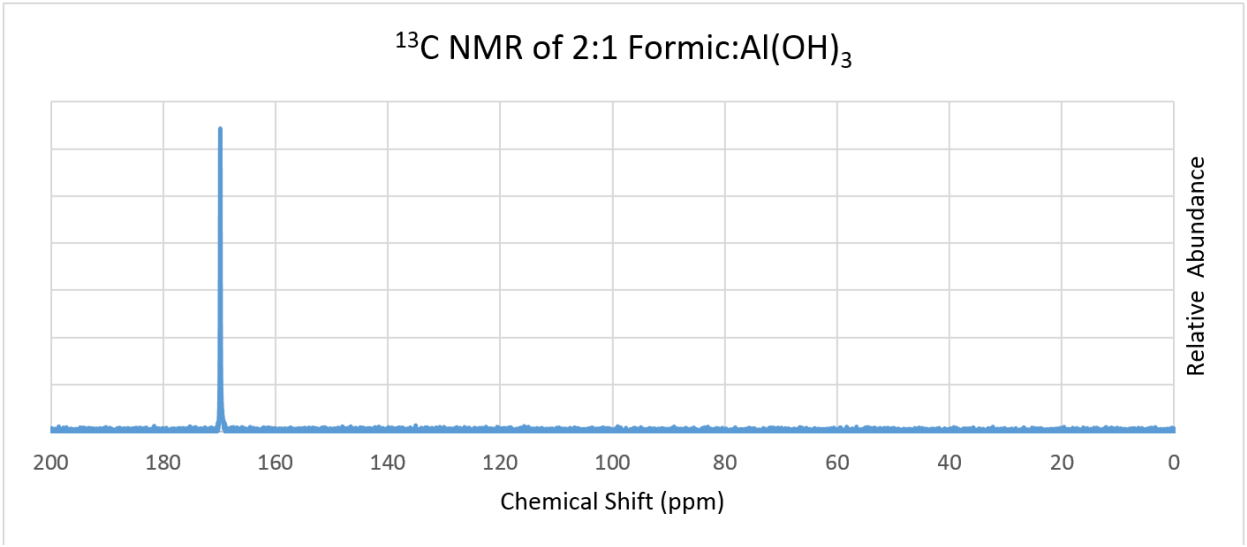

Figure 5.19 Representative ^{13}C NMR of the solution of 2:1 formic acid: $Al(OH)_3$ gel after 2 days at 90 °C. All other ^{13}C NMR's were identical at 169 ppm.

changing as they bind to each cluster slightly differently. Whether these changing NMR signals around 8.3 ppm indicate a change of aluminum speciation or simply a change in the formate location/mode of binding to the Al_{30} are both of interest. Each scenario indicates that isolating discrete aluminum clusters with formate adhered can be challenging due to the constant changing with aging. More precise studies looking at the aluminum speciation and relations with

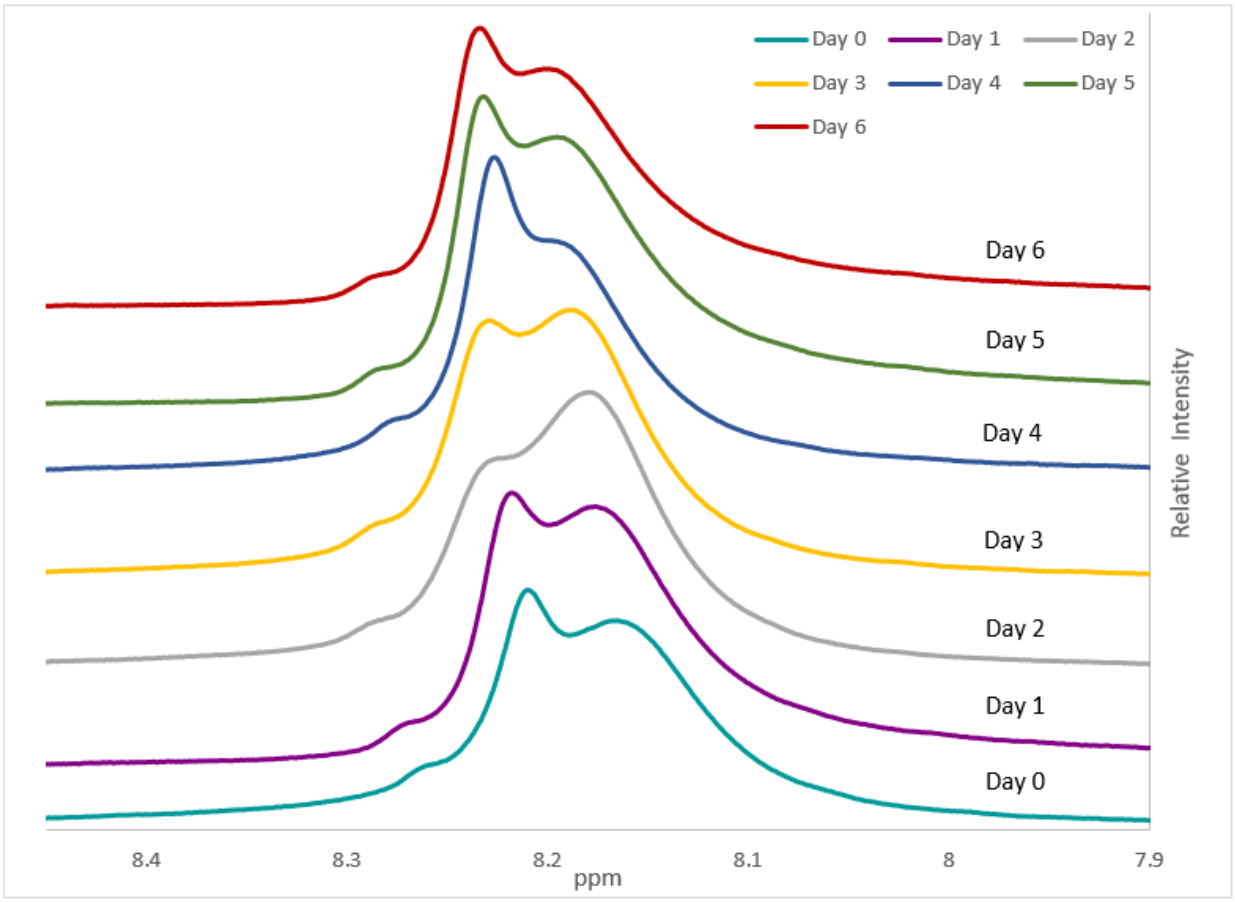

Figure 5.20 ^{1}H Solution NMR of 2:1 Formate:Aluminum hydroxide upon aging at 90 ^{o}C for 6 consecutive days. The peaks from 8.1 to 8.3 ppm are of the hydrogen attached to the carbon of formate. Peak F1 is indicated as the peak between ~ 8.23 and 8.25 ppm. Peak F2 is indicated as the peak between and ~ 8.17 and 8.21 ppm.

formate should be completed as small changes in the amount of heating could dramatically change the resulting cluster, including the interaction formate has with the cluster.

5.10 Conclusion

Waste streams rich in Al, including the Hanford Site, are incredibly complex and speciation in these systems are not well understood due to a fundamental lack of knowledge for Al^{3+} speciation in diverse matrices. Our investigation began with a well-studied system (Al_{30}) and added complexity in the form of both transition metal cations (Cu^{2+}) and organic molecules (formate, glycine). Similar to the previous studies on the Al_{30} nanocluster, there is evidence that formate will bind to the active site, but that there are several coordination modes that lead to

disorder in the crystallographic data. Upon addition of Cu^{2+}, there is competitive binding, leading to electron density at the site that can be modeled as a mixture of both the transition metal and the organic ligand. Upon the addition of copper to the mixture and we observe the binding to the Al_{30} become more complex. Notably, the active site now contains a mixture of formate and Cu binding, presumably competing for the site. These results indicate that transition metals and organic molecules will compete for the active site on the Al_{30} cluster in more complex matrices.

While previous work has shown that the active site will bind various metals cations, this work offers the first evidence of small organic ligands binding to the cap of the Al_{30} cluster. Nuclear waste streams will have large quantities of carboxylates due to separation processes. Under these relatively large concentrations or both formate and glycine, monodentate binding is shown to occur at the cap. This cap site was previously determining to be less reactive than the active site, noted by the shape (and/or electron deficiency) around the beltway region compared to the cap.[142] The addition of formate at the cap seems to be, at least in part, due to the copper occupying the active site that the formate may preferentially reside (as seen in Al_{30}-F).

5.11 Future Work

As stated previously, a better understanding of aluminum chemistry could aid in our treatment of nuclear waste that are plagued by challenges associated with metal hydrolysis. While the current work focuses on the more acidic pH region, additional work is needed to understand the formation of oligomers under high pH conditions. In addition, the development of better spectroscopic and scattering methods are needed to characterize these complexes in solution.

CHAPTER 6. CONCLUSIONS & FUTURE DIRECTIONS

6.1 Separation of Gallium and Actinides in Plutonium Nuclear Materials by Extraction Chromatography

Analysis of stable gallium in Pu nuclear materials for nuclear forensics applications and nuclear fuel certification has been demonstrated, utilizing radioisotopes that are becoming more popular for nuclear medicine applications. This creates a scenario in which these isotopes are becoming more widely available for alternative applications and provides opportunities for the development of new and innovative methodologies. This work not only utilized the nuclear medical radioisotope, ^{68}Ga, but resulted in the complete separation of Ga, Pu, U, Th, and Am using extraction chromatography. Precise determination of Ga enabled an accurate evaluation of the production method and aids in the development of methodology for production location identification– a useful metric for nuclear forensics. These advancements provided radioanalytical analysis of nuclear materials containing Ga, whether in nuclear weapon pits or in nuclear fuels for the purpose of energy production. These types of nuclear materials, such as MOX, are of interest due to their use in nuclear energy production and are formed as a byproduct of nuclear weapons disarmament. These materials need to be characterized and regulated so as to allow appropriate and responsible usage in nuclear energy production. The complete radioanalytical method for the separation of gallium and actinides has a use in numerous nuclear materials analyses, from nuclear forensics to nuclear fuels certification.

6.2 Disequilibrium of Naturally Occurring Radioactive Materials (NORM) in Drill Cuttings from a Horizontal Drilling Operation

Wastes associated with industrial activities have been a continual concern in recent years, notably in the area of domestic energy production and unconventional drilling techniques. These industries produce large volumes of wastes that may potentially create long-term undesirable environmental impacts. Due to large amounts of liquid wastes from hydraulic fracturing activities, radioactive-enriched liquid waste has become a public health concern and potential environmental contaminant. These liquid materials have exhibited enhanced NORM compared with normal background materials. These initial research results indicate that there is a need for increased monitoring of the liquid waste streams, but little was known regarding the solid-waste materials, particularly in landfill conditions. The work reported herein utilized new and more robust methods compared to previously reported methods that exhibited low radiochemical yields. Upon characterizing these solid wastes for NORM from the ^{238}U series, elevated levels of NORM were observed in samples collected from the Marcellus shale formation. Uranium-series disequilibrium was unexpectedly found, which indicates a need for a more detailed analysis of waste materials than previously utilized by regulatory agencies. Notably, there was disequilibrium between ^{226}Ra and ^{210}Pb, which is most likely due to the potential migration of gaseous ^{22}Rn, an intermediate radioactive decay product, in the subsurface environment.

Solid drill cuttings are typically disposed of in landfills, but there is a limited understanding of the mobility and transport of NORM, ^{238}U-series radionuclides, in these complex systems. Leachate studies were performed using a standard US EPA method and confirmed that as the pH of the leachate decreases, higher proportions of radionuclides leach out of the solid drill cuttings.

These results suggest a possibility that these materials could leach from the landfill and potentially enter surface waters. Disequilibrium among the isotopes of uranium leached was also observed, indicating that determination of ^{238}U-series radionuclides must include detailed radiochemical analysis of all relevant isotopes. The complexity of the complete radiochemical profile of the solid wastes and leachates underlines the importance of continued in-depth analysis and the development of new methodology for continued surveillance of NORM materials in heterogeneous environments.

6.3 Synthesis of Aluminum Hydroxide Octamer by a Simple Dissolution Method

A new, fast, and high-yielding synthesis of the aluminum oxyhydroxide octamer was achieved using amorphous aluminum hydroxide as a starting material. Clusters with similar topologies could also be an important constituent of complex nuclear wastes, such as materials currently undergoing reprocessing at the Hanford Site. A better overall understanding of Al chemistry, including identification of new clusters, could be invaluable for a more robust understand Al in these more complex systems. Identifying Al clusters in solution using spectroscopic methods continues to be problematic, but continued identification of these different types of cluster topologies will provide a means to develop the tools for in-situ identification in aqueous solutions.

6.4 Synthesis and Characterization of Novel Al_{30} Clusters Formed Through Dissolution of an Amorphous Aluminum Hydroxide Precursor: Relationships to Hanford Tank Waste

The Hanford Site exhibits a perfect example for the importance of a more complete and fundamental understanding of aluminum chemistry and speciation in complex systems. Along

that route, we isolated three new Al_{30} clusters, each of which has a unique set of archetypal contaminants bonded to its surface in specific locations on the cluster surface. Upon changing the chemical environment, we observed molecules bond in the previously described "active site" of the Al_{30} clusters and both formate and glycine are will coordinated to the "cap", which has not been previously reported in the literature. This could provide insight into the formation, stabilization, and reactivities of Al_{30} clusters in complex conditions, including waste scenarios. Changes in both the organics and the metals, both prevalent in these wastes, can dramatically affect the aluminum structures identified, which may play a crucial role in their bulk-phase chemistry, including nuclear waste scenarios such as that of the Hanford Site.

6.5 Future Directions

6.5.1 Quantification of Actinides and Stable Metals in Nuclear Materials

Further advancements in separation of actinides and Ga, specifically for applications in nuclear forensics, are needed to improve upon current methodology. These advancements include verifying the developed method herein on nuclear materials, including Pu-bearing nuclear weapons materials and MOX fuels. Along this line, testing MOX fuels both pre- and post-irradiation in a nuclear reactor broadens the scope of the method to more complex samples. Utilizing inductively coupled plasma-mass spectrometry (ICP-MS) for the gallium analysis could also further the method development. Certifying this method, including use of ICP-MS for stable metals analysis, would be crucial for its widespread use because ICP-MS is widely used in analysis laboratory for these analyses. The inclusion of ^{68}Ga as a radiotracer for this application would still be appropriate.

One complication with introducing previously irradiated nuclear materials (e.g. post-burnup MOX fuels) is the presence of fission products in the matrix. This new, very complex matrix could lead to additional problems with isobaric interferences with the stable gallium isotopes that could be measured by ICP-MS. Developing new methods or augmenting this method to account for these potential problems would be necessary so that irradiated nuclear materials can be effectively analyzed for these isotopes of interest.

Other future directions would be to continue to develop methods for other metrics that may act as important fingerprints in nuclear forensics applications and including nuclear medical isotopes in the design of new methodology. Other ratios of isotopes to stable metals could indicate the method or location of production of the nuclear material of interest. Determining what those may be, and developing a similar method to quantify them in nuclear materials, would be worthwhile efforts. Isotopes utilized in nuclear medicine applications could be used as a convenient tracer for other methods designed to quantify a stable metal. Creating other uses for isotopes used in nuclear medicine could help increase overall interest and use of them, allowing for better availability and lower costs for production. Using these new isotopes to quantify other elements that may currently lack an appropriate tracer could help develop methods that previously lacked quantitative approaches.

6.5.2 NORM Associated with Hydraulic Fracturing Wastes

Future endeavors would benefit greatly from the larger sample sizes that would come from increased access to these materials. We received just three solid state drill-bit samples after several years of searching and requesting them. Increased access to a wider range of samples could allow more monitoring and developing advanced techniques for these waste

forms. Eluting various solutions through columns of solid wastes could also aid our understanding regarding conditions that contribute to higher leaching rates. Other factors, such as pH, salinity, naturally occurring complexants, and so on could then also be studied with respect to their effect on NORM stability in these materials.

A further advancement would involve acquiring access to actual waste-isolation sites (i.e. landfills) containing these materials to conduct sampling of the leachates these sites produce. This would forgo the need for modeling and validate findings against a real-world sample. Factors such as landfill pH (both local and global), seasonal changes, weather effects, and others could also be analyzed if sample access were obtained. Public health research implications and directions could also be examined by analyzing different techniques for isolating and disposing of these materials, including the implications of their stability and potential impacts on surface waters and municipalities. These research directions could have dramatic implications for how we decide to characterize and dispose of these waste streams in the U.S.

6.5.3 Aluminum Speciation and Characterization in Wastes and Natural Environments

Our results indicate a crucial need to characterize the speciation of aluminum under more complex and basic conditions, such as that of liquid nuclear waste located at the Hanford Site. Understanding the intricacies of aluminum chemistry and its effects under these complex conditions is therefore useful for managing such nuclear wastes in the long term. The creation of synthetic samples of nuclear wastes and attempts to isolate aluminum clusters from them, could be a future direction that would provide immediate insights into the chemistry of this system. Radiolysis conditions in these nuclear wastes also adds a level of complexity not easily

analyzed under synthetic conditions, so utilizing the same procedures with actual nuclear waste forms could also be valuable. These samples have variability in many factors that could be adjusted that may affect speciation of Al, including radiolysis, temperature, pH, salinity, and ion/organic concentration.

Speciation is also very important with regard to aluminum contamination in the environment. This includes acid mine drainage and industrial wastes from Al industries that utilize the Bayer process for separating Al from ores. An example of the impact of these processes on the environment is the large spill of caustic wastes containing large amounts of Al and Fe into a river in Hungary, which caused a wildlife kill for many miles downstream. Identifying the aluminum and iron species present, along with their propensity to bind to other naturally occurring complexants, could provide insight into the long-term effects of spills. Obtaining samples from such spills would aid our ability to probe the chemistry occurring in these systems. There seems to be an interplay of Al and Fe chemistry in the environment, so exploring these elements and their interactions together is also a worthwhile avenue of investigation.

Another worthwhile endeavor would be the introduction of techniques that do not depend solely on isolation via single crystal XRD for the assumed identification of clusters in solution. Future advancements in this field will undoubtedly involve the incorporation of spectroscopic techniques that can identify specific Al species that exist in these complex systems, which may include mass spectrometry, two-dimensional femtosecond vibrational spectroscopy, small angle X-ray spectroscopy, and NMR techniques. This requires substantial investments in the near future to isolate and apply spectroscopic techniques to these Al structures and solutions under various conditions, allowing for discernment of their various spectroscopic fingerprints.

While some advancements have previously been made, we have not achieved precise and reliable quantification of polyaluminum species in solution.

REFERENCES

1. National Research Council, N. *Assuring a Future U.S.-Based Nuclear and Radiochemistry Expertise.*; National Academies Press: Washington, D.C., 2012.

2. University of Iowa, U. Radiochemistry at the University of Iowa. https://chem.uiowa.edu/radiochemistry (accessed 01/20/2017).

3. Seaborg, G. T.; McMillan, E. M.; Kennedy, J. W.; Wahl, A. C., Radioactive Element 94 from Deuterons on Uranium. *Physical Review* **1946,** *69* (7-8), 366-367.

4. Hanford B Reactor. http://www.hanford.gov/page.cfm/BReactor (accessed 03/01/2017).

5. Hecker, S. S., Challenges in Plutonium Science. *Los Alamos Science* **2000,** *No. 26*.

6. Federation of American Scientists; Kristensen, H. M. N., R. S. Status of World Nuclear Forces. https://fas.org/issues/nuclear-weapons/status-world-nuclear-forces/ (accessed 1/31/2017).

7. IAEA, I. A. E. A. IAEA Incident and Trafficking Database (ITDB) Incidents of nuclear and other radioactive material out of regulatory control 2016 Fact Sheet. https://www-ns.iaea.org/downloads/security/itdb-fact-sheet.pdf (accessed 1/25/2017).

8. Aggarwal, S. K., Nuclear forensics: what, why and how. *Current Science* **2016**.

9. UNODA, U. N. O. f. D. A. Treaty for the Non-Proliferation of Nuclear Weapons (NPT). https://www.un.org/disarmament/wmd/nuclear/npt/ (accessed 1/30/2016).

10. Wilson, D. F. B., E. C.; Besmann, T. M.; Devan, J. H.; Distefano, J. R.; Greene, S.R.; Rittenhouse, P. L.; Worley, B. A. , Potential effects of gallium on cladding material. US-DOE, Ed. 1997.

11. Wilkinson, W. D., Effects of Gallium on Materials at Elevated Temperatures. DOE, Ed. 1953.

12. Wilson, D. F. D., J. R.; Strizak, J.P.; King J.F.; Manneschmidt, E.T., Interactions of Zircaloy Cladding with Gallium: Final Report. US-DOE, Ed. 1998.

13. Au-Yeung, P. H.; Lukowski, J. T.; Heldt, L. A.; White, C. L., An auger spectrometric study of the crack tip surface chemistry for liquid metal embrittlement: Beta brass embrittled by gallium. *Scripta Metallurgica et Materialia* **1990,** *24* (1), 95-100.

14. US-DOE, Fuel Qualification Plan. US-DOE, Ed. 2001.

15. DeMuth, S. F., Preconceptual design for separation of plutonium and gallium by ion exchange. US-DOE, Ed. 1997.

16. DeMuth, S. F., ION EXCHANGE SEPARATION OF PLUTONIUM AND GALLIUM (1) Resource and Inventory Requirements, (2) Waste, Emissions, and Effluent, and (3) Facility Size US-DOE, Ed. 1997.

17. Kolman, D. G.; Griego, M. E.; James, C. A.; Butt, D. P., Thermally induced gallium removal from plutonium dioxide for MOX fuel production. *Journal of Nuclear Materials* **2000,** *282* (2–3), 245-254.

18. Eitrheim, E. S.; Knight, A. W.; Nelson, A. W.; Schultz, M. K., Separation of gallium and actinides in plutonium nuclear materials by extraction chromatography. *Journal of Radioanalytical and Nuclear Chemistry* **2015,** *303* (1), 123-130.

19. Schultz, M. K.; Mueller, D.; Baum, R. P.; Leonard Watkins, G.; Breeman, W. A., A new automated NaCl based robust method for routine production of gallium-68 labeled peptides. *Applied radiation and isotopes : including data, instrumentation and methods for use in agriculture, industry and medicine* **2013,** *76*, 46-54.

20. Gianquinto, J. M. D., J.S.; Keever, T.J., *Pushing the limits for detection of trace gallium impurities in MOX spent fuels*. Eichrom Technologies, LLC: 2012.

21. Rowan, E. L., Engle, M.A., Kirby, C.S., and Kraemer, T.F, Radium content of oil- and gas-field produced waters in the northern Appalachian Basin (USA)—Summary and discussion of data. *US Geological Survey Scientific Investigations Report* **2011,** (31), 5135.

22. Brown, V. J., Radionuclides in fracking wastewater: managing a toxic blend. *Environmental health perspectives* **2014,** *122* (2), A50-5.

23. Warner, N. R.; Christie, C. A.; Jackson, R. B.; Vengosh, A., Impacts of Shale Gas Wastewater Disposal on Water Quality in Western Pennsylvania. *Environmental Science & Technology* **2013,** *47* (20), 11849-11857.

24. Brian Schumacher, D. A., Bob Litman, Bob Shannon, Marinea Mehrhoff, Andrew Nelson, Michael Schultz, John Griggs, Development of Rapid Radiochemical Method for Gross Alpha and Gross Beta Activity Concentration in Flowback and Produced Waters from Hydraulic Fracturing Operations. EPA, U. E. P. A., Ed. 2014.

25. US Environmental Protection Agency, E., Method 900.0 Gross Alpha and Gross Beta in Drinking Water. 2007.

26. US Environmental Protection Agency, E., Analytical Methods Approved for Drinking Water ComplianceMonitoring of Radionuclides. 2014.

27. Nelson, A. W.; May, D.; Knight, A. W.; Eitrheim, E. S.; Mehrhoff, M.; Shannon, R.; Litman, R.; Schultz, M. K., Matrix complications in the determination of radium levels in hydraulic fracturing flowback water from Marcellus Shale. *Environmental Science & Technology Letters* **2014,** *1* (3), 204-208.

28. Zhang, T.; Gregory, K.; Hammack, R. W.; Vidic, R. D., Co-precipitation of radium with barium and strontium sulfate and its impact on the fate of radium during treatment of produced water from unconventional gas extraction. *Environ Sci Technol* **2014,** *48* (8), 4596-603.

29. Nelson, A. W.; Johns, A. J.; Eitrheim, E. S.; Knight, A. W.; Basile, M.; Bettis III, E. A.; Schultz, M. K.; Forbes, T. Z., Partitioning of naturally-occurring radionuclides (NORM) in Marcellus Shale produced fluids influenced by chemical matrix. *Environmental Science: Processes & Impacts* **2016,** *18* (4), 456-463.

30. Kondash, A. J.; Warner, N. R.; Lahav, O.; Vengosh, A., Radium and Barium Removal through Blending Hydraulic Fracturing Fluids with Acid Mine Drainage. *Environmental Science & Technology* **2014,** *48* (2), 1334-1342.

31. Doerner, H. A.; Hoskins, W. M., CO-PRECIPITATION OF RADIUM AND BARIUM SULFATES1. *Journal of the American Chemical Society* **1925,** *47* (3), 662-675.

32. Haluszczak, L. O.; Rose, A. W.; Kump, L. R., Geochemical evaluation of flowback brine from Marcellus gas wells in Pennsylvania, USA. *Applied Geochemistry* **2013,** *28*, 55-61.

33. National Nuclear Data Center, N. National Nuclear Data Center, NuDat 2 Database. http://www.nndc.bnl.gov/nudat2/: .

34. Swanson, V. E., *Geology and Geochemistry of Uranium in Marine Black Shales: A Review*. US Government Printing Office Washington, DC, 1961.

35. Nelson, A. W.; Knight, A. W.; May, D.; Eitrheim, E. S.; Schultz, M. K., *Naturally-Occurring Radioactive Materials (NORM) Associated with Unconventional Drilling for Shale Gas*. 2015; Vol. 1216.

36. Choppin, G. R. R., J.; Liljenzin, J-O.; Ekberg, C, *Radiochemistry and Nuclear Chemistry, Fourth Edition*. Academic Press, Elsevier: 2013.

37. Peate, D. W.; Hawkesworth, C. J., U series disequilibria: Insights into mantle melting and the timescales of magma differentiation. *Reviews of Geophysics* **2005,** *43* (1), n/a-n/a.

38. Fleischer, R. L., Isotopic disequilibrium of uranium: alpha-recoil damage and preferential solution effects. *Science* **1980,** *207* (4434), 979-81.

39. Osmond, J. K.; Cowart, J. B.; Ivanovich, M., Uranium isotopic disequilibrium in ground water as an indicator of anomalies. *The International Journal of Applied Radiation and Isotopes* **1983,** *34* (1), 283-308.

40. Nelson, A. W.; Eitrheim, E. S.; Knight, A. W.; May, D.; Mehrhoff, M. A.; Shannon, R.; Litman, R.; Burnett, W. C.; Forbes, T. Z.; Schultz, M. K., Understanding the radioactive ingrowth and decay of naturally occurring radioactive materials in the environment: an analysis of produced fluids from the Marcellus Shale. *Environmental Health Perspectives (Online)* **2015,** *123* (7), 689.

41. Eitrheim, E. S.; May, D.; Forbes, T. Z.; Nelson, A. W., Disequilibrium of Naturally Occurring Radioactive Materials (NORM) in Drill Cuttings from a Horizontal Drilling Operation. *Environmental Science & Technology Letters* **2016,** *3* (12), 425-429.

42. Nelson, A. W.; Eitrheim, E. S.; Knight, A. W.; May, D.; Wichman, M. D.; Forbes, T. Z.; Schultz, M. K., Polonium-210 accumulates in a lake receiving coal mine discharges—anthropogenic or natural? *Journal of Environmental Radioactivity* **2017,** *167*, 211-221.

43. West Virginia Department of Environmental Protection, W., Freedom of Information (FOIA) request. Protection, W. V. D. o. E., Ed. 2016.

44. Freidhoff, B., No Title. Nelson, A. W., Ed. 2015.

45. McMahon, J. Fracking Truck Sets Off Radiation Alarm At Landfill. https://www.forbes.com/sites/jeffmcmahon/2013/04/24/fracking-truck-sets-off-radiation-alarm-at-landfill/#4af56ee036e3 (accessed 03/01/2017).

46. Delegard, C. H. J., S.A., Chemical Disposition of Plutonium in Hanford Site Tank Wastes. Pacific Northwest National Laboratory, PNNL: Richland, Washington, USA, 2015.

47. Guillot, S., Aluminum Removal and Sodium Hydroxide Regeneration from Hanford Tank Waste by Lithium Hydrotalcite Precipitation. DOE, Ed. 2011.

48. Espana, J. S., The Behavior of Iron and Aluminum in Acid Mine Drainage: Speciation, Mineralogy, and Environmental Significance. In *Thermodynamics, Solubility and Environmental Issues*, Elsevier: 2007; pp 137-150.

49. Anjier, J. L.; Roberson, M. L.; Atchison, W. E., Bayer process production of alumina hydrate. Google Patents: 1985.

50. Day, D. Hungary threatened by 'ecological catastrophe' as toxic sludge escapes factory. http://www.telegraph.co.uk/news/worldnews/europe/hungary/8043969/Hungary-threatened-by-ecological-catastrophe-as-toxic-sludge-escapes-factory.html (accessed 03/07/2017).

51. Enserink, M., After Red Mud Flood, Scientists Try to Halt Wave of Fear and Rumors. *Science* **2010,** *330* (6003), 432-433.

52. Adya, V. C. T., S. K.; Kumar, M.; Purohit, P. J.; Mohapatra, M.; Seshagiri, T. K.; Godbole, S. V. , Determination of In and Ga in plutonium oxide matrix by ICP-AES after chemical separation. *Radiochim. Acta.* **2011,** *99*, 581-585.

53. Hecker, S. S.; Harbur, D. R.; Zocco, T. G., Phase stability and phase transformations in Pu–Ga alloys. *Progress in Materials Science* **2004,** *49* (3–4), 429-485.

54. Hecker, S. S.; Stan, M., Properties of plutonium and its alloys for use as fast reactor fuels. *Journal of Nuclear Materials* **2008,** *383* (1–2), 112-118.

55. Mahan, C.; Bonchin, S.; Figg, D.; Gerth, D.; Collier, C., Chromatographic extraction of plutonium and inorganic impurity analysis using ICP-MS and ICP-AES. *Journal of Analytical Atomic Spectrometry* **2000,** *15* (8), 929-935.

56. Mayer, K., Security: Expand nuclear forensics. *Nature* **2013,** *503*, 461-462.

57. Wilson, D. F. B., E. C.; Besmann, T. M.; Devan, J. H.; Distefano, J. R.; Greene, S. R.; Rittenhouse, P. L.; Worley, B. A., Potential effects of gallium on cladding materials. DOE, Ed. 1997.

58. Makarova, T. P.; Preobrazhenskaya, L. D.; Lovtsyus, A. V.; Fridkin, A. M.; Stepanov, A. V.; Lipovskii, A. A.; Belyaev, B. N., Application of isotope dilution method for

mass- and alpha-spectrometric determination of burn-up and uranium, plutonium and transplutonium element content in VVER-440 spent fuel. *Journal of Radioanalytical Chemistry* **1983,** *80* (1), 173-182.

59. Horwitz, E. P.; Dietz, M. L.; Chiarizia, R.; Diamond, H.; Maxwell, S. L.; Nelson, M. R., Separation and preconcentration of actinides by extraction chromatography using a supported liquid anion exchanger: application to the characterization of high-level nuclear waste solutions. *Analytica Chimica Acta* **1995,** *310* (1), 63-78.

60. Koma, Y. K., T.; Tanaka, Y. , *J. Nucl. Sci. Technol.* **1999,** *36*, 934-939.

61. Taylor, P. N., M.; Sano, Y.; Koma, Y.; Kamiya, M. , *J. Nucl. Sci. Technol.* **2012,** *44*, 373-381.

62. Harrison, J. J. Z., A.; Chisari, R.; Wong, H. K. Y. , *J. Environ. Radioact* **2011,** *102*, 896-900.

63. Maxwell, S. L. C., B. K.; Noyes, G. W., *Appl. Radiat. Isot.* **2010,** *68*, 2125-2131.

64. Kressln, I. K., *J. Anal. Chem.* **1977,** *49*, 842-846.

65. Maxwell, S. L. C., B. K.; Hutchison, J. B.; Spencer, R. B., *Journal of Radioanalytical and Nuclear Chemistry* **2013,** *298*, 1533-1542.

66. Inn, K. G. W. H., E.; Woodward, J. T.; Stewart, B.; Pollanen, R.; Selvig, L.; Turner, S.; Outola, I.; Nour, S.; Kurosaki, H.; LaRosa, J.; Schultz, M.; Lin, Z.; Yu, Z.; McMahon, C. , *Journal of Radioanalytical and Nuclear Chemistry* **2008,** *276*, 385-390.

67. Jackson, M. N.; Kamunde-Devonish, M. K.; Hammann, B. A.; Wills, L. A.; Fullmer, L. B.; Hayes, S. E.; Cheong, P. H. Y.; Casey, W. H.; Nyman, M.; Johnson, D. W., An overview of selected current approaches to the characterization of aqueous inorganic clusters. *Dalton Transactions* **2015,** *44* (39), 16982-17006.

68. Fu G.; Nazar, L. F. B., A.D., Aginng Processes of Alumina Sol-Gels: Characterization of New Aluminum Polyoxycations by 27Al NMR Spectroscopy. *Chemistry of Materials* **1991,** *3*, 602-610.

69. Thompson, A. R. K., A.C.; Gutowsky, H.S.; Oldfield, E., Oxygen-17 and aluminium-27 nuclear magnetic resonance spectroscopic investigations of aluminium(III) hydrolysis products. *Journal of the Chemical Society, Dalton Transactions* **1987**, 2317-2322.

70. Oliveri, A. F.; Colla, C. A.; Perkins, C. K.; Akhavantabib, N.; Callahan, J. R.; Pilgrim, C. D.; Smart, S. E.; Cheong, P. H. Y.; Pan, L.; Casey, W. H., Isomerization of Keggin Al13 Ions Followed by Diffusion Rates. *Chemistry – A European Journal* **2016,** *22* (52), 18682-18685.

71. Putnam, C. D.; Hammel, M.; Hura, G. L.; Tainer, J. A., X-ray solution scattering (SAXS) combined with crystallography and computation: defining accurate macromolecular structures, conformations and assemblies in solution. *Quarterly reviews of biophysics* **2007,** *40* (3), 191-285.

72. Akitt, J. W.; Elders, J. M., Multinuclear magnetic resonance studies of the hydrolysis of aluminium(III). Part 8. Base hydrolysis monitored at very high magnetic field. *Journal of the Chemical Society, Dalton Transactions* **1988,** (5), 1347-1355.

73. Jolivet, J.-P.; Chanéac, C.; Chiche, D.; Cassaignon, S.; Durupthy, O.; Hernandez, J., Basic concepts of the crystallization from aqueous solutions: The example of aluminum oxy(hydroxi)des and aluminosilicates. *Comptes Rendus Geoscience* **2011,** *343* (2–3), 113-122.

74. Abeysinghe, S.; Corum, K. W.; Neff, D. L.; Mason, S. E.; Forbes, T. Z., Contaminant Adsorption on Nanoscale Particles: Structural and Theoretical Characterization of Cu2+ Bonding on the Surface of Keggin-Type Polyaluminum (Al30) Molecular Species. *Langmuir* **2013,** *29* (46), 14124-14134.

75. Casey, W. H., Large Aqueous Aluminum Hydroxide Molecules. *Chemical Reviews* **2006,** *106* (1), 1-16.

76. Wang, W.; Wentz, K. M.; Hayes, S. E.; Johnson, D. W.; Keszler, D. A., Synthesis of the Hydroxide Cluster [Al13(μ3-OH)6(μ-OH)18(H2O)24]15+ from an Aqueous Solution. *Inorganic Chemistry* **2011,** *50* (11), 4683-4685.

77. Gatlin, J. T.; Mensinger, Z. L.; Zakharov, L. N.; MacInnes, D.; Johnson, D. W., Facile Synthesis of the Tridecameric Al13 Nanocluster Al13(μ3-OH)6(μ2-OH)18(H2O)24(NO3)15. *Inorganic Chemistry* **2008,** *47* (4), 1267-1269.

78. Seichter, W.; Mögel, H.-J.; Brand, P.; Salah, D., Crystal Structure and Formation of the Aluminium Hydroxide Chloride [Al13(OH)24(H2O)24]Cl15 · 13 H2O. *European Journal of Inorganic Chemistry* **1998,** *1998* (6), 795-797.

79. Johansson, G. L., G.; Sillen, L.G.; Soderquist, R., On the Crystal Structure of a Basic Aluminum Sulfate and the Corresponding Selenate. *Acta Chemica Scandanavica* **1960,** *14*, 769-771.

80. Smart, S. E.; Vaughn, J.; Pappas, I.; Pan, L., Controlled step-wise isomerization of the Keggin-type Al(13) and determination of the gamma-Al(13) structure. *Chemical communications (Cambridge, England)* **2013,** *49* (97), 11352-4.

81. Allouche, L.; Gerardin, C.; Loiseau, T.; Ferey, G.; Taulelle, F., Al(30): A Giant Aluminum Polycation. *Angewandte Chemie (International ed. in English)* **2000,** *39* (3), 511-514.

82. Abeysinghe, S.; Unruh, D. K.; Forbes, T. Z., Crystallization of Keggin-Type Polyaluminum Species by Supramolecular Interactions with Disulfonate Anions. *Crystal Growth & Design* **2012,** *12* (4), 2044-2051.

83. Casey, W. H.; Olmstead, M. M.; Phillips, B. L., A New Aluminum Hydroxide Octamer, [Al8(OH)14(H2O)18](SO4)5·16H2O. *Inorganic Chemistry* **2005,** *44* (14), 4888-4890.

84. Lokare, K. S.; Frank, N.; Braun-Cula, B.; Goikoetxea, I.; Sauer, J.; Limberg, C., Trapping Aluminum Hydroxide Clusters with Trisilanols during Speciation in Aluminum(III)-Water Systems: Reproducible, Large Scale Access to Molecular Aluminate Models. *Angewandte Chemie (International ed. in English)* **2016,** *55* (40), 12325-9.

85. Sposito, G., *The Environmental Chemistry of Aluminum*. CRC Press LLC: Boca Raton, FL, 1996.

86. Stewart, T. A.; Trudell, D. E.; Alam, T. M.; Ohlin, C. A.; Lawler, C.; Casey, W. H.; Jett, S.; Nyman, M., Enhanced Water Purification: A Single Atom Makes a Difference. *Environmental Science & Technology* **2009,** *43* (14), 5416-5422.

87. Armstrong, C. R.; Casey, W. H.; Navrotsky, A., Energetics of Al13 Keggin cluster compounds. *Proceedings of the National Academy of Sciences* **2011,** *108* (36), 14775-14779.

88. Akitt, J. W.; Greenwood, N. N.; Khandelwal, B. L.; Lester, G. D., 27Al nuclear magnetic resonance studies of the hydrolysis and polymerisation of the hexa-aquo-aluminium(III) cation. *Journal of the Chemical Society, Dalton Transactions* **1972,** (5), 604-610.

89. Akitt, J. W.; Elders, J. M., Aluminium-27 nuclear magnetic resonance studies of the hydrolysis of aluminium(III). Part 7.-Spectroscopic evidence for the cation [AlOH]2+ from line-broadening studies at high dilution. *Journal of the Chemical Society, Faraday Transactions 1: Physical Chemistry in Condensed Phases* **1985,** *81* (8), 1923-1930.

90. Fullmer, L. B.; Mansergh, R. H.; Zakharov, L. N.; Keszler, D. A.; Nyman, M., Nb2O5 and Ta2O5 Thin Films from Polyoxometalate Precursors: A Single Proton Makes a Difference. *Crystal Growth & Design* **2015,** *15* (8), 3885-3892.

91. Goberna-Ferrón, S.; Park, D.-H.; Amador, J. M.; Keszler, D. A.; Nyman, M., Amphoteric Aqueous Hafnium Cluster Chemistry. *Angewandte Chemie International Edition* **2016,** *55* (21), 6221-6224.

92. Oliveri, A. F.; Elliott, E. W.; Carnes, M. E.; Hutchison, J. E.; Johnson, D. W., Elucidating Inorganic Nanoscale Species in Solution: Complementary and Corroborative Approaches. *ChemPhysChem* **2013,** *14* (12), 2655-2661.

93. Johansson, G., The Crystal Structures of [Al2(OH)2(H2O)8](SO4)2 2H2O and [Al2(OH)2(H2O)8] (SeO4)2 2H2O. *Acta Chemica Scandanavica* **1962,** *16*, 403-420.

94. Perkins, C. K.; Mansergh, R. H.; Ramos, J. C.; Nanayakkara, C. E.; Park, D.-H.; Goberna-Ferrón, S.; Fullmer, L. B.; Arens, J. T.; Gutierrez-Higgins, M. T.; Jones, Y. R.; Lopez, J. I.; Rowe, T. M.; Whitehurst, D. M.; Nyman, M.; Chabal, Y. J.; Keszler, D. A., Low-index, smooth Al2O3 films by aqueous solution process. *Opt. Mater. Express* **2017,** *7* (1), 273-280.

95. S. W. Smith, W. W., D. A. Keszler, J. F. Conley, Solution based prompt inorganic condensation and atomic layer deposition of Al2O3 films: A side-by-side comparison. *J. Vac. Sci. Technol. A Vacuum, Surfaces, Film.* **2014,** *32*, 41501.

96. Menchetti, S. S., C., Alunogen: Its Structure and Twinning. *Tschermaks Mineralogische und Petrographische Mitteilungen* **1974,** *21*, 164-178.

97. Villars, P.; Cenzual, K., [Al(H2O)6]2(SO4)3·4.4H2O (Al2[SO4]3[H2O]17) Crystal Structure: Datasheet from "PAULING FILE Multinaries Edition – 2012" in SpringerMaterials. Villars, P.; Cenzual, K., Eds. Springer-Verlag Berlin Heidelberg & Material Phases Data System (MPDS), Switzerland & National Institute for Materials Science (NIMS), Japan: 2012.

98. Anderson, J. T.; Munsee, C. L.; Hung, C. M.; Phung, T. M.; Herman, G. S.; Johnson, D. C.; Wager, J. F.; Keszler, D. A., Solution-Processed HafSOx and ZircSOx Inorganic Thin-Film Dielectrics and Nanolaminates. *Advanced Functional Materials* **2007,** *17* (13), 2117-2124.

99. Falaise, C.; Nyman, M., The Key Role of U28 in the Aqueous Self-Assembly of Uranyl Peroxide Nanocages. *Chemistry – A European Journal* **2016,** *22* (41), 14678-14687.

100. Jiang, K.; Anderson, J. T.; Hoshino, K.; Li, D.; Wager, J. F.; Keszler, D. A., Low-Energy Path to Dense HfO2 Thin Films with Aqueous Precursor. *Chemistry of Materials* **2011,** *23* (4), 945-952.

101. Meyers, S. T.; Anderson, J. T.; Hong, D.; Hung, C. M.; Wager, J. F.; Keszler, D. A., Solution-Processed Aluminum Oxide Phosphate Thin-Film Dielectrics. *Chemistry of Materials* **2007,** *19* (16), 4023-4029.

102. Riverkeeper, C. More Tank Leaks Identified at Hanford Nuclear Site. http://columbiariverkeeper.org/top-stories/more-tank-leaks-identified-at-hanford-nuclear-site/ (accessed 04/30/2017).

103. Washington Department of Ecology, W. Hanford Quick Facts. http://www.ecy.wa.gov/programs/nwp/permitting/hdwp/CU/SST.html (accessed 03/15/2017).

104. Harden, B. M., D., Debate Intensifies on Nuclear Waste. *Washington Post* 06/02/2007, 2007, p A02.

105. Lichtner, P. C.; Felmy, A. R., Estimation of Hanford SX tank waste compositions from historically derived inventories. *Computers & Geosciences* **2003,** *29* (3), 371-383.

106. Campbell, J. A. M., G. M.; Clauss, S. A.; Sharma, A. K.; Hoppe, E. W. , ANALYSIS OF HANFORD TANK WASTES. DOE, Ed. Richland, WA, 2000.

107. Nash, K. L.; Borkowski, M.; Hancock, M.; Laszak, I., Oxidative Leaching of Plutonium from Simulated Hanford Tank-Waste Sludges. *Separation Science and Technology* **2005,** *40* (7), 1497-1512.

108. Babad, H. C., D. M., The Aging of Organic Chemicals in Hanford High-Level Wastes. In *Annual Waste Management Conference*, Tucson, AZ, 2000.

109. Baes, C. F. M., R. E., *The Hydrolysis of Cations*. John Wiley and Sons: 1976.

110. Chimie-Briere Aluminum. http://www.chimie-briere.com/problemes/Aluminium/Aluminiumcor.htm (accessed 03/15/2017).

111. Johansson, G., On the Crystal Structures of Some Basic Aluminum Salts. *Acta Chemica Scandanavica* **1960,** *14*, 771-773.

112. Arichi, J.; Pereira, M. M.; Esteves, P. M.; Louis, B., Synthesis of Keggin-type polyoxometalate crystals. *Solid State Sciences* **2010,** *12* (11), 1866-1869.

113. Keggin, F. J., The Structure and Formula of 12-Phosphotungstic Acid. *Proceedings of the Royal Society A* **1934**.

114. Sadakane, M.; Steckhan, E., Electrochemical Properties of Polyoxometalates as Electrocatalysts. *Chemical Reviews* **1998,** *98* (1), 219-238.

115. Mizuno, N.; Yamaguchi, K.; Kamata, K., Epoxidation of olefins with hydrogen peroxide catalyzed by polyoxometalates. *Coordination Chemistry Reviews* **2005,** *249* (17–18), 1944-1956.

116. Guo, Y.; Hu, C., Heterogeneous photocatalysis by solid polyoxometalates. *Journal of Molecular Catalysis A: Chemical* **2007,** *262* (1–2), 136-148.

117. Rohmer, M.-M.; Bénard, M.; Blaudeau, J.-P.; Maestre, J.-M.; Poblet, J.-M., From Lindqvist and Keggin ions to electronically inverse hosts: Ab initio modelling of the structure and reactivity of polyoxometalates. *Coordination Chemistry Reviews* **1998,** *178–180, Part 2*, 1019-1049.

118. Kholdeeva, O. A.; Maksimovskaya, R. I., Titanium- and zirconium-monosubstituted polyoxometalates as molecular models for studying mechanisms of oxidation catalysis. *Journal of Molecular Catalysis A: Chemical* **2007,** *262* (1–2), 7-24.

119. Uchida, S.; Mizuno, N., Design and syntheses of nano-structured ionic crystals with selective sorption properties. *Coordination Chemistry Reviews* **2007,** *251* (21–24), 2537-2546.

120. Mirzaei, M.; Eshtiagh-Hosseini, H.; Alipour, M.; Frontera, A., Recent developments in the crystal engineering of diverse coordination modes (0–12) for Keggin-type polyoxometalates in hybrid inorganic–organic architectures. *Coordination Chemistry Reviews* **2014,** *275*, 1-18.

121. Nomiya, K.; Sakai, Y.; Matsunaga, S., Chemistry of Group IV Metal Ion-Containing Polyoxometalates. *European Journal of Inorganic Chemistry* **2011,** *2011* (2), 179-196.

122. Ouahab, L., The polyoxometalates as precursors in molecular materials. *Comptes Rendus de l'Académie des Sciences - Series IIC - Chemistry* **1998,** *1* (5), 369-380.

123. Sun, C.-Y.; Liu, S.-X.; Liang, D.-D.; Shao, K.-Z.; Ren, Y.-H.; Su, Z.-M., Highly Stable Crystalline Catalysts Based on a Microporous Metal−Organic Framework and Polyoxometalates. *Journal of the American Chemical Society* **2009,** *131* (5), 1883-1888.

124. An, H.-Y.; Wang, E.-B.; Xiao, D.-R.; Li, Y.-G.; Su, Z.-M.; Xu, L., Chiral 3D Architectures with Helical Channels Constructed from Polyoxometalate Clusters and Copper–Amino Acid Complexes. *Angewandte Chemie International Edition* **2006,** *45* (6), 904-908.

125. Wang, X.-L.; Qin, C.; Wang, E.-B.; Su, Z.-M.; Li, Y.-G.; Xu, L., Self-Assembly of Nanometer-Scale [Cu24I10L12]14+ Cages and Ball-Shaped Keggin Clusters into a (4,12)-Connected 3D Framework with Photoluminescent and Electrochemical Properties. *Angewandte Chemie International Edition* **2006,** *45* (44), 7411-7414.

126. Song, J.; Luo, Z.; Britt, D. K.; Furukawa, H.; Yaghi, O. M.; Hardcastle, K. I.; Hill, C. L., A Multiunit Catalyst with Synergistic Stability and Reactivity: A Polyoxometalate–Metal Organic Framework for Aerobic Decontamination. *Journal of the American Chemical Society* **2011,** *133* (42), 16839-16846.

127. Lopez, X.; Carbo, J. J.; Bo, C.; Poblet, J. M., Structure, properties and reactivity of polyoxometalates: a theoretical perspective. *Chemical Society Reviews* **2012,** *41* (22), 7537-7571.

128. Baker, L. C. W.; Figgis, J. S., New fundamental type of inorganic complex: hybrid between heteropoly and conventional coordination complexes. Possibilities for geometrical isomerisms in 11-, 12-, 17-, and 18-heteropoly derivatives. *Journal of the American Chemical Society* **1970,** *92* (12), 3794-3797.

129. Chen, Z.; Fan, B.; Peng, X.; Zhang, Z.; Fan, J.; Luan, Z., Evaluation of Al30 polynuclear species in polyaluminum solutions as coagulant for water treatment. *Chemosphere* **2006,** *64* (6), 912-918.

130. Mertens, J.; Casentini, B.; Masion, A.; Pöthig, R.; Wehrli, B.; Furrer, G., Polyaluminum chloride with high Al30 content as removal agent for arsenic-contaminated well water. *Water Research* **2012,** *46* (1), 53-62.

131. Furrer, G.; Phillips, B. L.; Ulrich, K.-U.; Pöthig, R.; Casey, W. H., The Origin of Aluminum Flocs in Polluted Streams. *Science* **2002,** *297* (5590), 2245-2247.

132. Abeysinghe, S.; Unruh, D. K.; Forbes, T. Z., Surface Modification of Al30 Keggin-Type Polyaluminum Molecular Clusters. *Inorganic Chemistry* **2013,** *52* (10), 5991-5999.

133. Rustad, J. R., Molecular dynamics simulation of the titration of polyoxocations in aqueous solution. *Geochimica et Cosmochimica Acta* **2005,** *69* (18), 4397-4410.

134. Evans, C. C.; Sukarto, L.; Ward, M. D., Sterically Controlled Architectural Reversion in Hydrogen-Bonded Crystalline Clathrates. *Journal of the American Chemical Society* **1999,** *121* (2), 320-325.

135. Holman, K. T.; Martin, S. M.; Parker, D. P.; Ward, M. D., The Generality of Architectural Isomerism in Designer Inclusion Frameworks. *Journal of the American Chemical Society* **2001,** *123* (19), 4421-4431.

136. Russell, V. A.; Evans, C. C.; Li, W.; Ward, M. D., Nanoporous Molecular Sandwiches: Pillared Two-Dimensional Hydrogen-Bonded Networks with Adjustable Porosity. *Science* **1997,** *276* (5312), 575-579.

137. Cote, A. P.; Shimizu, G. K. H., The first example of a functional pillared metal sulfonate network. *Chemical Communications* **2001,** (3), 251-252.

138. Sheldrick, G. M., A short history of SHELX. *Acta Crystallographica Section A* **2008,** *64* (1), 112-122.

139. Spek, A. L., PLATON SQUEEZE: a tool for the calculation of the disordered solvent contribution to the calculated structure factors. *Acta crystallographica. Section C, Structural chemistry* **2015,** *71* (Pt 1), 9-18.

140. Brown, I. D., *The Chemical Bond in Inorganic Chemistry: The Bond Valence Model*. Oxford University Press: 2002.

141. Allmann, R., Beziehungen zwischen Bindungslängen und Bindungsstärken in Oxidstrukturen. *Monatshefte für Chemie / Chemical Monthly* **1975,** *106* (3), 779-793.

142. Corum, K. W.; Fairley, M.; Unruh, D. K.; Payne, M. K.; Forbes, T. Z.; Mason, S. E., Characterization of Phosphate and Arsenate Adsorption onto Keggin-Type Al30 Cations by Experimental and Theoretical Methods. *Inorganic Chemistry* **2015,** *54* (17), 8367-8374.

143. Sun, Z.; Wang, H.; Tong, H.; Sun, S., A Giant Polyaluminum Species S−Al32 and Two Aluminum Polyoxocations Involving Coordination by Sulfate Ions S−Al32 and S−K−Al13. *Inorganic Chemistry* **2011,** *50* (2), 559-564.

144. Reyes Lopez, S. Y. R., J.S.; Sueyoshi, S.S., Low-Temperature Formation of Alpha Alumina Powders via Metal Organic Synthesis. *The AZo Journal of Materials Online* **2006,** *2*.

145. Reyes Lopez, S. Y. A., R.S.; Lopez-Juarez, R.; Rodriguez, J.S., Analysis of the phase transformation og aluminum formate Al(O2CH)3 to alpha-alumina by Raman and infrared spectroscopy. *Journal of Ceramic Processing Research* **2013,** *14* (5), 627-631.

146. Pilgrim, C. D.; Callahan, J. R.; Colla, C. A.; Ohlin, C. A.; Mason, H. E.; Casey, W. H., 27Al MQMAS of the [small delta]-Al13-Keggin. *Dalton Transactions* **2017,** *46* (7), 2249-2254.

147. Matsui, Y.; Shirasaki, N.; Yamaguchi, T.; Kondo, K.; Machida, K.; Fukuura, T.; Matsushita, T., Characteristics and components of poly-aluminum chloride coagulants that enhance arsenate removal by coagulation: Detailed analysis of aluminum species. *Water Research* **2017,** *118*, 177-186.

148. Phillips, B. L.; Ohlin, C. A.; Vaughn, J.; Woerner, W.; Smart, S.; Subramanyam, R.; Pan, L., Solid-State 27Al NMR Spectroscopy of the γ-Al13 Keggin Containing Al Coordinated by a Terminal Hydroxyl Ligand. *Inorganic Chemistry* **2016,** *55* (23), 12270-12280.